TRIM25 and ZAP target the Ebola virus ribonucleoprotein complex to mediate interferon-induced restriction

Rui Pedro Galão[1,5,6], Harry Wilson[1,5], Kristina L Schierhorn[1], Franka Debeljak[1], Bianca S Bodmer[2], Daniel Goldhill[3], Thomas Hoenen[2], Sam J Wilson[4], Chad M Swanson[1] and Stuart J D Neil[1,6]

[1:] Department of Infectious Diseases, School of Immunology and Microbial Sciences, King's College London, UK

[2:] Institute for Molecular Virology and Cell Biology, Friedrich-Loeffler-Institut, Greifswald, Germany

[3:] Section of Virology, Department of Medicine, Imperial College London, London, UK.

[4:] MRC Centre for Virus Research, University of Glasgow, UK

[5:] These authors contributed equally to this work

[6:] Corresponding authors: stuart.neil@kcl.ac.uk; rui_pedro.galao@kcl.ac.uk

Running title: TRIM25 and ZAP target the EBOV vRNP

Highlights

- TRIM25 and ZAP play a major role on type I IFN-mediated inhibition of EBOV trVLP replication
- TRIM25 interacts with the EBOV NP and is recruited to vRNPs in the cytoplasm after viral entry
- TRIM25 ubiquitinates NP and displaces it from the viral genome, facilitating ZAP interaction
- ZAP targets CpGs in the EBOV genome to inhibit EBOV trVLP replication

Summary

Ebola virus (EBOV) causes highly pathogenic disease in primates. Through screening a library of human interferon-stimulated genes (ISGs), we identified TRIM25 as a potent inhibitor of EBOV transcription-and-replication-competent virus-like particle (trVLP) propagation. TRIM25 overexpression inhibited the accumulation of viral genomic and messenger RNAs independently of the RNA sensor RIG-I or secondary proinflammatory gene expression. Deletion of TRIM25 strongly attenuated the sensitivity of trVLPs to inhibition by type-I interferon. The antiviral activity of TRIM25 required ZAP and the effect of type-I interferon was modulated by the CpG dinucleotide content of the viral genome. We find that TRIM25 interacts with the EBOV vRNP, resulting in its autoubiquitination and ubiquitination of the viral nucleoprotein (NP). TRIM25 is recruited to incoming vRNPs shortly after cell entry, and leads to dissociation of NP from the vRNA. We propose that TRIM25 targets the EBOV vRNP, exposing CpG-rich viral RNA species to restriction by ZAP.

Keywords: Ebola virus, type I interferon, TRIM25, ZAP

Introduction

Type I interferons (IFN-I) are released as part of the innate immune response to viruses and induce the expression of an array of genes, many of which have direct antiviral activity (McNab et al., 2015; Schoggins et al., 2011). These proteins often target conserved structures or fundamental processes common to the replication of diverse viruses that cannot be avoided by simple point mutations in a given viral protein (Schneider et al., 2014). In turn, viruses encode mechanisms to inhibit either the detection of virally-expressed pathogen associated microbial patterns (PAMPs) by pattern recognition receptors (PRR), or the signalling through the IFN-I receptor complex (IFNAR1/2). These strategies are essential for efficient *in vivo* viral propagation and pathogenesis (Basler, 2015; Beachboard and Horner, 2016). However, viral evasion from innate immune responses is generally incomplete; acute viral infections are characterized by local and systemic IFN-I responses, and most viruses exhibit some degree of sensitivity to interferon treatment in their target cell types. Understanding the mechanisms by which IFN-I exerts its antiviral effects not only yields new understanding of how mammals have evolved to defend themselves against viral pathogens, but also reveals areas of vulnerability in virus replication that may be exploited therapeutically.

Ebola virus (EBOV, species *Zaire ebolavirus*) is the prototypic member of the ebolavirus genus of the *Filoviridae*, a family of filamentous enveloped non-segmented negative strand RNA viruses responsible for sporadic outbreaks in sub-Saharan Africa (Messaoudi et al., 2015). Ebola virus disease (EVD) is characterized by its high mortality rate (25%-90%), with symptoms including severe fever, vomiting, diarrhoea, that in some cases progress to haemorrhagic fever (Geisbert et al., 2003b). EBOV and other filoviruses are zoonotic infections in man, probably transmitted from bat species (Amman et al., 2014; Leroy et al., 2005), and are spread from person to person by close contact with bodily fluids (Vetter et al., 2016). Individuals that recover from EVD can harbour persistent virus, and men can shed infectious EBOV in the semen for many months after viremia becomes undetectable (Deen et al., 2017; Subissi et al., 2018; Thorson et al., 2021).

EBOV replicates in various tissues but is thought to primarily infect cells of the myeloid lineage (Geisbert et al., 2003a). After uptake by macropinocytosis, the virion membrane fuses with the host endosome following the interaction between a proteolytically processed form of its glycoprotein (GP) and the cellular receptor, NPC1 (Carette et al., 2011; Chandran et al., 2005; Cote et al., 2011). Fusion releases the viral genome into the cytoplasm, allowing the initiation of the replication cycle

(Muhlberger, 2007). The viral genomic RNA (vRNA) exists as a helical ribonucleoprotein complex (RNP) that contains the viral nucleoprotein (NP) and its cofactor VP35, as well as, at lower concentrations, the transcriptional regulator VP30, and the viral RNA-dependent RNA polymerase L (Noda et al., 2010). As with all negative-strand RNA viruses, the viral genome is first transcribed by L to generate mRNAs for viral gene products. L-mediated transcription initiates only at the 3' leader sequence of the vRNA. Viral genes are arrayed along the genome in an order correlating with their abundance in the infected cell; at the intergenic boundaries between each viral gene, L either dissociates from the genome, or reinitiates transcription, a process regulated by VP30 (Biedenkopf et al., 2016; Muhlberger, 2007). VP30 also acts as the molecular switch to promote the synthesis of a full length positive sense copy of the RNA genome (cRNA) (Kruse et al., 2018; Biedenkopf et al., 2013). The cRNA acts as template for the production of new copies of vRNA, that are then assembled into new vRNPs within cytoplasmic inclusion bodies, which are themselves induced by vRNP components (Hoenen et al., 2012). New vRNPs are then targeted to the plasma membrane (PM) where they interact with VP40, and bud from the surface as new virions (Martin-Serrano et al., 2001; Noda et al., 2002).

EBOV encodes two major activities that counteract the innate immune responses. First, VP35 counteracts recognition of viral RNA species by the PRR retinoic acid induced gene I (RIG-I), as well as by playing an incompletely defined role in disabling proinflammatory signalling downstream of PRR activation (Basler et al., 2003; Cardenas et al., 2006; Chang et al., 2009; Luthra P et al., 2013; Prins et al., 2009). Second, VP24 inhibits signalling through IFNAR1/2 by blocking nucleocytoplasmic transport of phosphorylated STAT1 (Shabman et al., 2011; Zhang et al., 2012). Additionally, the virus may antagonize certain antiviral proteins directly; notably the activity of tetherin/BST2 is counteracted by EBOV GP in some experimental systems (Kaletsky et al., 2009; Lopez et al., 2010). However, EBOV replication can still be inhibited by pre-treatment of target cells with IFN-I, and a number of ISGs have been proposed to have antiviral activities against EBOV (Huang et al., 2011; Kuroda et al., 2020; Okumura et al., 2008).

The requirement for high containment laboratories makes identifying host factors that facilitate or inhibit the replication of filoviruses challenging. To identify novel EBOV antiviral proteins, we used a well-established EBOV transcription- and replication-competent virus-like particle (trVLP) system to screen a human ISG library (Kane et al., 2016; Watt et al., 2014). Amongst these, we

identified tripartite-motif family member 25 (TRIM25) as a potent antiviral inhibitor of EBOV trVLP replication. TRIM25, an E3 ubiquitin ligase, until recently widely accepted as being a positive regulator of RIG-I-mediated pattern recognition of cytoplasmic viral RNA, has other emerging roles in innate immunity (Gack et al., 2007; Li et al., 2017; Martin-Vicente et al., 2017). Of note, a recent study has implicated nuclear forms of TRIM25 as having direct antiviral activity against the influenza A virus vRNP (Meyerson et al., 2017). Furthermore, TRIM25 is an important cofactor of the zinc-finger antiviral protein (ZAP, also known as ZC3HAV1 or PARP13), which broadly targets many RNA viruses (Li et al., 2017; Zheng et al., 2017). Recent evidence has shown that ZAP binds to RNAs with a high content of CpG dinucleotides (Chiu et al., 2018; Takata et al., 2017), targeting them for degradation. How TRIM25 regulates ZAP is unknown. Although TRIM25 interacts with and ubiquitinates ZAP, these events are not required for ZAP activity (Li et al., 2017; Zheng et al., 2017). Here we show that TRIM25 interacts with the EBOV vRNP and induces the dissociation of NP from the genomic RNA, thereby promoting CpG-dependent restriction by ZAP.

Results

EBOV trVLP replication is sensitive to type I interferon. The EBOV trVLP system is a reverse genetics system that models the entire replication cycle of the virus without the need for high containment laboratory facilities (Figure S1A)(Watt et al., 2014). trVLP stocks are produced in HEK293T cells (called passage 0 (p0) cells), which are then used to infect HEK293T or U87-MG target cells expressing the viral entry factor TIM-1 (passage 1 (p1) cells). Propagation of trVLPs requires co-transfection of plasmids encoding the vRNP components NP, VP35, VP30 and L prior to infection. trVLP replication can be measured by Renilla luciferase (Rluc) activity in lysates of target cells p1, and by assessing infectivity of harvested p1 supernatants on new target TIM-1 expressing HEK293T cells (passage 2 (p2) cells). p1 cells can also be used to assess the effects of exogenous treatments, and over-expression or knockdown/knockout of candidate cellular factors.

In order to identify candidate ISGs that inhibit EBOV replication, we first tested the sensitivity of trVLPs to IFN-I. HEK293T and U87-MG cells stably expressing TIM-1 were pre-treated overnight with various doses of universal type-I IFN-α and then infected with equal doses of EBOV trVLPs. Rluc activity was measured in p1 cells 24h after infection, and trVLP yield was assessed in the supernatants by infecting HEK293T-TIM1 p2 cells. IFN-I treatment of both cell types gave a robust

dose-dependent inhibition of Rluc activity in p1 and p2, although trVLP replication was more sensitive to IFN-I in U87-MG cells (Figure 1A). Given the distinct impact of IFN-α and IFN-ß on filoviruses pathogenesis in animal models and humans (Escudero-Perez et al., 2019), we tested their independent effect on EBOV trVLPs. As observed with the universal type-I IFN-α, both IFN-α2a and IFN-ß1a produced a dose-dependent inhibition of EBOV trVLPs on U87-MG cells, with IFN-ß1a being slightly more antiviral (Figure S1B), reproducing a previously reported observation (McCarthy et al., 2016). Using an EBOV VP40-Blam VLP-based entry assay, IFN-I pre-treatment of target cells resulted in a minor reduction in entry of particles pseudotyped with EBOV-GP, indicating the majority of the inhibition of trVLP replication was taking place post viral entry (Figure 1B). In keeping with this, IFN-I treatment resulted in a dose-dependent reduction of vRNA and mRNA species in the infected cells (Figure 1C), as well as concomitant reduction of new viral minigenomes in the supernatant that mirrored the effects on Rluc activity (Figure 1D). Importantly, IFN-I treatment did not affect the levels of the vRNP proteins expressed *in trans* (Figure S1C). Thus, human cells exposed to type I IFN exhibit a robust inhibition of filoviral replication through the induction of one or more ISGs targeting trVLP gene expression and minigenome replication.

A human arrayed ISG screen identifies TRIM25 as a potent inhibitor of EBOV trVLP replication

We then screened an expression library of 407 human ISGs individually cloned into mammalian expression vectors, and measured the impact of each ISG on EBOV trVLP replication (Kane et al., 2016). Briefly, individual expression vectors encoding a human ISG were transfected into HEK293T-TIM1 p1 cells alongside the vRNP components and a firefly luciferase (Fluc) transfection control. 24h later the cells were infected with a fixed dose of trVLPs. Rluc activity was measured at the harvest of supernatants 24h later. Supernatant infectivity was then assessed on p2 cells as before. Negative (GFP, empty vector) and positive (IRF1, BST2/tetherin) controls were included on each 96-well plate and Rluc activity in both p1 and p2 cells was normalized to the activity of control Fluc within individual wells and the effects of each individual gene was expressed as a percentage of the plate average (Figure 1E, Table S1). Both p1 and p2 outputs of the screen were normally distributed (Figure S1D), however we reasoned that outlier ISGs that directly inhibited EBOV replication should always display a phenotype in p2 as well as potentially in p1, reflecting likely effects on early and/or late viral replication stages. We focussed on ISGs that gave at least a 5-fold reduction of trVLP infectivity in p2, and discarded any hit in p1 that did not carry over. The top 50 hits were validated in three

independent experiments and ranked (Figure 1F). We then selected 20 of the top p2 hits from the validation for further characterization. First, we examined their effects on trVLP RNA using a primers-probe set in the *VP40* gene (that detects vRNA, cRNA and VP40 mRNA) and another set in the trVLP 5'-trailer region (that detects vRNA and cRNA) in p1 cell lysates, as well as measuring viral RNA levels in the supernatants as an indicator of released trVLP virions (Figure 1G). The majority of these ISGs, with the exception of TNK2, CTCFL, HERC5 and OAS2 affected the levels of cell-associated viral RNA. In addition to these, a few other ISGs had no significant impact on the viral RNA levels in the supernatants (ARHGEF3, SLFN12, P2RY6 and PABPC4). Several (FFAR2, UNC93B1, APOL6, SLC15A3, IFIH1 (MDA5), BST2, SLFN12 and PIM3) also reduced the expression of one or more of the viral RNP components expressed *in trans* (Figure S1E), potentially a confounding factor. Moreover, we noticed significant toxicity effects of FFAR2, C5ORF39, APOL6 and UNC93B1 consistent with previous reports of their proapoptotic activities (Figure S1F). Lastly, it is well known that many ISGs, and particularly pattern recognition receptors, can activate proinflammatory signalling pathways, indicating that antiviral activities measured could be mediated secondarily through upregulation of other ISGs or interferons. We therefore screened the selected 20 hits for their abilities to activate Fluc reporter genes driven by NFkB, IRF3 (ISG56/IFIT1) or IFN-induced ISGF3 (ISRE) dependent promoters (Figure S1G). As expected, expression of both IFIH1 (MDA5) and IRF1 activated ISG56 and ISRE promoters, indicating both an IRF3 and a secondary IFN-I-dependent response. IFIH1 (MDA5), FFAR2, P2YR6 and BST2 also triggered NFkB-dependent responses at both 24h and 48h. In contrast, TRIM25 only gave a detectable NFkB-dependent signal at 48h (i.e. 24h after p1 viral harvest). Importantly, TRIM25 overexpression robustly inhibited the accumulation of trVLP RNA species in p1 cells without affecting expression of vRNP components or demonstrating overt toxicity (Figures 1F, S1E and S1F). Moreover, recent evidence suggests that TRIM25 inhibits influenza virus independent of RIG-I (Meyerson et al., 2017). Thus, TRIM25 was one of the candidate EBOV antiviral factors taken forward for further analysis.

TRIM25 plays a major role in IFN-I-mediated inhibition of EBOV trVLP replication and reduces the abundance of viral RNA species. To further characterize the antiviral activity of TRIM25 we first showed that its ectopic expression in HEK293T-based p1 cells significantly blocked trVLP Rluc activity, both in these cells and subsequent carry over to p2 at increasing trVLP inputs (Figure 2A), without affecting entry of EBOV-GP pseudotyped lentiviral vectors (Figure 2B). The block to trVLP

198 replication correlated with reduced intracellular levels of viral mRNA, cRNA and vRNA, as well as
199 vRNA levels in the supernatant (Figure 2C). We then used lentiviral-based CRISPR/Cas9 vectors to
200 knockout TRIM25 in U87-MG and HEK293T cells (Figure 2D). In both cell types, TRIM25 is
201 expressed at readily detectable levels and this expression is further augmented upon IFN-I treatment.
202 Significantly, whereas IFN-I pre-treatment of control U87-MG cells carrying an irrelevant sgRNA
203 targeting E.coli *LacZ* gene resulted in a 20-30 fold inhibition of trVLP infectivity in p1 target cells,
204 knockout of TRIM25 significantly attenuated this block to trVLP production (Figure 2E), correlating
205 with a rescue of viral RNA species in the corresponding cell lysates and supernatants (Figure 2F).
206 Similarly, the antiviral effects of IFN-α2a or IFN-ß1a on EBOV trVLPs were also attenuated on U87-
207 MG TRIM25 knockout cells (Figure 2G). Importantly, this effect of TRIM25 knockout was specific to
208 the EBOV trVLPs, as IFN-I reduced the infectivity of VSV-G-pseudotyped HIV-1-based vectors
209 equally in control sgRNA (LacZ) and knockout U87-MG cell lines (Figure 2H). Furthermore, in the
210 absence of IFN treatment, TRIM25 knockout HEK293T cells gave significantly higher Rluc activity in
211 p0 producer cells and yielded significant higher levels of virus (p1 infectivity) (Figure 2I). Thus,
212 TRIM25 restricts trVLP production, and is an important component for the IFN-induced antiviral
213 restriction of EBOV.
214 **TRIM25-mediated restriction of EBOV requires components of the cytoplasmic RNA pattern**
215 **recognition machinery, but not proinflammatory signal transduction.** The best characterized role
216 of TRIM25 is as a cofactor of the cytoplasmic RNA sensor RIG-I (Gack et al., 2007). TRIM25 and/or
217 Riplet mediate Lys63-linked polyubiquitination of RIG-I and promote the binding of this PRR to viral
218 RNAs and its interaction with the full-length (FL) mitochondrial antiviral protein (MAVS) isoform. This
219 is essential for the propagation of proinflammatory signalling downstream of RIG-I and its related
220 helicases (Loo and Gale, 2011). We therefore used CRISPR/Cas9 to delete both RIG-I and MAVS in
221 HEK293T and U87-MG cells (Figure 3A and B). Whilst RIG-I expression is only detectable after IFN-
222 treatment of the control sgRNA cells (LacZ), FL-MAVS and a shorter isoform known as miniMAVS
223 (Brubaker et al., 2014) are readily detected in both cell lines at steady state. Both isoforms are
224 expressed as alternative translation products from the same mRNA. miniMAVS localizes and interacts
225 with FL-MAVS, but having no CARD domains, cannot interact with RIG-like helicases and activate
226 antiviral signal. Moreover, its interference with FL-MAVS activity has suggested it as a negative
227 regulator of RNA sensing (Brubaker et al., 2014). We designed sgRNA guides that would target exons

upstream or downstream of the miniMAVS start codon and thus generated FL-MAVS knockout, or FL-MAVS and miniMAVS double-knockout cells (DKO). We then examined the effects of these knockouts on the antiviral activity of ectopically expressed TRIM25. Whilst TRIM25 retained antiviral activity when overexpressed in RIG-I knockout cells it lost this activity in FL-MAVS/miniMAVS double-knockout cells (Figure 3C). Furthermore, there was no effect of RIG-I knock-out on the sensitivity of trVLPs to IFN-I in U87-MG cells (Figure 3D). By contrast, trVLP replication was significantly rescued from IFN-I antiviral effect in FL-MAVS/miniMAVS DKO cells, with FL-MAVS alone KO presenting only a partial rescue (Figure 3E). To clarify the potential requirement of each MAVS isoform for the antiviral activity of ectopically expressed TRIM25, we performed rescue experiments in which the expression of miniMAVS and/or FL-MAVS was stably reconstituted in HEK293T MAVS DKO cells (Figure 3F). The antiviral effect of TRIM25 against EBOV trVLP was rescued by the simultaneous reintroduction of CRISPR-resistant forms of miniMAVS and FL-MAVS ($MAVS^{CR}$), whilst still significantly attenuated when FL-MAVS ($M142A^{CR}$) or miniMAVS ($M1A^{CR}$) were expressed separately (Figure 3G). Thus, the TRIM25 and IFN-I antiviral activities against EBOV trVLPs required both signalling active and inactive MAVS isoforms, but not RIG-I, suggesting a mechanism distinct from classical RLR signalling. To further rule out classical RNA sensing as the mechanism, we knocked out TBK1, which is the essential kinase downstream of MAVS for IFN and ISG induction (Figure 3H). As with RIG-I knockout, depletion of TBK1 did not affect TRIM25- or IFN-I-mediated inhibition of trVLP replication (Figures 3I and 3J). Moreover, TRIM25 overexpression in all knockout cell lines induced indistinguishable NFκB-dependent reporter activity at 48h irrespective of its antiviral effect, arguing against an indirect role of TRIM25-mediated signalling (Figure 3K). Taken together, these data indicate that the TRIM25/IFN-I-dependent antiviral restriction of EBOV trVLP replication requires both MAVS isoforms, but is independent of the proinflammatory signal generated by classical cytoplasmic RLR sensing.

Potent IFN-mediated inhibition of EBOV trVLP propagation requires ZAP and is modulated by CpG content of the viral genome. TRIM25 has been implicated in the regulation of ZAP, which has antiviral activity against numerous mammalian RNA viruses (Bick et al., 2003; Gao et al., 2002; Li et al., 2017; Zheng et al., 2017). ZAP is expressed as long (L) and short (S) splice variants, the latter lacking the catalytically inactive PARP-like domain (Kerns et al., 2008). ZAP-L has more potent antiviral activities against some viruses and has a stronger interaction with TRIM25 than ZAP-S

(Charron et al., 2013; Goodier et al., 2015; Kerns et al., 2008; Li et al., 2017). Whilst ZAP-S is the major IFN-regulated isoform (Goodier et al., 2015; Hayakawa et al., 2011) and was included in our ISG screen, it did not score as a hit. By contrast, however, overexpression of ZAP-L had a potent antiviral activity against EBOV trVLP replication in HEK293T-TIM1 p1 and p2 cells, which manifested as significant reductions in viral mRNA, vRNA and cRNA species (Figures 4A and S2A). We then generated HEK293T and U87-MG ZAP CRISPR knockout cells (Figure 4B), and found that like TRIM25 knockout cells, they exhibited a significantly reduced restriction of trVLP replication and viral RNA accumulation after pre-treatment with IFN-I (Figures 4C and 4D). We also observed an attenuated effect of IFN-α2a and IFN-ß1b on trVLP propagation (Figure S2B) and increased viral yields from p0 cells (Figure S2C). Furthermore, ZAP and TRIM25 interdependence was confirmed by showing that the antiviral effect conferred by their individual overexpression was abolished in cells lacking the other gene (Figure 4E). In contrast, while we could confirm the report (Meyerson et al., 2017) that overexpression of TRIM25 targets the influenza vRNP, the magnitude of this activity was unaffected by ZAP knockout (Figure S2D).

ZAP has previously been shown to inhibit the expression of EBOV proteins (Muller et al., 2007), particularly the RdRp L which we supply here *in trans*. However, whilst we could demonstrate significant reductions in L mRNA and protein levels in p1 cells transfected with ZAP-L (Figure 4F and S2E), the same reductions were observed in TRIM25 KO cells where ZAP overexpression had limited impact in reducing the levels of EBOV genomic RNA or antiviral activity (Figure S2F and 4E). Moreover, our earlier observations that IFN-I treatment did not affect the expression levels of vRNP components (Figure S1C) further argued against the reduction in L expression as the major contributor to the TRIM25/ZAP-mediated restriction of EBOV trVLPs under these experimental conditions.

Most mammalian viral RNA genomes exhibit marked suppression of CpG dinucleotides (Fros et al., 2017; Takata et al., 2017). In the case of HIV-1, artificial increase in CpG concentration in the viral genome impairs replication through ZAP-mediated inhibition, with evidence that ZAP binds directly to the CpGs themselves and induces RNA degradation or translational repression (Takata et al., 2017). The EBOV genome contains just over half of the number of CpGs expected by chance for its nucleotide composition (Figure S2G). These CpGs are widely distributed across the genome, both in the protein coding genes and intergenic regions with the notable exception of the intergenic region

between GP and VP30 (Figure S2H). The trVLP CpG content is moderately higher, with 61 CpGs in the *Rluc* reporter gene that replaces NP as first ORF. Since the *RLuc* coding sequence does not contain any necessary viral *cis*-acting regulatory elements, this gave us the opportunity to test whether CpG content could impact upon IFN-sensitivity of the virus. We generated a trVLP in genome in which all the CpGs in *Rluc* were silently mutated, reducing the observed vs expected CpG content of the trVLP to 0.45 (CpG low, Figures S2G and S2H). This modification had no detectable effect on trVLP yield or replication (Figure 4G). However, the CpG-low containing trVLP exhibited partial rescue from ZAP-L restriction (Figure 4G), which correlated with increased intracellular levels of viral mRNA, cRNA and vRNA on these cells, as well as vRNA levels in the supernatant (Figure 4H). Furthermore, the CpG-low containing trVLP was also less sensitive than the parental trVLP to IFN-I (Figure 4I). Since Renilla expression is not required for trVLP replication and both of these phenotypes were measured in p2 cells, these data imply that a major target of ZAP-mediated restriction is the CpG dinucleotides in the trVLP. These data further suggest that CpG content of the genomes of RNA virus can sensitize them to type I IFNs in a ZAP-dependent manner. Finally, ZAP-mediated targeting of CpG-containing retroviral RNA for degradation was shown to depend not only on TRIM25, but also on the cytoplasmic protein KHNYN, which predictably confers the nuclease activity that is lacking in both ZAP isoforms (Ficarelli et al., 2019). However, in contrast to ZAP-mediated restriction of retroviruses, this does not seem to be dependent on KHNYN, as depletion of this protein in U87-MG cells did not attenuate the antiviral effect of IFN-I on EBOV trVLPs replication (Figure S4I and S4J).

TRIM25 interacts with the EBOV vRNP and promotes ubiquitination of NP.

While the role of TRIM25 as a ZAP cofactor is established, how it facilitates ZAP targeting of viral RNAs is not understood. However, given the previously reported interaction between TRIM25 and influenza virus (Meyerson et al., 2017), we hypothesized that it could act directly on EBOV vRNP components to promote ZAP-mediated restriction. We noted that overexpression of TRIM25 induced a smear of higher molecular weight species above NP in western blots of transfected HEK293T cell lysates during the screen (Figure S1E), so we therefore first examined whether TRIM25 could interact with the EBOV NP and its cofactor VP35. NP co-immunoprecipitated with TRIM25, whereas VP35 only pulled-down with TRIM25 in the presence of NP (Figure 5A). Furthermore, reciprocal immunoprecipitation of NP from p1 cells brought down both VP35 and TRIM25, indicating that TRIM25 could interact with the vRNP in an NP-dependent manner (Figure S3A). This interaction was

resistant to RNAse treatment, suggesting that the vRNA was not bridging the interaction between TRIM25 and NP (Figure S3B). Endogenous ZAP-L, but not ZAP-S, could also be detected in TRIM25/NP coprecipitates. However, in cells lacking ZAP, TRIM25 could still interact with NP (Figure S3C). To determine if TRIM25 localized to viral replication compartments, we analysed endogenous TRIM25 expression by immunofluorescence. TRIM25 re-localized to NP-containing viral inclusion bodies in cells transfected with the vRNP proteins (Figure 5B). NP expression was sufficient for this re-localization, but it was markedly enhanced in the presence of VP35 which is known to regulate the conformational dynamics of NP in the vRNP (Kirchdoerfer et al., 2015).

Like many TRIM family members, TRIM25 consists of a N-terminal RING domain containing E3-ubiquitin ligase activity, two B-Box domains, a coiled-coil domain that allows it to form antiparallel dimers, and a C-terminal PRYSPRY substrate recognition domain (D'Cruz et al., 2013; Gack et al., 2007; Sanchez et al., 2014) (Figure 5C). Using deletion mutants of TRIM25, we found that the mutants lacking the PRYSPRY domain, but not the RING domain, lost their ability to interact with NP in co-immunoprecipitations (Figure 5C). However, both PRYSPRY and RING domains were essential for antiviral activity against EBOV trVLPs when overexpressed in HEK293T-TIM1 p1 cells (Figure 5D). When activated by their cognate ligands, many TRIM proteins undergo autoubiquitination as well as inducing ubiquitination of target proteins (Tomar and Singh, 2015). Consistent with this, in the presence of HA-tagged ubiquitin, co-expression of TRIM25 and NP induced the appearance of higher molecular weight species of both proteins, that could be precipitated with anti-HA and NP antibodies, indicating the presence of ubiquitin molecules (Figure 5E). Ubiquitinated species of NP and TRIM25 could not be detected in cells transfected with the RING-deleted TRIM25 mutant, indicating the RING E3 ligase activity was essential (Figure S3D). However, in HEK293T cells lacking either ZAP or FL-MAVS and miniMAVS where TRIM25 antiviral activity is curtailed, TRIM25 and NP co-expression could still lead to ubiquitination of both proteins (Figures S3E and S3F). To exclude the possibility that our observations are product of an artefact associated with overexpressing HA-tagged ubiquitin, we pulled-down EBOV NP following its co-expression with YFP or TRIM25 under endogenous levels of ubiquitin, and treated this fraction with Ubiquitin Specific Peptidase 2 (USP2). The typical smear of higher molecular weight observed above NP when TRIM25 is ectopically expressed disappeared upon treatment with USP2, reinforcing our initial finding that TRIM25 promotes the ubiquitination of NP (Figure 5F). Of note, we did not detect evidence of a differential NP degradation in the absence of

TRIM25 (Figure S3G). Thus, the ubiquitin ligase activity of TRIM25, and specifically the ubiquitination of NP and auto-ubiquitination of TRIM25, are necessary but not sufficient to explain its antiviral activity against EBOV.

Recent evidence has suggested that activation of TRIM25 E3 ligase activity requires its binding to RNA, with two distinct RNA interaction domains being described – a basic patch with 7 lysine residues in the linker between the coiled-coil and the PRYSPRY domain, and an RNA-binding domain (RBD) in the N-terminal region of the PRYSPRY itself. Activation is also strictly dependent on the multimerization of TRIM25 dimers through dimerization of N-terminal RING domains (Sanchez et al., 2018). In order to further probe the determinants of TRIM25-mediated antiviral activity, we made a series of mutations in these functional domains (Figure 6A). Compared to the wildtype protein, some of the targeted mutations in the RING dimerization interface, the catalytic site itself, or the PRYSPRY domain significantly impaired antiviral activity (Figure 6A). Of these RING dimerization mutants N66A, L69A and V72A lost all antiviral activity (Figure 6A). Similarly, deletion of the RBD or mutation of the linker region basic patch (7KA) led to lost activity. Targeted mutations predicted to disrupt the coiled-coil (Sanchez et al., 2014) were not significantly defective in restricting trVLP replication. Western blot analyses indicated that antiviral potency appeared to correlate well with NP ubiquitination under endogenous levels of ubiquitin (Figure 6B). While most RING dimerization mutants blocked ubiquitination of NP, individual mutations in the catalytic site reduced, but did not completely, abolish it. Furthermore, the effectively antiviral coiled-coil mutants Y254A and Y252A, together with the BBox2 RHK mutant, were still capable to induce NP ubiquitination. Interestingly the putative RNA-binding activity mutants, particularly the RBD, were also impaired in NP ubiquitination. Unlike the full deletion of the PRYSPRY domain, all functional RING mutants of TRIM25 tested retained the ability to interact with NP in coimmunoprecipitations as did the RBD deletion (Figure 6C). Surprisingly, the 7K mutant lost NP interaction, suggesting that it may affect PRYSPRY-mediated NP interaction.

TRIM25 is recruited to incoming vRNPs and reduces NP association with trVLP vRNA and promotes its interaction with ZAP.

The data presented above support the hypothesis that TRIM25 and ZAP target the EBOV vRNP to block its transcription and/or replication. To examine this in detail we first tested whether incoming vRNPs alone were capable of re-localizing endogenous TRIM25. HEK293T LacZ CRISPR-TIM1 cells were infected with concentrated trVLP supernatants in the absence of transfection of vRNP

components, then fixed and stained for NP and TRIM25 3 to 6 hours post-infection. In approximately 5% of cells, distinct NP positive foci were detected in the cytoplasm, associated with an aggregation of endogenous TRIM25 (Figure 7A, left panel). To ensure this re-localisation was specific for cells in which trVLPs had entered, we made use of HEK293T-TIM1 cells in which the endosomal EBOV fusion receptor NPC1 had been deleted by CRISPR, thus rendering them uninfectable by VLPs pseudotyped with EBOV GP (Figure S4A-S4C). By contrast, in these cells we saw no evidence of cytoplasmic NP structures or TRIM25 re-localization (Figure 7A, right panel), suggesting that TRIM25 can only associate with incoming EBOV vRNPs after fusion of the viral membrane and release of the vRNPs into the cytoplasm.

We then asked whether TRIM25 or ZAP could affect the integrity of the vRNP. As a control we could show that neither overexpression of TRIM25, nor ZAP, affected total cell-associated trVLP genomes 3 hours post-infection (Figure S4D). mRNA abundance is very low at this timepoint, showing that any primary transcription is below the limit of detection. Thus, under conditions in which no vRNP components were ectopically expressed, we performed RNA-IPs of NP-associated genomic trVLP vRNA after UV-crosslinking of cells overexpressing GFP, TRIM25 or ZAP. Immunoprecipitation of NP under these conditions consistently brought down 5-to-10% of the input genomes. Interestingly, overexpression of TRIM25 or ZAP significantly reduced the levels of trVLP genome associated with incoming NP (Figure 7B), independently of using WT or CpG low EBOV trVLPs (Figure S4E). Importantly, TRIM25 and ZAP did not dissociate EBOV trVLP RNA from NP in NPC1 CRISPR knockout cells where cell associated virions will remain unfused in endosomal compartments (Figure 7B). Furthermore, whilst TRIM25 overexpression in ZAP KO cells could still reduce NP/genome association, ZAP overexpression could not mediate the same effect in TRIM25 KO cells (Figure 7C), indicating that TRIM25, not ZAP, was essential for this effect, while the CpG content of the viral genome does not influence the targeting of the RNP by TRIM25 (Figure S4F). Furthermore, neither RING nor PRYSPRY-deletion mutants of TRIM25 could promote NP/genome dissociation (Figure 7D), neither could the RNA-binding or RING mutants (Figure 7E), consistent with their lack of antiviral activity.

Since transcription of viral genes by the vRNP-associated RdRp is the one of the first events in EBOV replication after cellular entry, we performed the experiment in Figure 7B in the presence of 250μM of the L inhibitor T705, which is sufficient to inhibit trVLP RLuc expression by 90% (Figure

S4G and S4H). Importantly, we found that T705 did not prevent TRIM25 overexpression from dissociating NP from the genome of incoming viruses (Figure 7F). Together these data indicate vRNP interaction, RNA-binding and activation of E3 ligase activity are required for TRIM25 to dissociate NP from the viral genome of incoming EBOV vRNPs, and thus facilitate interaction with ZAP.

We then performed a similar crosslinking-IP in cells, this time precipitating overexpressed ZAP. This markedly enriched for the trVLP viral genome at the same timepoint that NP/genome association was reduced (Figure 7G). However, immunoprecipitation from TRIM25 KO cells under the same experimental conditions showed no evidence of ZAP association with the trVLP genome, indicating that this correlated with TRIM25-mediated NP/genome dissociation. To further address the importance of the CpG content for ZAP association, we used a monocistronic genome containing the *Rluc* gene flanked by the leader and trailer regions of EBOV, from which we generated a low CpG variant in which all the CpGs in *Rluc* were silently mutated (Figure S4I). As expected, ZAP overexpression impacts in the replication of the WT monocistronic genome, whilst its effect is attenuated upon reduction of the CpG content (Figure S4J). This correlated with the significant impairment of ZAP association with the CpG low monocistronic genome when compared with the wild-type (Figure S4K), thus highlighting the important role of the viral genome CpG content for ZAP-mediated antiviral effect.

Finally, we asked if the NP/genome dissociation could be recapitulated following an IFN-I treatment. HEK293T LacZ-TIM1 cells, or those lacking TRIM25 or ZAP were treated overnight with IFN-I and then infected for 3h with trVLPs and similarly subjected to UV-crosslinked RNA-IP of NP. In HEK293T LacZ-TIM1 cells, IFN-I pre-treatment reduced the NP/genome association to a similar extent to the ectopic overexpression of TRIM25, without affecting total cell-associated trVLP vRNA. However, in TRIM25 knockout cells, there was no significant reduction in NP/genome association. In ZAP knockout cells, whilst NP/genome interactions were largely restored, there remained a small reduction in trVLP vRNA recovered after NP immunoprecipitation (Figure 7H). Thus, the TRIM25 dependent dissociation of NP from the trVLP genome can be demonstrated in cells after IFN-I stimulation, implying the relevance of these observations to the antiviral mechanism.

In order to further investigate whether we could observe the antiviral effect of TRIM25 and ZAP in an alternative model of the trVLP system based only in infection, we created an EBOV minigenome that expressed a nanoluciferase in place of the Renillla, resulting in a more sensitive

reporter capable of reliably detecting at low enough quantities to observe primary transcription. The observed primary transcription could be quantified specifically as luciferase signal was not observed with either ΔGP trVLPs or in NPC1 CRISPR knockout cells (Figure S4L). We then investigated the effect of TRIM25 and ZAP and observed that the antiviral activity of IFN-I treatment on primary transcription was attenuated in either TRIM25 or ZAP knockout cells at lower concentrations (Figure 7I). Furthermore, we also observed that TRIM25 overexpression was also antiviral in this system (Figure S4M). These observations indicate that both TRIM25 and ZAP are important for the cellular defence against EBOV in an infection only based model.

Discussion

Through screening of a human ISG library we provide evidence that TRIM25 and ZAP are major effectors of interferon-induced antiviral restriction of EBOV trVLP. The data presented herein lead us to propose the following model for the mechanism of this restriction (Figure 7J). TRIM25 interacts with the viral NP and is recruited to the incoming vRNP shortly after fusion of the virion with the cellular endosomal membrane. This results in the ubiquitination of both NP and TRIM25, and the apparent displacement of NP from the viral genome, facilitating ZAP binding to the vRNA. The antiviral inhibition of the subsequent transcription and replication of the virus is dependent on this interaction, and the overall sensitivity of the virus to both ZAP and IFN-I can be modulated by the CpG content of the viral genomic RNA. This activity of TRIM25 is completely independent of RIG-I-mediated sensing of viral RNA and proinflammatory signalling but requires both isoforms of MAVS. As such we propose this as a direct antiviral restriction mechanism associated with, but independent of, classical cytoplasmic RNA pattern recognition.

Until recently, TRIM25 was thought to be an essential cofactor for the RIG-I helicase to recognise viral RNA species, particularly those with exposed 5’ triphosphates (Gack et al., 2007; Okamoto et al., 2017). However, new data implicates Riplet as the essential E3 ligase in RIG-I activation (Cadena et al. 2019). Upon activation, RIG-I and MAVS undergo a prion-like polymerization into extended filaments that directly activate the kinase TBK1, and thus promote proinflammatory signalling (Cai et al., 2014), and it is still unclear whether TRIM25 plays further roles in the pathway. However, neither RIG-I nor TBK1 are necessary for TRIM25 to inhibit EBOV trVLP replication, implying a role distinct from classical RNA sensing.

The PRYSPRY domain of TRIM25 binds to and activates ZAP (Li et al., 2017; Zheng et al., 2017), which has long been known as an antiviral effector targeting various RNA viruses (Bick et al., 2003; Gao et al., 2002; Takata et al., 2017). For a number of positive sense RNA viruses, ZAP binds to the RNA genome and restricts replication by blocking its translation and/or targets viral RNA for degradation by the 3'-5' exosome (Bick et al., 2003; Li et al., 2017; Zheng et al., 2017). ZAP exists as two isoforms, ZAP-L and ZAP-S, the latter being a splice variant lacking the C-terminal catalytically inactive poly-ADP ribosyl polymerase (PARP) domain (Kerns et al., 2008). Whilst antiviral activity has been ascribed to both isoforms, ZAP-L is more active against some viruses (Bick et al., 2003; Gao et al., 2002; Li et al., 2017; Zheng et al., 2017). Upon overexpression, ZAP-L restricts EBOV trVLP more potently than ZAP-S, and we find that only ZAP-L coprecipitates with TRIM25 and NP. Overexpression of a rat ZAP has been previously shown to have an antiviral activity against EBOV, by blocking the translation of the L mRNA (Muller et al., 2007). While we also see an effect on both L mRNA and protein expression upon ZAP overexpression in our assays, this is also observable in TRIM25 KO cells where ZAP has no antiviral activity, in contrast with the impact of ZAP overexpression on EBOV genomic RNA levels which occurs in a TRIM25-dependent manner. Moreover, the TRIM25/ZAP-mediated block induced by IFN-I does not affect the expression of any viral protein expressed *in trans* and ZAP activity is modulated by the CpG content in *Renilla*, suggesting that ZAP is targeting the viral genome rather than just blocking the synthesis of L.

ZAP has been implicated in driving the evolution of RNA viruses towards suppression of their genomic CpG content (Fros et al., 2017; Takata et al., 2017). Most RNA viruses have a lower abundance of CpGs than would be expected by chance, and in the case of HIV-1, artificially increasing the CpG content in parts of the genome renders the virus sensitive to ZAP (Ficarelli et al, 2019; Odon et al., 2019; Takata et al., 2017). Evidence suggests ZAP directly binds to viral RNAs with high CpG content and promotes their degradation (Chiu et al., 2018; Takata et al., 2017). EBOV exhibits less CpG suppression than HIV (observed vs expected ratio of 0.5 compared to 0.2). However, if we change this CpG content in either the trVLP or monocistronic systems we modulate the viral sensitivity to ZAP, and in the case of the latter, enrich ZAP/RNA interactions. Since *RLuc* expression is not required for the trVLP propagation, this result implies that ZAP can target CpGs in the EBOV genome itself.

How TRIM25 activates ZAP remains unclear. TRIM25 interacts with and ubiquitinates ZAP, but the latter activity is not required for its cofactor activity (Li et al., 2017; Zheng et al., 2017). Our data showing that TRIM25 displaces NP from the genome shortly after entry and that ZAP binds the vRNA in a TRIM25-dependent manner raises the possibility that its role is to expose viral RNA rather than acting directly on ZAP itself. Importantly, through this TRIM25/ZAP axis, we show that the CpGs in the genome render EBOV sensitive to IFN-I. While both TRIM25 and ZAP are IFN-inducible, they are constitutively expressed in most cells and only increase modestly at the protein level upon IFN stimulation. Therefore, despite being essential effectors targeting EBOV trVLP replication, whether this increase in their expression fully explains the IFN-regulated antiviral activity, or whether other IFN-inducible components are required needs further study (Kuroda et al. 2020).

Our results indicate that TRIM25 may target the structure of the EBOV (and perhaps other negative strand RNA virus) vRNP in a manner analogous to antiviral restriction by other mammalian proteins. While we see no evidence of TRIM25-dependent NP degradation, TRIM25 does appear to displace it from the viral RNA, which would likely dysregulate viral transcription and RNA replication. Similar to rhesus TRIM5 and HIV CA, as well as TRIM21 and its antibody opsonised targets (Fletcher et al., 2015; James, 2014), we see evidence of NP ubiquitination. While this correlates with antiviral activity, we do not yet know whether that is itself essential. TRIM25 forms an antiparallel dimer through its coiled-coil domain (Sanchez et al., 2014) and can then further assemble into multimers through RING domain dimerization. This positions the RING moieties at either end of the dimer, with the ligand-binding PRYSPRY located more centrally, either side of the coiled-coil. To act as an E3 ligase the TRIM25 RING domain must also dimerize, which can only happen through association with another TRIM25 dimer. This has been demonstrated to be facilitated by the binding of the PRYSPRY domain to one of its cognate ligands, the RIG-I 2CARD, generating the catalytically active domain that can interact with E2 ligases (Sanchez et al., 2016). Thus, TRIM25 is only active as a multimer of dimers when bound to its target. Two possibilities exist for the conformation of these multimers from the current structural studies of TRIM25; either two TRIM25 dimers multimerize into a closed dimer of dimers, or end-to-end multimerization of RING domains could lead to extended polymers of TRIM25 (Sanchez et al., 2016). We find evidence that TRIM25 interaction with NP depends on its PRYSPRY domain. Antiviral activity, however, was blocked by mutations that impair RING dimerization as well as catalytic activity, suggesting that multimerization of TRIM25 on the EBOV vRNP is also essential.

Since this is a helical ribonucleoprotein complex, it is possible that end-to-end multimers of TRIM25 could form over such a structure, driving its disassembly, and thus recruit other RNA-directed antiviral factors and sensors.

Several studies have suggested that TRIM25 is an RNA-binding protein itself and that this is important for the activation of the E3 ligase activity. Two RNA binding sites have been identified. A tyrosine-rich segment of loops 2 and 3 of the PRYSPRY domain has been shown to bind the Let7 miRNA both *in vitro* and *in cellulo*, and CLIP analyses has revealed many cellular TRIM25-associated RNAs with a preference for G-rich regions (Choudhury et al., 2017). A second domain, a basic patch in the unstructured region that links the coiled coil to the PRYSPRY, had also been shown to bind RNA *in vitro* (Sanchez et al., 2018). In both cases, RNA-binding has been shown to promote E3 ligase activity *in vitro*, and mutation of these sites has been shown to block the substrate ubiquitination. It is unknown whether both domains are functionally independent, or whether their mutation have effects other than RNA-binding on TRIM25 substrate recognition. Interestingly, in the case of EBOV restriction we find distinct phenotypes for either site. Mutation of the PRYSPRY RBD loses antiviral activity and NP ubiquitination, but retains NP interaction consistent with this being RNAse insensitive. Mutation of the basic patch (7KA) similarly loses antiviral activity, but unlike the RBD deletion, also loses NP interaction similar to a full PRYSPRY deletion. Given that the basic patch lies within a linker between the coiled-coil and the PRYSPRY, it is possible that such a change may affect the spacing and positioning of the PRYSPRY relative to the coiled-coil for multimeric substrate engagement, as is well-known for other TRIM-family members. The implication of RNA-binding in TRIM25's antiviral mechanism is attractive in the light of our data that shows that it can dissociate NP from the genome even when transcription is inhibited. Cryo-EM structures of the EBOV vRNP show RNA tightly wound around helical NP assemblies, with each protomer engaging 6bp of RNA (Su et al., 2018; Wan et al., 2017). The RNA is clamped into a cleft, reducing its accessibility to cellular factors. In such a configuration, TRIM25 would have to interact with NP to access the vRNA, which is consistent with our mutagenesis data. Recent studies have shown that nuclear TRIM25 associates with influenza virus vRNPs to block transcriptional elongation (Meyerson et al., 2017). While there are differences in these studies taken together, these observations raise the possibility that TRIM25 may have a broad direct antiviral activity against negative-strand RNA viruses with helical vRNPs. More

widely, these data also suggest that TRIM25 can act as a ZAP cofactor by disassembling RNA/protein structures to expose CpG-rich RNAs.

Further to their direct antiviral restriction, several TRIMs ligand-induced synthesis of K63 polyubiquitin chains act as platforms for the activation of TAK1 and subsequently NFkB-dependent proinflammatory gene expression (Fletcher et al., 2015; Pertel et al., 2011). TRIM5 acts effectively as a pattern recognition receptor for the hexameric array of retroviral capsids, and TRIM21 for antibody-bound microbes entering the cytoplasm. This therefore raises the question of whether the “classical” cytoplasmic sensing mechanisms themselves are linked to a direct virus restriction. The requirement for MAVS in TRIM25/ZAP-mediated restriction of EBOV replication would suggest that this may be the case for the cytoplasmic RNA sensing pathway. Intriguingly, we find that both isoforms of MAVS are required. Since signalling through MAVS is not required for the direct antiviral activity, we suggest that it may act as a regulatory part of the complex. MAVS localizes primarily to mitochondrial associated membranes and peroxisomes, and as such forms a platform for RNA sensing via RIG-I and MDA5, and we suggest that this platform may also allow the recruitment of directly acting antiviral factors, as well as a link to the ultimate disposal of viral components by the cell. Various studies have linked MAVS, and its functional paralogue in DNA sensing, STING, to autophagic degradation upon activation (Liu et al., 2018; Zhao et al., 2012).

TRIM25 is a common target for antagonism by RNA viruses. Influenza A virus NS1 blocks TRIM25 activity to disable RIG-I in infected cells (Gack et al., 2009), whereas dengue virus encodes a subgenomic RNA that functions analogously (Manokaran et al., 2015). We see no evidence of a direct counteractivity for human TRIM25 encoded by EBOV. VP24, which blocks signalling from IFNAR1/2, prevents the upregulation of ISGs after IFN-I exposure. In cells already exposed to IFN-I at the time of infection, VP24 would not be expected to have any effect, and in any case is encoded by the trVLP. VP35, is expressed *in trans* in the trVLP system and counteracts RIG-I and protein kinase R (PKR) but has no known activity to inhibit TRIM25 (Basler, 2015). However, humans are not the virus’ natural host, and it is possible that filoviruses do have a countermeasure/resistance mechanism to TRIM25/ZAP in other mammals, particularly putative bat reservoir species. Interestingly, adaptation of EBOV to infection of both mice and guinea pigs is associated with amino acid changes in NP. Furthermore, lethality of mouse adapted EBOV in C57BL/6 mice requires the knockout of *mavs* (Dutta et al., 2017). Whilst this has been interpreted to be due to enhanced RNA sensing, given our

observations that both MAVS isoforms are required for TRIM25/ZAP-mediated antiviral activity, it is also possible that differences in direct restriction of the vRNP underlie this species-specific tropism. Both ZAP and TRIM25 are under high levels of positive selection in mammals, suggesting a continuous adaptation to new viral pathogens (Kerns et al., 2008).

In summary, our studies have revealed that TRIM25 and ZAP are major contributors to an IFN-induced restriction of EBOV replication. We provide evidence that TRIM25 directly associates with the incoming vRNP and dissociates NP from the genome. These data further suggest TRIM25 as a key restriction factor for EBOV, and that its role is to expose CpG rich areas of the viral genome to ZAP, which could then degrade or inhibit translation of the viral RNAs.

Material and Methods

Cell lines

HEK293T and U87-MG cells were obtained from ATCC. HEK293T-TIM1 and U87-MG-TIM1 cells were produced by transduction of the parental cell lines with a MLV-based lentiviral vector packaging a pCMS28 vector genome (Gallois-Montbrun et al., 2007) encoding the TIM1 construct, and selecting the cells in puromycin. Alternatively, some of the CRISPR KO cell lines (described below) were derived to stably express TIM1 by transduction with a MLV-based retroviral vector packaging a pLHCX (Clontech) vector genome encoding TIM1, and selecting in hygromycin. All cells used on this study were maintained in high glucose DMEM supplemented with GlutaMAX, 10% fetal bovine serum (FBS), 20µg/mL gentamicin, and incubated at 37^{o}C with 5% CO_2.

Generation of CRISPR Knock-Out cell lines

CRISPR guides targeting *E.coli* LacZ gene, or human TRIM25, ZAP, RIG-I, FL-MAVS, FL-MAVS/ miniMAVS, TBK1 and KHNYN genes were cloned into *BsmBI* restriction enzyme sites in the lentiviral CRISPR plasmid lentiCRISPRv2 (Addgene). LentiCRISPR VLPs were produced on HEK293T cells seeded on a 10cm dish, and transfected with 8µg of lentiCRISPRv2-Guide, 8µg of pCRV1-HIV-Gag Pol (Neil et al., 2008) and 4µg of pCMV-VSV-G (Neil et al., 2008). Supernatants were harvested 48

hours later and used to transduce HEK293T or U87-MG cells, followed by selection in puromycin. Furthermore, MAVS isoforms expression were rescued on HEK293T FL-MAVS & miniMAVS CRISPR DKO by transduction with a MLV-based lentiviral vector packaging a pCMS28 vector genome encoding CRISR-resistant MAVS (MAVS^{CR}), miniMAVS (MAVS M1A^{CR}) or FL-MAVS (MAVS M142A^{CR}) constructs, and selecting cells in Blasticidin.

Additionally, the CRISPR guide targeting NPC1 gene was cloned into lentiCRISPR_v2_GFP as above (Addgene). The generated plasmid was transfected into HEK293T-TIM1 cells, which were subsequently sorted by flow cytometry, on a BD FACSCantoII, on the basis of their GFP expression. Finally, NPC1 expression was rescued on these HEK293T NPC1 CRISPR KO-TIM1 cells by transduction with a MLV-based lentiviral vector packaging a pCMS28 vector genome encoding NPC1 construct, and selecting the cells in Blasticidin to generate the HEK293T NPC1 CRISPR KO-TIM1 + NPC1 cell line.

All CRISPR guides sequences are in Table S2.

Generated Plasmids

TRIM25wt, TRIM25 ΔRING and TRIM25 ΔSPRY were PCR amplified from the ISG library plasmid pcDNA-DEST40-TRIM25 (Kane et al., 2016) using forward and reverse primers encoding 5' overhangs with, respectively, *EcoRI* and *XhoI* restriction sites. Purified amplification products were then inserted into the corresponding sites on a pcDNA3.1 backbone. pcDNA3.1-TRIM25 ΔRINGΔSPRY was generated by PCR amplification using pcDNA3.1-TRIM25 ΔRING as template and sub-cloning the PCR product into pcDNA3.1 backbone as above.

pcDNA3.1-TRIM25wt CR (CRISPR-resistant) was generated by overlapping PCR from pcDNA3.1-TRIM25wt, using internal primers that inserted silent mutations on the CRISPR-guides target sequence and the above mentioned TRIM25 ORF flanking forward and reverse primers with *EcoRI* and *XhoI* restriction sites as 5' overhangs. pcDNA3.1-TRIM25wt CR was used as template for all CRISPR-resistant TRIM25 mutants used on this study. These mutants were generated, unless otherwise mentioned, by overlapping PCR using internal primers that inserted silent mutations, and the above mentioned forward and reverse primers encoding 5' overhangs with *EcoRI* and *XhoI* restriction sites. TRIM25 L7A CR was generated by PCR amplification of TRIM25wt CR with L7A_CR_Fwd primer with a 5' *EcoRI* overhang and the above mentioned TRIM25_*XhoI* Rev primers.

Purified amplification products were then inserted into the corresponding sites on a pcDNA3.1 backbone.

pCMS28-Blast-MAVS^{CR} was constructed by overlapping PCR from pCR3.1-MAVS (Pertel et al. 2011), using internal primers that inserted a silent mutation in the NGG PAM of the CRISPR guide target sequence alongside forward and reverse primers encoding 5' overhangs with *NotI* and *XhoI* restriction sites respectively. pCMS28-Blast-MAVS^{CR} was then used as a template and backbone for the MAVS CRISPR resistant plasmids used in this study. pCMS28-Blast-M142A^{CR}, expressing only the FL-MAVS isoform, was created by overlapping PCR from pCMS28-Blast-MAVS^{CR} using internal primers substituting the methionine for an alanine at position 142, in conjunction with the above mentioned forward and reverse primers with *NotI* and *XhoI* 5' overhangs. Furthermore, pCMS28-Blast-M1A^{CR} was created by PCR amplification using forward and reverse primers encoding 5' overhangs with *NotI* and *XhoI* restriction sites respectively, where the forward primer also encoded for a mutation in the first methionine thus disrupting the expression of the FL-MAVS isoform. Amplified DNA fragments were then inserted into the pCMS28-Blast backbone digested with *NotI* and *XhoI*.

pCMS28-TIM1 was generated by sub-cloning the product of pCAGGS-TIM1 digestion with *EcoRI* and *NotI* enzymes into the corresponding sites in pCMS28 backbone. Additionally, pCAGGS-TIM1 served also as template for the PCR amplification of TIM1, and the product inserted into *XhoI* and *NotI* sites on pLHCX backbone to generate pLHCX-TIM1.

Finally, pBABE-NPC1 (Carette et al., 2011) served as template for the PCR amplification of NPC1, and the PCR product was digested with *EcoRI*/*XhoI* and inserted into the corresponding restriction sites in pCMS28-Blasticidin to generate pCMS28-Blast-NPC1.

All primers used for cloning are described on Table S3.

To generate p4cis-vRNA-CpG low RLuc we have synthesised a 2141nt-long DNA fragment (sequence available upon request), with 61 silent mutations that removed all CpG dinucleotides present in the *Renilla* luciferase gene of the p4cis-vRNA-RLuc sequence. This DNA fragment was digested with *ApaI* and *BlpI* and inserted into the corresponding sites in the original p4cis-vRNA-RLuc minigenome plasmid. On the other hand, the monocistronic plasmid pT7-1cis-vRNA-CpG low-EBOV-

hrluc expressing a Renilla luciferase with no CpG's was constructed by overlapping PCR using p4cis-vRNA-CpG low as template. Briefly, two fragments were amplified by PCR with the primers P4 cis Low CpG TRAIL F and P4 cis vRNA *XmaI* R (size 793bp) and P4 cis Low CpG TRAIL R and P4 cis vRNA *BlpI* F (size 1626bp). These DNA fragments were joined together by PCR using the outer primers with the *BlpI* and *XmaI* restriction sites in their 5' overhangs, digested with these enzymes and cloned into the pT7-1cis-vRNA-EBOV-hrluc plasmid to create a low CpG renilla monocistronic EBOV plasmid.

Ebola transcription- and replication-competent virus-like particle (trVLP) assays

Unless otherwise stated, EBOV trVLPs (Watt et al., 2014) were produced in HEK293T producer cells (also called p0 cells) seeded in a 10 cm dish, and transfected with 625ng of pCAGGS-NP, 625ng of pCAGGS-VP35, 375ng of pCAGGS-VP30, 5µg of pCAGGS-L, 400ng of p4cis-vRNA-Rluc (or corresponding CpG low variant of this minigenome), and 250ng of pCAGGS-T7, using TransIT-LT1 transfection reagent. Medium was exchanged 4-6 hours post-transfection, and trVLP-containing supernatants were harvested 48-72 hours later and cleared by centrifugation for 5 minutes at 300xg. Typically, 5 to 50µl of cleared supernatants were transferred to p1 target cells that had been seeded on 24-well plates, and transfected 24 hours previously with 31.25ng of pCAGGS-NP, 31.25ng of pCAGGS-VP35, 18.75ng of pCAGGS-VP30, 250ng of pCAGGS-L (or pCAGGS-L-HA where mentioned) and 5ng of pFluc per well. In specific experiments, cells were also co-transfected at this stage with 125ng of the ISG of interest. Furthermore, if p1 target cells were not stably expressing TIM1, they were additionally co-transfected with 62.5ng of pCAGGS-TIM1 per well. Medium was changed 4-6 hours post-transfection and, in experiments performed either with interferons or T705 (Favipiravir), increasing amounts of universal IFN-I, IFN alpha 2a, IFN beta 1a (PBL Interferon Source) or T705 (AdooQ) were added to the cells at this stage. Cells were infected the following day and medium was again changed 4-6 hours after infection of p1 target cells, and 24 hours later cells were lysed with Passive Lysis 1x and reporter activities measured with Dual Luciferase Reporter Kit (Promega). At the same time supernatants from p1 cells were cleared by centrifugation and passaged onto fresh HEK293T-TIM1 p2 target cells, seeded in 24-well plates and transfected 24 hours earlier exclusively with the EBOV RNP components and pFluc (same quantities as above). These cells were lysed 24 hours post infection and reporter activities measured as already described.

Specific experiments required the use of concentrated EBOV trVLPs. For that purpose trVLPs were produced as above, and treated for 2 hours with 10U/ml DNase-I (Roche) before being concentrated by ultracentrifugation through a 20% sucrose/PBS cushion (28,000 rpm on a Sorvall Surespin rotor, for 90 min at 4^{o}C), and resuspended overnight in serum-free DMEM medium.

ISG Screen

ISG screen was conducted on HEK293T-TIM1 cells in a 96-well plate format, using a library of human ISGs encoded by pcDNA-DEST40 (Kane et al., 2016). 50ng of individual ISG-expressing plasmids were co-transfected onto p1 target cells together with EBOV RNP expressing plasmids and pFluc, as described above in the trVLP assay. p1 target cells were infected with EBOV trVLPs 24 hours post-transfection and medium changed 4 hours later. 24 hours post-infection the cells were lysed with Passive Lysis 1x and reporter activities measured with Dual Luciferase Reporter Kit. At the same time supernatants from p1 cells were used to infect fresh HEK293T-TIM1 p2 target cells, seeded in 96-well plates and transfected 24 hours earlier exclusively with the EBOV RNP components (as described above). These cells were lysed 24 hours post infection and reporter activities measured as already previously described. For each ISG, the yield of infectious virions was expressed as a percentage of the mean value across each library plate.

Ebola monocistronic genome assays

VLPs carrying the monocistronic EBOV genomes were produced in HEK293T cells seeded in 10cm dishes, and transfected with 625ng of pCAGGS-NP, 625ng of pCAGGS-VP35, 375ng of pCAGGS-VP30, 300ng of pCAGGS-VP24, 5µg of pCAGGS-L, 1.25µg of pCAGGS-VP40, 1.25µg of pCAGGS GP, 1.25µg of pCAGGS-T7, 1.25µg of pT7-1cis-vRNA-EBOV-hrluc (or corresponding CpG low variant) and 125ng of pFLuc, using TransIT-LT1 transfection reagent. Medium was exchanged 4-6 hours post-transfection and supernatants harvested 72 hours later as described before. Experiments with these monocistronic VLPs were performed following the same proceeding described above for the EBOV trVLPs.

Nanoluciferase experiments

EBOV trVLPs were produced containing a minigenome that encoded Nanoluciferase rather than Renilla luciferase using the protocol previously described for EBOV trVLP production under section heading Ebola transcription- and replication-competent virus-like particle (trVLP) assays. Target cells were plated in a 96 well format and spinfected with 200µl of cleared p0 supernatant the next day. Cells were then washed three times in medium 6 hours after infection. Cells were lysed with passive lysis buffer 48 hours after infection and reporter activity was then measured with a Nano-Glo luciferase assay system (Promega). For IFN-I based experiments increasing amounts of IFN-I were added 16 hours before infection and for TRIM25 overexpression experiments cells were reverse transfected with either TRIM25 or YFP as well as TIM1 24 hours before infection.

Reporter Gene Assays

For transient reporter gene assays, HEK293T cells were seeded on 24-well plates and transfected with 100ng of control pcDNA-DEST40-GFP or pcDNA-DEST40 expressing individual ISG of interest in combination with 10ng of 3xkB-pCONA-Fluc (Mankouri et al., 2010), or pTK-ISG56-Luc (kindly provided by Greg Towers, UCL), or pNL(NlucP/ISRE/Hygro) (Promega) luciferase reporters and 10ng of pCMV-RLuc (Mankouri et al., 2010). Cells were lysed with 1x Passive Lysis buffer 24 or 48 hours post-transfection, and Firefly and Renilla luciferase activities in the lysates were measured using a dual luciferase kit (Promega).

Influenza A Minigenome Assay

Influenza A polymerase activity was determined using a minigenome reporter containing the Firefly luciferase gene in a negative sense, flanked by the non-coding regions of the influenza NS gene segment transcribed from a species-specific pol I plasmid with a mouse terminator sequence (Moncorge et al., 2010; Pleschka et al., 1996). Each viral polymerase component was expressed from separate pCAGGS plasmids encoding A/H1N1/Eng/195 NP, PA, PB1 and PB2 (Moncorge et al., 2013). To analyse polymerase activity, HEK293T LacZ, HEK293T RIG-I CRISPR and HEK293T ZAP CRISPR cells were seeded in 24-well plates 24 hours prior transfection with 10ng PB1, 10ng PB2, 5ng PA, 15ng NP, 10ng pHPMO1-Firefly, 2.5ng pCAGGS-Renilla (transfection control, (Cauldwell et al., 2013) and increasing amounts of pcDNA3.1-TRIM25 using Trans-IT LT1. Cells were lysed 24

765 hours post-transfection with 1x Passive Lysis and reporter activities measured using a dual luciferase
766 kit (Promega).
767
768 **Lentiviral Assay**
769 HIV-based lentiviral VLPs expressing GFP were produced on HEK293T cells seeded on a 10cm dish,
770 and transfected with 6µg of pHR' Sin CSGW (Demaison et al., 2002), 4 µg of pCRV-HIV Gag Pol and
771 2µg of pCMV-VSV-G using TransIT-LT1. Medium was changed 4-6 hours post transfection and VLP-
772 containing supernatants harvested 48 hours later and cleared by centrifugation (5 minutes, 1200rpm).
773 U87-MG LacZ CRISPR control and U87-MG TRIM25 CRISPR KO cells were treated overnight with
774 increasing amounts of IFN-I and then transduced with a fixed amount of pCSGW-HIV GP-VSVG
775 VLPs prepared as above. 48 hours post-transduction cells were harvested and analysed for GFP
776 expression by flow cytometry.
777
778
779 **Blam Assay**
780 Ebola BlamVP40-Ebola GP and Ebola BlaVP40-VSVg VLPs were produced on HEK293T cells. For
781 that purpose, cells were plated in 10cm dishes and transfected with 6µg of pcDNA3.1-EBOV BlaVP40
782 (Tscherne and Garcia-Sastre, 2011) and 15µg of either pCAGGS-Ebola GP (Long et al., 2015) or
783 pCMV-VSVG using PEI max, and media was changed to OptiMEM 4-6 hours post-transfection.
784 Supernatants were harvested past 48 hours and cleared by centrifugation (5 minutes, 1500rpm)
785 before storage.
786 HEK293TIM-1 cells pre-treated with IFN-I, or transfected with either GFP or TRIM25, were 24 hours
787 later transduced with Blam VLPs prepared as above, and incubated for 3-5 hours. After incubation
788 cells were washed once with RPMI 1640 (no phenol red) medium (RPMI), and incubated in 1x loading
789 solution of LiveBLAzer FRET-B/G Loading Kit (Life Technologies) with CCF2-AM for 1 hour (dark,
790 room temperature). Following, cells were washed with 2.5mM Probenecid (Sigma) in RPMI and
791 incubated in the same medium overnight (dark, room temperature). Next day, cells were analyzed by
792 flow cytometry using BD FACSCanto II. Cells were gated on live cells and analyzed for CCF2
793 cleavage as readout for Blam VLP entry with Pacific Blue (cleaved) and FITC (not cleaved) laser
794 channels, and using FlowJo 10.4.2 software for analysis.

Production and Purification of anti-EBOV antibodies

Rabbit antibodies against Ebola virus proteins NP, VP35 and VP30 were produced by Lampire Biological Laboratories using their standard protocol. In brief, two rabbits per each viral peptide were immunized with 0.50mg of antigen mixed with 0.5ml of Complete Freund's adjuvant. Two further boosts were performed in the same conditions at days 21 and 42. Serums used in this manuscript were collected by day 50. The sequences of the viral protein peptides used in the immunizations are as follow:

NP: DEDDEDTKPVPNRSTKGGQ

VP35: EAYWAEHGQPPPGPSLYEE

VP30: QLNITAPKDSRLANPTADD

For microscopy staining of the Ebola NP protein (see below), we have purified a fraction of the serum collected from rabbits immunized with the viral NP peptide. For that purpose, protein A beads (Invitrogen) were equilibrated by washing them with PBS, and then incubated with the serum for 2 hours at room temperature. Following, the beads were added into a column cartridge and washed 3 times with 10ml of PBS. IgGs were then eluted with 0.1M Glycine pH 3.5 in 5 batches of 1ml. IgG eluates were adjusted to pH 7.0 with 2M Tris Base, pH 9.0, and concentrated on Amicon Ultra centrifugal filter units (MWCO 10kDa) (SIGMA) with buffer exchanged to PBS. Approximate concentration of purified antibodies was determined by spectrometry (280nm) and fragments analyzed on SDS-PAGE.

Analysis of cellular and viral proteins expression

Cells used in this study were seeded on 24-well plates, and transfected the following day with EBOV RNP-expressing plasmids as described above, either in combination with 150ng of individual ISG-expressing plasmids per well or followed by the addition 4 hours post-transfection of increasing amounts of type-I interferon. 24 hours later cellular lysates were subjected to SDS-PAGE and western blots performed using mouse monoclonal antibodies anti-HSP90 (Santa Cruz), anti-HA (Covance) or anti-TRIM25 (Abcam), or rabbit antibodies anti-EBOV NP, anti-EBOV VP35, anti-EBOV VP30, anti-TRIM25 (Abcam), anti-RIG-I (Enzo), anti-MAVS/VISA (Bethyl), anti-TBK1 (Abcam), anti-ZCCHV/ZAP

(Abcam) or anti-NPC1 (Thermo Fisher). Visualizations were done by Image-Quant using either HRP-linked anti-mouse or anti-rabbit secondary antibodies (Cell Signaling).

Immunoprecipitations

To address the interaction of TRIM25 with EBOV-NP proteins cells were seeded in 6-well plates and transfected with 500ng of either pcDNA3.1-GFP or pcDNA3.1-TRIM25wt, or mutants thereof, in combination with 125ng of pCAGGS-NP and/or 125ng of pCAGGS-VP35. At 24 hours post-transfection cells were lysed with a RIPA buffer containing 50mM Tris-HCl (pH 7.4), 150mM NaCl, 0.1% SDS, 0.5% sodium deoxycholate, 1% NP-40 and protease inhibitors (Roche). Following sonication, lysates were immunoprecipitated overnight with either rabbit anti-TRIM25 (Abcam) or rabbit anti-EBOV NP antibodies and protein G beads at 4^{o}C on a tube rotator. On specific experiments, cellular lysates were treated prior immunoprecipitation with 10µg/ml of RNAseA (SIGMA) for 2 hours at 37^{o}C.

For ubiquitination-related pull-downs cells were plated similarly in 6-well plates and transfected with 500ng of either pcDNA3.1-GFP or pcDNA3.1-TRIM25wt, in combination with 125ng of pCAGGS-VP35, 90ng of pCAGGS-VP30 and 1.2µg pCAGGS-L together with 125ng of pCAGGS-NP and/or 100ng of pMT123-HA-Ub (Treier et al., 1994). At 24 hours post-transfection cells were lysed with a buffer containing 50mM Tris-HCl (pH 7.4), 150mM NaCl, 5mM EDTA, 5% Glycerol, 1% Triton-X 100, 10mM N-Ethylmaleimide (NEM) and protease inhibitors. Lysates were treated as above and immunoprecipitated overnight either with rabbit anti-EBOV-NP or mouse anti-HA (Covance).

Cell lysates and pull-down samples were subjected to SDS-PAGE and Western blots performed using antibodies against HSP90 (Santa Cruz), TRIM25 (Abcam), EBOV-NP, EBOV-VP35, HA-tag (Rockland) and ZAP (Abcam). Blots were visualized by ImageQuant using anti-mouse or anti-rabbit HRP-linked antibodies (Cell Signaling).

RNA Immunoprecipitation

Cells were plated on 10cm dishes and transfected in the absence of EBOV RNP expressing plasmids with 2.5µg of pcDNA3.1-GFP, pcDNA3.1-TRIM25wt (or mutants thereof), or pcDNA4-ZAP-L (Kerns et al., 2008) and medium changed 4-6 hours later. Alternatively, cells were treated overnight with 1000U/ml of IFN-I or 250µM of T705. The following day cells were infected for 3 hours with 3ml of

wild-type- or CpG low-EBOV trVLPs, or alternatively with the same volume of EBOV monocistronic VLPs, and then gently washed in PBS prior to 'on dish' irradiation with 400mJ/cm2 using a UV Stralinker 2400. Cells were subsequently lysed in 1ml of RIPA buffer (see above for composition) and sonicated. Cleared lysates were immunoprecipitated overnight at 4^{o}C with rabbit anti-EBOV NP or rabbit anti-ZAP antibodies and protein G beads. Following 3 washes with RIPA buffer, the beads were resuspended in 200µl of RIPA and boiled for 10min to decouple protein/RNA complexes from the beads. Finally, input and pulldown samples were incubated with proteinase K (Thermo Fisher, 2mg/ml) for 1hr at 37^{o}C, and then boiled for 10 minutes to inactivate the enzyme. Samples were stored at -20^{o}C for downstream processing.

RNA Purification and Quantitative RT-PCR

Total RNA was isolated and purified from EBOV trVLP infected cells using a QIAGEN RNAeasy kit, while viral RNA was extracted from supernatants using a QIAGEN QIAmp Viral mini kit, both accordingly with the manufacture instructions. Unless otherwise stated, 50ng of purified RNA was reverse transcribed by random hexamer primers using a High Capacity cDNA Reverse Transcription kit (Applied Biosystems). Alternatively, strand-specific reverse transcription primers were used to generate cDNAs for viral genomic RNA (-vRNA, EBOV -vRNA RT primer), complementary RNA (+cRNA, EBOV +cRNA RT primer), or viral mRNA (oligo dT). Of the reaction, 5µl were subjected to quantitative PCR using primer/probe sets for human *Gapdh* (Applied Biosystems), and EBOV trVLP 5'-trailer region, L-Pol RNA or VP40 RNA (primer/probe sequences in Table S4). Quantitative PCRs were performed on a QuantStudio 5 System (Thermo Fischer) and absolute quantification data analyzed using Thermo Fisher's Cloud Connect online software.

Input and pulldown samples from RNA immunoprecipitations were first resuspended in QIAzol (QIAGEN), and passed through QIAshredder columns (QIAGEN) for homogenization, and then passed to phase lock gel tubes (VWR) prior to addition of chloroform (SIGMA). After manually shaking the tubes, samples were centrifuged full-speed, for 15min at 4^{o}C. The aqueous phase was passed to a new tube, and isopropanol added. After 10 minutes at room temperature, tubes were centrifuged as before and supernatants removed. RNA pellets were subsequently washed with 75% Ethanol, and span at 7500xg, for 5 minutes at 4^{o}C. Following aspiration of the supernatants, RNA

884 pellets were left to dry and then resuspended in RNAse-free water. Downstream processing for
885 reverse transcription and quantitative RT-PCR was done as detailed above.
886
887 **Deubiquitinase Assays**
888 Prior to the deubiquitinase reactions, immunoprecipitations were performed using similar conditions to
889 the ones described above for ubiquitination-related pull-downs. Briefly, HEK293T TRIM25 CRISPR
890 KO cells were plated in 6 well plates and transfected with 500ng of either pcDNA3.1-YFP or
891 pcDNA3.1-TRIM25^{CR} in combination with 125ng of pCAGGS-VP35, 90ng of pCAGGS-VP30, 1.2µg of
892 pCAGGS-L and 125ng of pCAGGS-NP, in the absence of ectopically expressed ubiquitin. Cells were
893 lysed 48 hours post-transfection and lysates immunoprecipitated overnight with rabbit anti-EBOV-NP
894 antibody using protein G agarose beads. Following immunoprecipitation, beads were treated with
895 UbiCREST Deubiquitinase Enzyme Kit (BostonBiochem) following manufacturer's instructions. Briefly,
896 beads were washed several times before being equally split into separate tubes and treated with
897 either USP2 or left untreated (NTC, non-treated control), for 30 minutes at 37^{o}C. Input lysates and
898 pull-down beads were subjected to SDS-PAGE and Western blots performed using antibodies against
899 HSP90 (Santa Cruz), TRIM25 (Abcam) and EBOV-NP. Blots were visualized by ImageQuant using
900 anti-mouse or anti-rabbit HRP-linked antibodies (Cell Signaling).
901
902 **Microscopy**
903 Cells were seeded on 24-well plates on top of coverslips pre-treated with poly-L-lysine to improve
904 their adherence. For transient assays, cells were transfected with different combinations of EBOV
905 RNP plasmids using the amounts described previously. Alternatively, cells were infected with 30µl of
906 concentrated EBOV trVLPs in the absence of ectopically expressed EBOV RNP components.
907 Cells were fixed 24 hours post-transfection, or 3 hours post-infection, with 4% paraformaldehyde for
908 15 minutes at room temperature, and then washed first with PBS, followed by a second wash with
909 10mM Glycine. Next, cells were permeabilized for 15 minutes with a PBS solution complemented with
910 1% BSA and 0.1% Triton-X. Subsequently, cells were stained with mouse anti-TRIM25
911 (Abcam,10µg/ml) and purified rabbit anti-EBOV NP (1:50) antibodies diluted in PBS/0.01% Triton-X
912 for an hour at room temperature. Cells were washed 3 times in PBS/0.01% Triton-X, followed by an
913 incubation with Alexa Fluor 594 anti-mouse and Alexa Fluor 488 anti-rabbit antibodies (Molecular

Probes, 1:500 in PBS/0.01% Triton-X) for 45 minutes in the dark. Finally, coverslips were washed once again 3 times with PBS/0,01% Triton-X and then mounted on slides with Prolong Diamond Antifade Mountant with DAPI (Invitrogen). Imaging was performed on a Nikon Eclipse Ti Inverted Microscope, equipped with a Yokogawa CSU/X1-spinning disk unit, under 60-100x objectives and Laser wavelengths of 405nm, 488nm and 561nm. Image processing and co-localization analysis was performed with NIS Elements Viewer and Image J (Fiji) software.

Statistical Analysis

Statistical significance was determined using paired two-tailed t tests calculated using the Prism software. Significance was ascribed to p values as follows: *p > 0.05, **p > 0.01, and ***p > 0.001. Data relative to viral based assays, signalling reporter assay and Blam assays were performed in duplicate in at least 3 independent experiments, and error bars represent +/-SEM.

For RNA IP experiments each data point is represented as average of three independent experiments +/-SD.

Contact for Reagents and Resources Sharing

Further information and requests for resources and reagents should be directed to and will be fulfilled by the Lead Contact, Stuart J.D. Neil (stuart.neil@kcl.ac.uk). Distribution of the CRISPR cell lines, antibodies, EBOV p4cis-CpG low-vRNA-Rluc and pT7-1cis-vRNA CpG low-EBOV-hrluc minigenomes generated in the course of this work will require signing of Material Transfer Agreements (MTA) in accordance with policies of King's College London. All requests for other trVLP components should be directed to Thomas Hoenen (thomas.hoenen@fli.de).

Author Contributions

Conceptualization: RPG, HW, SJW, CMS, SJDN ; Methodology: RPG, HW, KLS, FD, BSB, DG, TH, SJW, CMS, SJDN; Investigation: RPG, HW, KLS, FD, BSB; Visualisation: RPG, HW, KLS, FD, CMS, SJDN; Supervision: SJDN; Project Administration: SJDN; Funding Acquisition: SJDN; Writing –

943 Original Draft: RPG, HW, SJDN; Writing - Review and Editing: RPG, HW, KLS, FD, TH, SJW, CMS,
944 SJDN

945

946 **Acknowledgments**

947 We thank other members of the Neil and Swanson laboratories for helpful discussions and Wendy S
948 Barclay (Imperial College London) for materials. We are grateful to Stefan Becker and his group for
949 advice. These studies were funded by an MRC Discovery Award MC/PC/15068 and a Wellcome Trust
950 Senior Research Fellowship (WT098049AIA) to SJDN, a Guy's and St Thomas's Charity Challenge
951 Fund grant to CMS and SJDN and MRC research grant MR/M019756/1 to CMS. This project has
952 received funding from the European Union's Horizon 2020 research and innovation programme under
953 the Marie Skłodowska-Curie grant agreement No. 750621 (KLS).

954

955 **Conflict of interests**

956 All authors declare no conflict of interests.

957

References

Amman, B.R., Nyakarahuka, L., McElroy, A.K., Dodd, K.A., Sealy, T.K., Schuh, A.J., Shoemaker, T.R., Balinandi, S., Atimnedi, P., Kaboyo, W., *et al.* (2014). Marburgvirus resurgence in Kitaka Mine bat population after extermination attempts, Uganda. Emerg Infect Dis *20*, 1761-1764.

Basler, C.F. (2015). Innate immune evasion by filoviruses. Virology *479-480*, 122-130.

Basler, C.F., Mikulasova, A., Martinez-Sobrido, L., Paragas, J., Muhlberger, E., Bray, M., Klenk, H.D., Palese, P., and Garcia-Sastre, A. (2003). The Ebola virus VP35 protein inhibits activation of interferon regulatory factor 3. J Virol *77*, 7945-7956.

Beachboard, D.C., and Horner, S.M. (2016). Innate immune evasion strategies of DNA and RNA viruses. Curr Opin Microbiol *32*, 113-119.

Bick, M.J., Carroll, J.W., Gao, G., Goff, S.P., Rice, C.M., and MacDonald, M.R. (2003). Expression of the zinc-finger antiviral protein inhibits alphavirus replication. J Virol *77*, 11555-11562.

Biedenkopf, N., Hartlieb, B., Hoenen, T., and Becker, S. (2013). Phosphorylation of Ebola virus VP30 influences the composition of the viral nucleocapsid complex: impact on viral transcription and replication. J Biol Chem *288*, 11165-11174.

Biedenkopf, N., Schlereth, J., Grunweller, A., Becker, S., and Hartmann, R.K. (2016). RNA Binding of Ebola Virus VP30 Is Essential for Activating Viral Transcription. J Virol *90*, 7481-7496.

Brubaker, S.W., Gauthier, A.E., Mills, E.W., Ingolia, N.T., and Kagan, J.C. (2014). A bicistronic MAVS transcript highlights a class of truncated variants in antiviral immunity. Cell *156*, 800-811.

Cadena, C., Ahmad, S., Xavier, A., Willemsen, J., Park, S., Park, J.W., Oh, S-W., Fujita, T., Hou, F., Binder, M., Hur, S. (2019). Ubiquitin-Dependent and -Independent Roles of E3 Ligase RIPLET in Innate Immunity. Cell 16;177(5):1187-1200.e16.

Cai, X., Chen, J., Xu, H., Liu, S., Jiang, Q.X., Halfmann, R., and Chen, Z.J. (2014). Prion-like polymerization underlies signal transduction in antiviral immune defense and inflammasome activation. Cell *156*, 1207-1222.

Cardenas, W.B., Loo, Y.M., Gale, M., Jr., Hartman, A.L., Kimberlin, C.R., Martinez-Sobrido, L., Saphire, E.O., and Basler, C.F. (2006). Ebola virus VP35 protein binds double-stranded RNA and inhibits alpha/beta interferon production induced by RIG-I signaling. J Virol *80*, 5168-5178.

Carette, J.E., Raaben, M., Wong, A.C., Herbert, A.S., Obernosterer, G., Mulherkar, N., Kuehne, A.I., Kranzusch, P.J., Griffin, A.M., Ruthel, G., *et al.* (2011). Ebola virus entry requires the cholesterol transporter Niemann-Pick C1. Nature *477*, 340-343.

Cauldwell, A.V., Moncorge, O., and Barclay, W.S. (2013). Unstable polymerase-nucleoprotein interaction is not responsible for avian influenza virus polymerase restriction in human cells. J Virol *87*, 1278-1284.

Chandran, K., Sullivan, N.J., Felbor, U., Whelan, S.P., and Cunningham, J.M. (2005). Endosomal proteolysis of the Ebola virus glycoprotein is necessary for infection. Science *308*, 1643-1645.

Chang, T-H., Kubota, T., Matsuoka, M., Jones, S., Bradfute, S.B., Bray, M., Ozato, K. (2009). Ebola Zaire virus blocks type I interferon production by exploiting the host SUMOS modification machinery. PLoS Pathog. Jun;5(6):e1000493.

Charron, G., Li, M.M., MacDonald, M.R., and Hang, H.C. (2013). Prenylome profiling reveals S-farnesylation is crucial for membrane targeting and antiviral activity of ZAP long-isoform. Proc Natl Acad Sci U S A *110*, 11085-11090.

Chiu, H.P., Chiu, H., Yang, C.F., Lee, Y.L., Chiu, F.L., Kuo, H.C., Lin, R.J., and Lin, Y.L. (2018). Inhibition of Japanese encephalitis virus infection by the host zinc-finger antiviral protein. PLoS Pathog *14*, e1007166.

Choudhury, N.R., Heikel, G., Trubitsyna, M., Kubik, P., Nowak, J.S., Webb, S., Granneman, S., Spanos, C., Rappsilber, J., Castello, A., *et al.* (2017). RNA-binding activity of TRIM25 is mediated by its PRY/SPRY domain and is required for ubiquitination. BMC Biol *15*, 105.

Cote, M., Misasi, J., Ren, T., Bruchez, A., Lee, K., Filone, C.M., Hensley, L., Li, Q., Ory, D., Chandran, K., *et al.* (2011). Small molecule inhibitors reveal Niemann-Pick C1 is essential for Ebola virus infection. Nature *477*, 344-348.

D'Cruz, A.A., Kershaw, N.J., Chiang, J.J., Wang, M.K., Nicola, N.A., Babon, J.J., Gack, M.U., and Nicholson, S.E. (2013). Crystal structure of the TRIM25 B30.2 (PRYSPRY) domain: a key component of antiviral signalling. Biochem J *456*, 231-240.

Deen, G.F., Broutet, N., Xu, W., Knust, B., Sesay, F.R., McDonald, S.L.R., Ervin, E., Marrinan, J.E., Gaillard, P., Habib, N., *et al.* (2017). Ebola RNA Persistence in Semen of Ebola Virus Disease Survivors - Final Report. N Engl J Med *377*, 1428-1437.

Demaison, C., Parsley, K., Brouns, G., Scherr, M., Battmer, K., Kinnon, C., Grez, M., and Thrasher, A.J. (2002). High-level transduction and gene expression in hematopoietic repopulating cells using a human immunodeficiency [correction of imunodeficiency] virus type 1-based lentiviral vector containing an internal spleen focus forming virus promoter. Hum Gene Ther *13*, 803-813.

Dutta, M., Robertson, S.J., Okumura, A., Scott, D.P., Chang, J., Weiss, J.M., Sturdevant, G.L., Feldmann, F., Haddock, E., Chiramel, A.I., *et al.* (2017). A Systems Approach Reveals MAVS Signaling in Myeloid Cells as Critical for Resistance to Ebola Virus in Murine Models of Infection. Cell Rep *18*, 816-829.

1051 Escudero-Pérez, B. and Muñoz-Fontela, C. (2019). Role of Type I Interferons on Filovirus
1052 Pathogenesis. Vaccines (Basel) Feb 20;7(1):22.
1053
1054 Ficarelli, M., Wilson, H., Galão, R.P., Mazzon, M., Antzin-Anduetza, I., Marsh, M., Neil, S.J.D.,
1055 Swanson, C.M. (2019). KHNYN is essential for the zinc finger antiviral protein (ZAP) to
1056 restrict HIV-1 containing clustered CpG dinucleotides. Elife Jul 9;8:e46767.
1057
1058 Fletcher, A.J., Mallery, D.L., Watkinson, R.E., Dickson, C.F., and James, L.C. (2015). Sequential
1059 ubiquitination and deubiquitination enzymes synchronize the dual sensor and effector
1060 functions of TRIM21. Proc Natl Acad Sci U S A *112*, 10014-10019.
1061
1062 Fros, J.J., Dietrich, I., Alshaikhahmed, K., Passchier, T.C., Evans, D.J., and Simmonds, P.
1063 (2017). CpG and UpA dinucleotides in both coding and non-coding regions of echovirus 7
1064 inhibit replication initiation post-entry. Elife *6*.
1065
1066 Gack, M.U., Albrecht, R.A., Urano, T., Inn, K.S., Huang, I.C., Carnero, E., Farzan, M., Inoue, S.,
1067 Jung, J.U., and Garcia-Sastre, A. (2009). Influenza A virus NS1 targets the ubiquitin ligase
1068 TRIM25 to evade recognition by the host viral RNA sensor RIG-I. Cell Host Microbe *5*, 439-
1069 449.
1070 Gack, M.U., Shin, Y.C., Joo, C.H., Urano, T., Liang, C., Sun, L., Takeuchi, O., Akira, S., Chen, Z.,
1071 Inoue, S.*, et al.* (2007). TRIM25 RING-finger E3 ubiquitin ligase is essential for RIG-I-mediated
1072 antiviral activity. Nature *446*, 916-920.
1073
1074 Gallois-Montbrun, S., Kramer, B., Swanson, C.M., Byers, H., Lynham, S., Ward, M., and
1075 Malim, M.H. (2007). Antiviral protein APOBEC3G localizes to ribonucleoprotein complexes
1076 found in P bodies and stress granules. J Virol *81*, 2165-2178.
1077
1078 Gao, G., Guo, X., and Goff, S.P. (2002). Inhibition of retroviral RNA production by ZAP, a
1079 CCCH-type zinc finger protein. Science *297*, 1703-1706.
1080
1081 Geisbert, T.W., Hensley, L.E., Larsen, T., Young, H.A., Reed, D.S., Geisbert, J.B., Scott, D.P.,
1082 Kagan, E., Jahrling, P.B., and Davis, K.J. (2003a). Pathogenesis of Ebola hemorrhagic fever in
1083 cynomolgus macaques: evidence that dendritic cells are early and sustained targets of
1084 infection. Am J Pathol *163*, 2347-2370.
1085
1086 Geisbert, T.W., Young, H.A., Jahrling, P.B., Davis, K.J., Larsen, T., Kagan, E., and Hensley, L.E.
1087 (2003b). Pathogenesis of Ebola hemorrhagic fever in primate models: evidence that
1088 hemorrhage is not a direct effect of virus-induced cytolysis of endothelial cells. Am J Pathol
1089 *163*, 2371-2382.
1090
1091 Goodier, J.L., Pereira, G.C., Cheung, L.E., Rose, R.J., and Kazazian, H.H., Jr. (2015). The Broad-
1092 Spectrum Antiviral Protein ZAP Restricts Human Retrotransposition. PLoS Genet *11*,
1093 e1005252.
1094
1095 Hayakawa, S., Shiratori, S., Yamato, H., Kameyama, T., Kitatsuji, C., Kashigi, F., Goto, S.,
1096 Kameoka, S., Fujikura, D., Yamada, T.*, et al.* (2011). ZAPS is a potent stimulator of signaling
1097 mediated by the RNA helicase RIG-I during antiviral responses. Nat Immunol *12*, 37-44.

Hoenen, T., Shabman, R.S., Groseth, A., Herwig, A., Weber, M., Schudt, G., Dolnik, O., Basler, C.F., Becker, S., and Feldmann, H. (2012). Inclusion bodies are a site of ebolavirus replication. J Virol *86*, 11779-11788.

Huang, I.C., Bailey, C.C., Weyer, J.L., Radoshitzky, S.R., Becker, M.M., Chiang, J.J., Brass, A.L., Ahmed, A.A., Chi, X., Dong, L., *et al.* (2011). Distinct patterns of IFITM-mediated restriction of filoviruses, SARS coronavirus, and influenza A virus. PLoS Pathog *7*, e1001258.

James, L.C. (2014). Intracellular antibody immunity and the cytosolic Fc receptor TRIM21. Curr Top Microbiol Immunol *382*, 51-66.

Kaletsky, R.L., Francica, J.R., Agrawal-Gamse, C., and Bates, P. (2009). Tetherin-mediated restriction of filovirus budding is antagonized by the Ebola glycoprotein. Proc Natl Acad Sci U S A *106*, 2886-2891.

Kane, M., Zang, T.M., Rihn, S.J., Zhang, F., Kueck, T., Alim, M., Schoggins, J., Rice, C.M., Wilson, S.J., and Bieniasz, P.D. (2016). Identification of Interferon-Stimulated Genes with Antiretroviral Activity. Cell Host Microbe *20*, 392-405.

Kerns, J.A., Emerman, M., and Malik, H.S. (2008). Positive selection and increased antiviral activity associated with the PARP-containing isoform of human zinc-finger antiviral protein. PLoS Genet *4*, e21.

Kirchdoerfer, R.N., Abelson, D.M., Li, S., Wood, M.R., and Saphire, E.O. (2015). Assembly of the Ebola Virus Nucleoprotein from a Chaperoned VP35 Complex. Cell Rep *12*, 140-149.

Kruse, T., Biedenkopf, N., Hertz, E.P.T., Dietzel, E., Stalmann, G., Lopez-Mendez, B., Davey, N.E., Nilsson, J., and Becker, S. (2018). The Ebola Virus Nucleoprotein Recruits the Host PP2A-B56 Phosphatase to Activate Transcriptional Support Activity of VP30. Mol Cell *69*, 136-145 e136.

Kuroda, M., Halfmann, P.J., Hill-Batorski, L., Ozawa, M., Lopes, T.J.S., Neumann, G., Schoggins, J.W., Rice, C.M., Kawaoka, Y. (2020). Identification of interferon-stimulated genes that attenuate EBOV infection. Nat Commun Jun 11;11(1)2953.

Leroy, E.M., Kumulungui, B., Pourrut, X., Rouquet, P., Hassanin, A., Yaba, P., Delicat, A., Paweska, J.T., Gonzalez, J.P., and Swanepoel, R. (2005). Fruit bats as reservoirs of Ebola virus. Nature *438*, 575-576.

Li, M.M., Lau, Z., Cheung, P., Aguilar, E.G., Schneider, W.M., Bozzacco, L., Molina, H., Buehler, E., Takaoka, A., Rice, C.M., *et al.* (2017). TRIM25 Enhances the Antiviral Action of Zinc-Finger Antiviral Protein (ZAP). PLoS Pathog *13*, e1006145.

Liu, Y., Gordesky-Gold, B., Leney-Greene, M., Weinbren, N.L., Tudor, M., and Cherry, S. (2018). Inflammation-Induced, STING-Dependent Autophagy Restricts Zika Virus Infection in the Drosophila Brain. Cell Host Microbe *24*, 57-68 e53.

1144 Long, J., Wright, E., Molesti, E., Temperton, N., and Barclay, W. (2015). Antiviral therapies
1145 against Ebola and other emerging viral diseases using existing medicines that block virus
1146 entry. F1000Res *4*, 30.
1147
1148 Loo, Y.M., and Gale, M., Jr. (2011). Immune signaling by RIG-I-like receptors. Immunity *34*,
1149 680-692.
1150
1151 Lopez, L.A., Yang, S.J., Hauser, H., Exline, C.M., Haworth, K.G., Oldenburg, J., and Cannon,
1152 P.M. (2010). Ebola virus glycoprotein counteracts BST-2/Tetherin restriction in a sequence-
1153 independent manner that does not require tetherin surface removal. J Virol *84*, 7243-7255.
1154
1155 Luthra, P., Parameshwaran, R., Mire, C.E., Weisend, C., Tsuda, Y., Yen, B., Liu, G., Leung,
1156 D.W., Geisbert, T.W., Ebihara, H., *et al.* (2013). Mutual antagonism between the Ebola virus
1157 VP35 protein and the RIG-I activator PACT determines infection outcome. Cell Host Microbe
1158 Jul 17;14(1):74-84.
1159
1160 Mankouri, J., Fragkoudis, R., Richards, K.H., Wetherill, L.F., Harris, M., Kohl, A., Elliott, R.M.,
1161 and Macdonald, A. (2010). Optineurin negatively regulates the induction of IFNbeta in
1162 response to RNA virus infection. PLoS Pathog *6*, e1000778.
1163
1164 Manokaran, G., Finol, E., Wang, C., Gunaratne, J., Bahl, J., Ong, E.Z., Tan, H.C., Sessions,
1165 O.M., Ward, A.M., Gubler, D.J., *et al.* (2015). Dengue subgenomic RNA binds TRIM25 to
1166 inhibit interferon expression for epidemiological fitness. Science *350*, 217-221.
1167
1168 Martin-Serrano, J., Zang, T., and Bieniasz, P.D. (2001). HIV-1 and Ebola virus encode small
1169 peptide motifs that recruit Tsg101 to sites of particle assembly to facilitate egress. Nature
1170 medicine *7*, 1313-1319.
1171
1172 Martin-Vicente, M., Medrano, L.M., Resino, S., Garcia-Sastre, A., and Martinez, I. (2017).
1173 TRIM25 in the Regulation of the Antiviral Innate Immunity. Front Immunol *8*, 1187.
1174
1175 McCarthy, S.D.S., Majchrzak-Kita, B., Racine, T., Kozlowski, H.N., Baker, D.P., Hoenen, T.,
1176 Kobinger, G.P., Fish, E.N., Branch, D.R. (2016). A Rapid Screening Assay Identifies
1177 Monotherapy with Interferon-ß and Combination Therapies with Nucleoside Analogs as
1178 Effective Inhibitors of Ebola Virus. PLoS Negl Trop Dis Jan 11;10(1):e0004364.
1179
1180 McNab, F., Mayer-Barber, K., Sher, A., Wack, A., and O'Garra, A. (2015). Type I interferons in
1181 infectious disease. Nat Rev Immunol *15*, 87-103.
1182
1183 Messaoudi, I., Amarasinghe, G.K., and Basler, C.F. (2015). Filovirus pathogenesis and
1184 immune evasion: insights from Ebola virus and Marburg virus. Nat Rev Microbiol *13*, 663-
1185 676.
1186
1187 Meyerson, N.R., Zhou, L., Guo, Y.R., Zhao, C., Tao, Y.J., Krug, R.M., and Sawyer, S.L. (2017).
1188 Nuclear TRIM25 Specifically Targets Influenza Virus Ribonucleoproteins to Block the Onset
1189 of RNA Chain Elongation. Cell Host Microbe *22*, 627-638 e627.
1190

Moncorge, O., Long, J.S., Cauldwell, A.V., Zhou, H., Lycett, S.J., and Barclay, W.S. (2013). Investigation of influenza virus polymerase activity in pig cells. J Virol *87*, 384-394.

Moncorge, O., Mura, M., and Barclay, W.S. (2010). Evidence for avian and human host cell factors that affect the activity of influenza virus polymerase. J Virol *84*, 9978-9986.

Muhlberger, E. (2007). Filovirus replication and transcription. Future Virol *2*, 205-215.

Muller, S., Moller, P., Bick, M.J., Wurr, S., Becker, S., Gunther, S., and Kummerer, B.M. (2007). Inhibition of filovirus replication by the zinc finger antiviral protein. J Virol *81*, 2391-2400.

Neil, S.J., Zang, T., and Bieniasz, P.D. (2008). Tetherin inhibits retrovirus release and is antagonized by HIV-1 Vpu. Nature *451*, 425-430.

Noda, T., Hagiwara, K., Sagara, H., and Kawaoka, Y. (2010). Characterization of the Ebola virus nucleoprotein-RNA complex. J Gen Virol *91*, 1478-1483.

Noda, T., Sagara, H., Suzuki, E., Takada, A., Kida, H., and Kawaoka, Y. (2002). Ebola virus VP40 drives the formation of virus-like filamentous particles along with GP. J Virol *76*, 4855-4865.

Odon, V., Fros, J.J., Goonawardane, N., Dietrich, I., Ibrahim, A., Alshaikhahmed, K., Nguyen, D., Simmonds, P. (2019). The role of ZAP and OAS3/RNAse L pathways in the attenuation of an RNA virus with elevated frequencies of CpG and UpA dinucleotides. Nucleic Acids Res 5;47(15):8061-8083.

Okamoto, M., Kouwaki, T., Fukushima, Y., and Oshiumi, H. (2017). Regulation of RIG-I Activation by K63-Linked Polyubiquitination. Front Immunol *8*, 1942.

Okumura, A., Pitha, P.M., and Harty, R.N. (2008). ISG15 inhibits Ebola VP40 VLP budding in an L-domain-dependent manner by blocking Nedd4 ligase activity. Proc Natl Acad Sci U S A *105*, 3974-3979.

Pertel, T., Hausmann, S., Morger, D., Zuger, S., Guerra, J., Lascano, J., Reinhard, C., Santoni, F.A., Uchil, P.D., Chatel, L.*, et al.* (2011). TRIM5 is an innate immune sensor for the retrovirus capsid lattice. Nature *472*, 361-365.

Pleschka, S., Jaskunas, R., Engelhardt, O.G., Zurcher, T., Palese, P., and Garcia-Sastre, A. (1996). A plasmid-based reverse genetics system for influenza A virus. J Virol *70*, 4188-4192.

Prins, K.C., Cardenas, W.B., and Basler, C.F. (2009). Ebola virus protein VP35 impairs the function of interferon regulatory factor-activating kinases IKKepsilon and TBK-1. J Virol *83*, 3069-3077.

Sanchez, J.G., Chiang, J.J., Sparrer, K.M.J., Alam, S.L., Chi, M., Roganowicz, M.D., Sankaran, B., Gack, M.U., and Pornillos, O. (2016). Mechanism of TRIM25 Catalytic Activation in the Antiviral RIG-I Pathway. Cell Rep *16*, 1315-1325.

Sanchez, J.G., Okreglicka, K., Chandrasekaran, V., Welker, J.M., Sundquist, W.I., and Pornillos, O. (2014). The tripartite motif coiled-coil is an elongated antiparallel hairpin dimer. Proc Natl Acad Sci U S A *111*, 2494-2499.

Sanchez, J.G., Sparrer, K.M.J., Chiang, C., Reis, R.A., Chiang, J.J., Zurenski, M.A., Wan, Y., Gack, M.U., and Pornillos, O. (2018). TRIM25 Binds RNA to Modulate Cellular Anti-viral Defense. J Mol Biol *430*, 5280-5293.

Schneider, W.M., Chevillotte, M.D., and Rice, C.M. (2014). Interferon-stimulated genes: a complex web of host defenses. Annu Rev Immunol *32*, 513-545.

Schoggins, J.W., Wilson, S.J., Panis, M., Murphy, M.Y., Jones, C.T., Bieniasz, P., and Rice, C.M. (2011). A diverse range of gene products are effectors of the type I interferon antiviral response. Nature *472*, 481-485.

Shabman, R.S., Gulcicek, E.E., Stone, K.L., and Basler, C.F. (2011). The Ebola virus VP24 protein prevents hnRNP C1/C2 binding to karyopherin alpha1 and partially alters its nuclear import. J Infect Dis *204 Suppl 3*, S904-910.

Su, Z., Wu, C., Shi, L., Luthra, P., Pintilie, G.D., Johnson, B., Porter, J.R., Ge, P., Chen, M., Liu, G., *et al.* (2018). Electron Cryo-microscopy Structure of Ebola Virus Nucleoprotein Reveals a Mechanism for Nucleocapsid-like Assembly. Cell *172*, 966-978 e912.

Subissi, L., Keita, M., Mesfin, S., Rezza, G., Diallo, B., Van Gucht, S., Musa, E.O., Yoti, Z., Keita, S., Djingarey, M.H., *et al.* (2018). Ebola Virus Transmission Caused by Persistently Infected Survivors of the 2014-2016 Outbreak in West Africa. J Infect Dis.

Takata, M.A., Goncalves-Carneiro, D., Zang, T.M., Soll, S.J., York, A., Blanco-Melo, D., and Bieniasz, P.D. (2017). CG dinucleotide suppression enables antiviral defence targeting non-self RNA. Nature *550*, 124-127.

Thorson, A.E., Deen, G.F., Bernstein, K.T., Liu, W.J., Yamba, F., Habib, N., Sesay, F.R., Gaillard, P., Massaquoi, T.A., McDonald, S.L.R., *et al.* (2021). Persistence of Ebola virus in semen among Ebola virus disease survivors in Sierra Leone: A cohort study of frequency, duration, and risk factors. PLoS Med. Feb 10;18(2):e1003273.

Tomar, D., and Singh, R. (2015). TRIM family proteins: emerging class of RING E3 ligases as regulator of NF-kappaB pathway. Biol Cell *107*, 22-40.

Treier, M., Staszewski, L.M., and Bohmann, D. (1994). Ubiquitin-dependent c-Jun degradation in vivo is mediated by the delta domain. Cell *78*, 787-798.

Tscherne, D.M., and Garcia-Sastre, A. (2011). An enzymatic assay for detection of viral entry. Curr Protoc Cell Biol *Chapter 26*, Unit 26 12.

Vetter, P., Fischer, W.A., 2nd, Schibler, M., Jacobs, M., Bausch, D.G., and Kaiser, L. (2016). Ebola Virus Shedding and Transmission: Review of Current Evidence. J Infect Dis *214*, S177-S184.

Wan, W., Kolesnikova, L., Clarke, M., Koehler, A., Noda, T., Becker, S., and Briggs, J.A.G. (2017). Structure and assembly of the Ebola virus nucleocapsid. Nature *551*, 394-397.

Watt, A., Moukambi, F., Banadyga, L., Groseth, A., Callison, J., Herwig, A., Ebihara, H., Feldmann, H., and Hoenen, T. (2014). A novel life cycle modeling system for Ebola virus shows a genome length-dependent role of VP24 in virus infectivity. J Virol *88*, 10511-10524.

Zhang, A.P., Bornholdt, Z.A., Liu, T., Abelson, D.M., Lee, D.E., Li, S., Woods, V.L., Jr., and Saphire, E.O. (2012). The ebola virus interferon antagonist VP24 directly binds STAT1 and has a novel, pyramidal fold. PLoS Pathog *8*, e1002550.

Zhao, Y., Sun, X., Nie, X., Sun, L., Tang, T.S., Chen, D., and Sun, Q. (2012). COX5B regulates MAVS-mediated antiviral signaling through interaction with ATG5 and repressing ROS production. PLoS Pathog *8*, e1003086.

Zheng, X., Wang, X., Tu, F., Wang, Q., Fan, Z., and Gao, G. (2017). TRIM25 Is Required for the Antiviral Activity of Zinc Finger Antiviral Protein. J Virol *91*.

Figure Legends

Figure 1. Human ISG-expression screening identifies novel candidates with antiviral activity against EBOV trVLP.

(A) EBOV trVLP normalized reporter activity on HEK293T- and U87-MG-stably expressing TIM1 transfected with EBOV RNP proteins and pre-treated with increasing amounts of IFN-I 24 hours prior infection (p1 target cells, blue). Supernatants from p1 cells were harvested 24 hpi, and used to infect HEK293T-TIM1 cells and reporter activities measured 24 hours later (p2 target cells, red).

(B) HEK293T-TIM1 cells were pre-treated with IFN-I (1000U/ml) prior to transduction with BlaVP40-EBOV-GP virus-like particles. 24 hours later, viral particle entry was measured as percentage of cells presenting cleavage of CCF2-AM dye by flow cytometry.

(C) Relative quantification of intracellular viral RNA levels on HEK293T-TIM1 (grey) and U87-MG-TIM1 (blue) p1 target cells pre-treated with IFN-I, and infected with EBOV trVLPs as in (A). Random hexamer primers were used to generate cDNAs and RT-qPCR analysis was performed using qPCR primers/probe sets targeting the 5'-trailer region of the trVLP 4cis minigenome (vRNA and cRNA, left panel), VP40 RNA (vRNA, cRNA and mRNA, right panel) or *gapdh* as endogenous control. Data presented as fold change compared to control (no IFN) based on $\Delta\Delta$Ct values.

(D) Relative quantification of viral transcripts present on supernatants from (C). cDNA synthesis performed as above and RT-qPCR performed with primers/probe set targeting EBOV VP40 RNA. Data shown as fold change compared to control (no IFN) based on absolute copy numbers.

(E) Results of the arrayed human ISG screen. HEK293T-TIM1 target cells (p1) were pre-transfected with plasmids expressing individual ISGs together with EBOV RNP components and Firefly transfection control, and infected with EBOV trVLPs 24 hours later. Supernatants from p1 cells were harvested 24 hpi and used to infect p2 target cells pre-transfected solely with vRNP components and pFluc. EBOV trVLP reporter activities for p1 (blue dots) and p2 target cells (red dots) were measured as in (A). Each dot represents one ISG. Infectivity measured for each ISG-expressing well was normalized to the activity of Fluc control within the well, and values are represented as percentage of the screen plate average, which is indicated as log of 100%.

(F) Confirmatory assays for selected top candidate inhibitory ISGs. EBOV-trVLP infection was performed on HEK293T-TIM1 cells as in the primary screen. Normalized reporter activities for p1

(upper panels) and p2 target cells (lower panels) are represented as percentage of EBOV trVLP replication on cells transfected with GFP (white bars).

(G) Relative quantification of intracellular (left and middle panels) and supernatant (right panel) viral RNA levels on HEK293T-TIM1 target cells (p1) transfected with EBOV RNP components and the top inhibitory ISG candidates and infected as before. cDNA synthesis and RT-qPCR analysis performed as in (C) and (D).

All the represented EBOV trVLP Rluc reporter activities are normalized to control Fluc values obtained in the same lysates. Universal Type I IFN-α was used to pre-treat cells in panels (A-D). *p > 0.05, **p > 0.01 and ***p > 0.001 as determined by two-tailed paired t-test. All error bars represent ± SEM of at least three independent experiments.

Figure 2. TRIM25 is required for type-I IFN-mediated restriction of EBOV trVLP replication.

(A) EBOV trVLP normalized reporter activity on HEK293T-TIM1 cells transfected with EBOV RNP proteins and either GFP (grey) or TRIM25 (blue) prior to infection with increasing amounts of EBOV trVLPs (p1 target cells, left panel). Supernatants from p1 cells were harvested 24 hpi and used to infect p2 target cells (right panel), and reporter activities measured 24 hours later.

(B) HEK293T-TIM1 cells were transfected with plasmids expressing either GFP (grey) or TRIM25 (blue), and transduced with BlaVP40-EBOV-GP virus like particles 24 hours later. Viral particle entry was determined 24 hours post-transduction by measuring the percentage of cells with cleaved CCF2-AM dye by flow cytometry.

(C) Quantification of viral RNA transcripts present on cell lysates (left panel) and supernatants (right panel) of HEK293T-TIM1 cells transfected and infected as in (A). Strand-specific reverse transcription primers were used on total RNA extracted from cells to generate cDNAs for minigenomic RNA (vRNA), complementary RNA (cRNA), and mRNA, which were subsequently analysed by RT-qPCR. Random hexamer primers were used to generate cDNAs from total viral RNA extracted from supernatants, and qPCR analysis performed using primers/probe sets targeting 5' trailer region of the 4cis genome or VP40 RNA.

(D) U87-MG- and HEK293T-based CRISPR cells lines were treated with increasing amounts of IFN-I, and lysed 24 hours later for analysis. Protein levels of HSP90 and TRIM25 were determined by western blot on LacZ CRISPR control cells and corresponding TRIM25 CRISPR KO cell lines.

(E) EBOV trVLP reporter activities on U87-MG LacZ CRISPR-TIM1 (grey) and U87-MG TRIM25 CRISPR KO-TIM1 (blue) target cells (p1) transfected with EBOV RNP proteins, and pre-treated with increasing amounts of IFN-I prior to infection.

(F) Relative quantification of intracellular and supernatant trVLP RNA levels on U87-MG LacZ CRISPR-TIM1 (grey) and U87-MG TRIM25 CRISPR KO-TIM1 cells (blue) from (E). Random hexamer primers were used to generate cDNAs and RT-qPCR analysis was performed using primers/probe sets targeting trVLP 4cis genome trailer region (vRNA and cRNA, left panel), or VP40 RNA (intracellular vRNA, cRNA and mRNA, middle panel; minigenomic RNA in the supernatant, right panel). Data shown as fold change compared to control (no IFN) based on absolute copy numbers.

(G) EBOV trVLP reporter activities on U87-MG LacZ CRISPR-TIM1 (solid lines) and U87-MG TRIM25 CRISPR KO-TIM1 (dashed lines) target cells transfected with EBOV RNP proteins and pre-treated with increasing amounts of IFN-α2a (blue) or IFN-ß1b (red) prior to infection.

(H) U87-MG LacZ CRISPR (grey) and U87-MG TRIM25 CRISPR KO cells (blue) were treated with increasing amounts of IFN-I, and transduced the following day with a VSV-G pseudo-typed lentiviral vector expressing GFP (CSGW). The percentage of GFP-positive cells was determined 24 hours later by flow cytometry.

(I) HEK293T LacZ CRISPR (grey) and HEK293T TRIM25 CRISPR KO (blue) were used as producer cells (p0) of EBOV trVLPs and reporter activities measured 48 hours post-transfection. Supernatants from p0 cells were used to infect HEK293T-TIM1 target cells (p1), and reporter activities determined 24 hours later.

All the represented EBOV trVLP RLuc reporter activities are normalized to control FLuc values obtained in the same lysates. *p > 0.05, **p > 0.01 and ***p > 0.001 as determined by two-tailed paired t-test. All error bars represent ± SEM of at least three independent experiments.

Figure 3. TRIM25 antiviral effect against EBOV trVLPs is independent of RIG-I and downstream pro-inflammatory signal transduction.

(A, B, H) U87-MG- and/or HEK293T-based CRISPR cells lines were treated with increasing amounts of IFN-I, and lysed 24 hours later for protein analysis. Protein levels of HSP90 (A, B and H), RIG-I (A), FL-MAVS/mini-MAVS (B) and TBK1 (H) were determined by western blot on LacZ CRISPR control cells and corresponding CRISPR knock-out (KO) cells lines.

(C, I) HEK293T-based CRISPR cell lines depicted in the figures were transfected with plasmids expressing EBOV RNP proteins and TIM-1 together with either GFP (grey bars) or TRIM25 (blue bars), and later infected with a fixed amount of EBOV trVLPs. 24 hpi cells were lysed and trVLP reporter activities measured.

(D) EBOV trVLP reporter activities on U87-MG LacZ CRISPR (grey) and U87-MG RIG-I CRISPR KO (blue) target cells (p1), transfected with TIM-1 and EBOV RNP proteins, and pre-treated overnight with increasing amounts of IFN-I prior to infection. Luciferase activities measured 24 hours post-infection.

(E) EBOV trVLP reporter activities on U87-MG LacZ CRISPR (grey), U87-MG FL-MAVS KO (blue) and FL-MAVS/miniMAVS CRISPR DKO (red) target cells (p1), transfected with TIM-1 and EBOV RNP proteins, and pre-treated overnight with increasing amounts of IFN-I prior to infection. Luciferase activities measured 24 hours post-infection.

(F) Protein levels of HSP90 and MAVS determined by western blot lysates from HEK293T LacZ control cells, and HEK293T-MAVS DKO cells lines engineered to stably express CRISPR-resistant variants of both MAVS isoforms ($MAVS^{CR}$), miniMAVS ($M1A^{CR}$) or FL-MAVS ($M142A^{CR}$).

(G) HEK293T LacZ CRISPR and engineered HEK293T-MAVS DKO cell lines from (F) were co-transfected with plasmids expressing EBOV RNP components and TIM-1 together with either GFP (grey bars) or TRIM25 (blue bars), and later infected with EBOV trVLPs. Reporter activities were measured 24 hours later.

(J) U87-MG LacZ CRISPR and U87-MG TBK1 CRISPR KO cells were transfected with RNP proteins and TIM-1, followed by a IFN-I pre-treatment prior to infection with a fixed amount of EBOV trVLPs. EBOV trVLP reporter activities in p1 were measured 24 hours after infection.

(K) Fold activation of a firefly luciferase NF-kB reporter in the depicted HEK293T-based CRISPR cells lines transiently transfected with TRIM25 compared to control GFP vector. Cells were harvested 48 hours post-transfection and FLuc reporter values normalised to control Renilla luciferase activity in the same lysates.

All the represented EBOV trVLP Renilla reporter activities are normalized to control Firefly luciferase values obtained in the same lysates. *$p > 0.05$, **$p > 0.01$ and ***$p > 0.001$ as determined by two-tailed paired t-test. All error bars represent ± SEM of at least three independent experiments.

Figure 4. TRIM25 and ZAP are inter-dependent for their antiviral activity against EBOV trVLP.

(A) EBOV trVLP normalized reporter activity on HEK293T-TIM1 cells transfected with EBOV RNP proteins and either GFP (grey) or ZAP-L (red) prior to infection with increasing amounts of EBOV trVLPs (p1 target cells, left panel). Supernatants from p1 cells were harvested and used to infect p2 target cells (right panel), and reporter activities measured 24 hours later.

(B) HEK293T- and U87-MG-based CRISPR cells lines were treated with increasing amounts of IFN-I, and lysed 24 hours later for analysis. Protein levels of HSP90 and ZAP were determined by western blot on LacZ CRISPR control cells and corresponding ZAP CRISPR KO cell lines.

(C) EBOV trVLP reporter activities on U87-MG LacZ CRISPR-TIM1 (grey) and U87-MG ZAP CRISPR KO-TIM1 (red) target cells (p1), transfect with RNP proteins and pre-treated with increasing amounts of IFN-I prior to infection. Reporter activities measured 24 hours after infection.

(D) Quantification of intracellular and supernatant viral RNA levels on U87-MG LacZ CRISPR-TIM1 (grey) and U87-MG ZAP CRISPR KO-TIM1 target cells (red) that were transfected with EBOV RNP proteins and pre-treated with IFN-I, prior to infection with EBOV trVLPs as in (C). Random hexamer primers were used to generate cDNAs and RT-qPCR analysis was performed using primers/probe sets targeting either the trailer region of the viral genome (vRNA and cRNA, left panel), or VP40 RNA (intracellular vRNA, cRNA and mRNA, middle panel; minigenomic RNA in the supernatant, right panel). Data presented as fold change compared to control (no IFN) based on absolute copy numbers.

(E) EBOV trVLP normalized reporter activities on HEK293T LacZ CRISPR, HEK293T TRIM25 CRISPR KO and HEK293T ZAP CRISPR KO cells stably expressing TIM1, that were transfected with EBOV RNP plasmids together with GFP (grey), ZAP L (red) or TRIM25 (blue), prior to infection with a fixed amount of EBOV trVLPs (p1 target cells). Supernatants from p1 were then harvested and used to infect HEK293T-TIM1 cells (p2 target cells).

(F) Relative quantification of EBOV L-Polymerase RNA transcripts on cell lysates of HEK293T LacZ CRISPR-TIM1 and HEK293T TRIM25 CRISPR KO-TIM1 cells transfected EBOV RNP plasmids in combination with either with GFP (grey) or ZAP-L (red), and infected with a fixed amount of EBOV trVLPs. Random hexamer primers were used to generate cDNAs from total RNA, and RT-qPCR analysis performed using a primers/probe sets targeting EBOV L-polymerase and *gapdh*. Data

normalized to L-polymerase RNA levels on HEK293T LacZ CRISPR-TIM1 cells transfected with GFP based on ΔΔCt values.

(G) EBOV trVLP normalized reporter activity on p2 target cells. HEK293T-TIM1 p1 cells were transfected with EBOV RNP proteins, and either GFP (grey) or ZAP-L (red) prior to infection with increasing amounts of wild-type EBOV trVLPs (trVLPwt, solid lines) or a variant with no CpG dinucleotides on the *Renilla* ORF of the 4cis genome (CpG low, dashed lines). Supernatants from p1 were harvested and used to infect HEK293T-TIM1 p2 target cells.

(H) Quantification of viral RNA transcripts present intracellularly (upper and middle panels) and in supernatants (lower panel) of 293T-TIM1 cells transfected as in (G), and infected with a fixed amount of EBOV trVLP WT or CpG low. Random hexamer primers were used to generate cDNAs from total RNA and RT-qPCR analysis was performed as in (D).

(I) EBOV trVLP normalized reporter activity on HEK293T-TIM1 p2 target cells. HEK293T LacZ CRISPR-TIM1 (grey) and HEK293T ZAP CRISPR KO-TIM1 cells (red) were transfected with EBOV RNP proteins and pre-treated with increasing amounts of IFN-I prior to infection with wild-type EBOV trVLPs (solid lines) or CpG Low EBOV trVLP (dashed lines). Supernatants from p1 were harvested and used to infect HEK293T-TIM1 p2 target cells. Reporter activities measured 24 hours post-infection.

All the represented EBOV trVLP Renilla reporter activities are normalized to control Firefly luciferase values obtained in the same lysates. $P > 0.05$, $^{**}p > 0.01$ and $^{***}p > 0.001$ as determined by two-tailed paired t-test. All error bars represent ± SEM of at least three independent experiments.

Figure 5. TRIM25 interacts with EBOV NP and promotes its ubiquitination.

(A) Lysates of HEK293T-TIM1 cells transfected either with GFP or TRIM25, in combination with EBOV NP and/or EBOV VP35, were immunoprecipitated with an anti-TRIM25 antibody. Cellular lysates and pull-downs were analysed by western blot for HSP90, TRIM25, EBOV NP and VP35.

(B) Panels show representative fields for the localization of EBOV NP and endogenous TRIM25 on HEK293T-TIM1 cells left untreated (Null), or transfected with EBOV NP protein alone, or in combination either with VP35 or all remaining RNP proteins (VP35, VP30 and L). Cells were stained with anti-TRIM25 (red) and anti-NP (green) antibodies, as well as with DAPI (blue). White arrows point to the localization of TRIM25 intracellular aggregates.

(C) Schematic representation of functional domains within TRIM25 (upper panel). Lysates of HEK293T-TIM1 cells transfected with EBOV NP in combination with GFP, TRIM25 or mutants thereof, were immunoprecipitated with an anti-TRIM25 antibody. Input and pull-down samples were blotted for HSP90, TRIM25 and EBOV NP (lower panel). (*) indicates the detected heavy-chains (HC) from the antibody used in the pull-down.

(D) EBOV trVLP normalized reporter activity on HEK293T-TIM1 cells transfected with EBOV RNP proteins in combination with GFP (grey), TRIM25 wild-type (blue), TRIM25 ΔRING (red) or TRIM25 ΔSPRY (orange) mutants, prior to infection with increasing amounts of EBOV trVLPs (p1 target cells). EBOV trVLP Rluc reporter activities were measure 24 hpi and normalized to control Fluc values obtained in the same lysates. EBOV trVLP Renilla reporter activities are normalized to control Firefly luciferase values obtained in the same lysates. *p > 0.05, **p > 0.01 and ***p > 0.001 as determined by two-tailed paired t-test. All error bars represent ± SEM of at least three independent experiments.

(E) HEK293T-TIM1 cells were transfected either with GFP or TRIM25, in combination with EBOV NP and/or a plasmid expressing a HA-tagged Ubiquitin (HA-Ub). Lysates from these cells were immunoprecipitated with an anti-HA antibody (left panels) or an anti-NP antibody (right panels). Cellular lysates and pull-down samples were analysed by western blot for HSP90, TRIM25, EBOV NP and HA (ubiquitin).

(F) Lysates from HEK293T cells co-transfected with EBOV NP and YFP or TRIM25 were immunoprecipitated with an anti-NP antibody, and pulled-down fractions treated with USP2 deubiquitinase enzyme. Cellular lysates and pull-downs were analysed by western blot for HSP90, TRIM25 and EBOV NP.

Figure 6. Determinants of TRIM25 antiviral activity and NP interaction

(A) Upper Panel: schematic representation of TRIM25 with the localization of the RING dimerization mutants (light blue), E3-Ligase catalytic mutants (pink), Bbox2 & coiled-coil mutants (orange) and SPRY-domain and RNA-binding mutants (light green) generated on a TRIM25 CRISPR-resistant background. Lower Panel: EBOV trVLP normalized reporter activity on HEK293T TRIM25 CRISPR KO-TIM1 cells transfected with EBOV RNP proteins in combination with GFP (grey), CRISPR-resistant (CR) TRIM25 wild-type (dark blue), or mutants thereof (see upper panel), prior to infection with EBOV trVLPs (p1 target cells). EBOV trVLP Rluc reporter activities were measure 24 hpi and

normalized to control Fluc values obtained in the same lysates. All error bars represent ± SEM of four independent experiments. *p > 0.05, **p > 0.01 and ***p > 0.001 as determined by Oneway-ANOVA. Statistics represented above graphic bars were calculated as multiple comparisons to TRIM25 wild-type, while the statistics within graphic bars are represented in function of multiple comparison to YFP.

(B) HEK293T TRIM25 CRISPR KO cells were transfected with plasmids expressing the EBOV RNP proteins together with YFP, CRISPR-resistant TRIM25 or mutants thereof. Cell lysates were analysed 48 hours later by western blot for the expression of HSP90, TRIM25 and EBOV NP.

(C) Lysates of HEK293T cells transfected with EBOV NP in combination with either YFP or CRISPR-resistant TRIM25 (or mutants thereof) were immunoprecipitated with a rabbit anti-TRIM25 antibody. Cellular lysates and pull-down samples were analysed by western blot for HSP90, TRIM25 and EBOV NP.

Figure 7. TRIM25 and ZAP promote the dissociation of EBOV trVLP genomic RNA from the viral ribonucleoprotein.

(A) Typical confocal microscopy fields from HEK293T LacZ CRISPR-TIM1 (left panels) or HEK293T NPC1 CRIPSR KO-TIM1 cells (right panels) left untreated (Null) or infected with EBOV trVLPs concentrated on a 20% sucrose-cushion. Cells were stained 4 to 6 hours post-infection with anti-TRIM25 (red), anti-EBOV NP (green) and DAPI (blue). White arrows show localization of TRIM25 intracellular aggregates.

(B) Relative quantification of intracellular RNA levels (grey) and NP-associated RNA (blue) on HEK293T LacZ CRISPR-TIM1 and HEK293T NPC1 CRISPR KO-TIM1 cells transfected with GFP, TRIM25 or ZAP-L prior to infection with EBOV trVLPs. 3 hours post-infection cells were UV cross-linked, and EBOV NP from incoming virions was immunoprecipitated from lysates with an anti-NP antibody. Following proteinase K treatment, pulled-down RNA was extracted with Qiazol / chloroform, and random hexamer primers were used to generate cDNAs, and RT-qPCR analysis performed using a primers/probe set targeting EBOV VP40 RNA. Values are presented as percentage of absolute RNA copy numbers on cells transfected with GFP.

(C) HEK293T LacZ CRISPR, HEK293T ZAP CRISPR KO and HEK293T TRIM25 CRISPR KO cells stably expressing TIM1 were transfected with GFP, TRIM25 or ZAP-L as depicted in the panels, and

later infected with EBOV trVLPs. Relative quantification of intracellular viral RNA levels (grey) and NP-associated RNA (coloured bars) were determined as in (B).

(D) HEK293T-TIM1 cells were transfected with GFP, wild-type TRIM25 or mutants thereof prior to infection with EBOV trVLPs. Relative quantification of intracellular viral RNA levels (grey) and NP-associated RNA (blue) were determined as in (B).

(E) HEK293T TRIM25 CRISPR KO-TIM1 cells were transfected with GFP (grey), or CRISPR-resistant versions of TRIM25 (wild-type, dark blue; or mutants thereof, as depicted in the figure, light blue) prior to infection with EBOV trVLPs. Relative quantification of NP-associated RNA was determined as in (B).

(F) Prior to infection with EBOV trVLPs, HEK293T LacZ CRISPR-TIM1 cells were transfected with GFP or TRIM25 and either treated with 250µM of T705 (Favipiravir), or the equivalent volume of the diluent (DMSO). Relative quantification of intracellular viral RNA levels (grey) and NP-associated RNA (coloured bars) were determined as in (B). Values are presented as percentage of absolute RNA copy numbers on cells transfected with GFP.

(G) Relative quantification of ZAP-associated RNA on HEK293T LacZ CRISPR-TIM1 and HEK293T TRIM25 CRISPR KO-TIM1 cells transfected with GFP (grey) or ZAP-L (red) prior to infection with EBOV trVLPs. 3 hours post-infection cells were UV cross-linked, and ZAP was immunoprecipitated from lysates. RNA extraction, cDNA synthesis and RT-qPCR analysis were performed as in (B). Values were normalized to the respective inputs and are presented relative to absolute RNA copy numbers on cells transfected with GFP.

(H) HEK293T LacZ CRISPR, HEK293T TRIM25 CRISPR KO and HEK293T ZAP CRISPR KO cells stably expressing TIM1 were either untreated or pre-treated with 1000U/ml of IFN-I prior to infection with EBOV trVLPs. Relative quantification of intracellular viral RNA levels (grey) and NP-associated RNA (coloured bars) were determined as in (B). Values are presented as percentage of absolute RNA copy numbers on cells non-treated with IFN.

(I) HEK293T LacZ CRISPR, HEK293T TRIM25 CRISPR and HEK293T ZAP CRISPR KO cells stably expressing TIM1 were pre-treated overnight with increasing concentrations of IFN-I prior to infection with EBOV nanoluciferase trVLPs. EBOV trVLP nanoluc reporter activities were measured 48 hpi and data is shown as a percentage of untreated for each cell line individually.

(J). Proposed model for the mechanism associated with the antiviral activities of TRIM25 and ZAP against EBOV trVLP. EBOV viral particle enters the cells by macropinocytosis, followed by NPC1-dependent fusion with the cellular endosomal membrane. Once in the cytoplasm, TRIM25 is recruited to the viral particle through an interaction with EBOV NP protein, leading to the ubiquitination of both viral target and TRIM25 itself. This results in the displacement of the viral RNA genome from the vRNP, followed by its recognition by ZAP in a way dependent of the genome's CpG content and subsequent impact in the transcription and replication of EBOV trVLP.

Supplemental Figure Legends

Supplemental Figure S1 (related to Figure 1). EBOV trVLP assay and characterization of top candidate inhibitory ISGs.

(A) Upper panels: Graphical representations of the Ebola virus genome, and of the tetra-cistronic minigenome (4cis) encoding Renilla luciferase (*Rluc*) used in the transcription- and replication-competent (trVLP) assay. Lower panel: Schematic representation of the EBOV trVLP assay. Plasmids expressing ISGs of interest were co-transfected with viral RNP proteins into p1 target cells. Alternatively, p1 target cells were pre-treated with IFN-I prior infection with EBOV trVLPs (detailed description on Methods).

(B) U87-MG-Tim1 cells were transfected with plasmids expressing EBOV's RNP components and pre-treated with increasing amounts of Universal type-I IFN-α, IFN-α2a or IFN-ß1a, 16-24 hours prior to EBOV trVLP infection. Reporter activities were measured 24 hours later.

(C) U87-MG-TIM1 and HEK293T-TIM1 cells were transfected with plasmids expressing EBOV NP, VP35, VP30 and a HA-tagged version of L-polymerase, before being treated with increasing amounts of IFN-I prior to EBOV trVLP infection as in Figure 1A. Cells were lysed 24 hours post-transfection and lysates analysed by western blot for the expression of the EBOV RNP proteins and HSP90.

(D) ISG Screen Validation. Normal distribution of EBOV trVLP Rluc values in the presence of individually over-expressed ISGs on p1 (left panel, blue dots) and p2 (right panel, red dots) target cells, normalized to Fluc levels on the same well. The number (n) of ISGs within standard deviation (s.d. or z score) ranges is shown in the boxes.

(E) HEK293T-TIM1 cells were transfected with plasmids expressing the EBOV RNP proteins together with selected ISGs. Cells lysates were analysed 48 hours later by western blot as in (C).

(F) HEK293T-TIM1 cells were transfected with individual ISGs and EBOV RNP-expressing plasmids as in (E), and tested for cellular viability 48 hours later using Cell-Titer Glo luminescence-based assay (Promega). As positive control for toxicity (red bar), cells were treated for 48h with a concentration of MG132 (25μM) sufficient to reduce in 50 percent the ATP levels in the supernatant. Values are represented as percentage of luminescence obtained in control wells transfected with GFP (grey bar), and toxicity cut-off represented as a dashed line.

(G) Fold activation of Firefly luciferase NF-kB, ISG56/IFIT1 or ISRE reporters (top, middle or bottom panels, respectively) in HEK293T cells transiently transfected with selected individual ISGs compared

to control GFP vector. Cells were harvested either 24 hours (blue) or 48 hours (grey) post-transfection.

Supplemental Figure S2 (related to Figure 4). Overexpression of ZAP-L impacts on EBOV trVLP viral RNA levels

(A) Quantification of viral RNA transcripts present intracellularly (left panel) and in supernatants (right panel) of HEK293T-TIM1 cells transfected as in Figure 4A, and infected with a fixed amount of EBOV trVLPs. Strand-specific reverse transcription primers were used on total RNA extracted from cells to generate cDNAs for minigenomic RNA (vRNA), complementary RNA (cRNA), and mRNA, followed by RT-qPCR analysis. Random hexamer primers were used to generate cDNAs from total RNA extracted from supernatants, and qPCR analysis performed using primers targeting the 5' trailer region of the 4cis minigenome or VP40 RNA.

(B) EBOV trVLP reporter activities on U87-MG LacZ CRISPR-TIM1 (solid lines) and U87-MG ZAP CRISPR KO-TIM1 (dashed lines) target cells transfected with EBOV RNP proteins and pre-treated with increasing amounts of IFN-α2a (blue) or IFN-ß1b (red) prior to infection.

(C) HEK293T LacZ CRISPR (grey) and HEK293T ZAP CRISPR KO (red) were used as producer cells (p0) for EBOV trVLPs, and reporter activities measured 48 hours post-transfection. Supernatants from p0 were used to infect HEK293T-TIM1 target cells (p1), and reporter activities determined 24 hours later.

(D) Influenza A minigenome assay was performed in HEK293T LacZ CRISPR (grey), HEK293T ZAP CRISPR KO (red) and HEK293T RIG-I CRISPR KO (blue) cells transfected with Influenza polymerase components (NP, PB1, PB2 and PA) and increasing amounts of TRIM25. Normalized Fluc values are presented as percentage relative to a GFP control in each cell line.

(E) HEK293T LacZ CRISPR, and HEK293T TRIM25 CRISPR KO cells were transfected with plasmids expressing the EBOV NP, VP35, VP30 proteins and a HA-tagged L Polymerase together with either pcDNA4 or ZAP-L. Cells lysates were analysed 48 hours later by western blot for the expression of HSP90, TRIM25, ZAP and the EBOV RNP complex proteins.

(F) Relative quantification of intracellular viral RNA transcripts on cell lysates of HEK293T LacZ CRISPR-TIM1 and HEK293T TRIM25 CRISPR KO-TIM1 cells transfected EBOV RNP plasmids in combination with either with GFP (grey) or ZAP-L (red), and infected with a fixed amount of EBOV

trVLPs. Random hexamer primers were used to generate cDNAs from total RNA, and RT-qPCR analysis performed using a primers/probe sets targeting VP40 (mRNA,cRNA and vRNA, left), Trailer (cRNA and vRNA, right) and *gapdh*. Data normalized to HEK293T LacZ CRISPR-TIM1 cells transfected with GFP based on ΔΔCt values.

(G) Graphical representation of the ratio between observed and expected CpG dinucleotide frequencies in the full-length EBOV genomic RNA (grey), in the wild-type trVLP 4cis genome (dark blue) and in the trVLP genomic variant with no CpG dinucleotides in the *Renilla* reporter sequence (CpG low, light blue).

(H) Graphical representation of CpG dinucleotides localization on full-length EBOV genome (upper panel), on EBOV trVLP 4cis genome (middle panel) and on a 4cis genome with no CpG on the *Renilla* ORF (lower panel). CpG dinucleotides present on intergenic regions are represented in blue, while the ones present on viral ORFs are represented in red. In yellow are represented the CpG dinucleotides present on the *Renilla* reporter gene.

(I) U87-MG LacZ CRISPR and U87-MG KHNYN CRISPR KO cells were transfected with RNP proteins and TIM-1, followed by a IFN-I pre-treatment prior to infection with a fixed amount of EBOV trVLPs. EBOV trVLP reporter activities in p1 were measured 24 hours after infection.

(J) Relative quantification of intracellular viral RNA levels on cellular lysates from (I). Random hexamer primers were used to generate cDNAs and RT-qPCR analysis was performed using qPCR primers/probe sets targeting the VP40 RNA (vRNA, cRNA and mRNA, left panel) or the 5'-trailer region of the trVLP 4cis minigenome (vRNA and cRNA, right panel). Data presented as fold change compared to control (no IFN) based on absolute copy numbers.

Supplemental Figure S3 (related to Figure 5). TRIM25-mediated ubiquitination of EBOV NP is independent of ZAP and MAVS

(A) Lysates of HEK293T-TIM1 cells transfected either with GFP or TRIM25, in combination with EBOV NP and/or EBOV VP35 were immunoprecipitated with an anti-NP antibody. Cellular lysates and pull-downs were analysed by western blot for HSP90, TRIM25, EBOV NP and VP35.

(B) Lysates of HEK293T-TIM1 cells transfected either with EBOV NP and/or TRIM25 were left untreated (NT), or treated with RNase A prior to immunoprecipitation with an anti-TRIM25 antibody. Cellular lysates and pull-downs were analysed by western blot for HSP90, TRIM25 and EBOV NP.

(C) Lysates of HEK293T LacZ CRISPR and HEK293T ZAP CRISPR KO cells transfected either with GFP or TRIM25 and/or EBOV NP were immunoprecipitated with anti-TRIM25 antibody. Cellular lysates and pull-down samples were analysed by western blot for HSP90, TRIM25, EBOV NP and ZAP.

(D) HEK293T-TIM1 cells were transfected either with GFP, TRIM25 wild-type or TRIM25 ΔRING mutant, in combination with EBOV NP and/or a plasmid expressing a HA-tagged Ubiquitin (HA-Ub). Lysates from these cells were immunoprecipitated 48 hours later with an anti-HA antibody. Cellular lysates and pull-down samples were analysed by western blot for HSP90, TRIM25, NP and HA (ubiquitin).

(E) HEK293T LacZ CRISPR and HEK293T ZAP CRISPR KO cells were transfected either with GFP or TRIM25, in combination with EBOV NP and/or Ub-HA. Lysates from these cells were immunoprecipitated 48 hours later with an anti-HA antibody. Cellular lysates and pull-down samples were analysed by western blot as in (D).

(F) HEK293T LacZ control and HEK293T FL-MAVS/miniMAVS CRISPR DKO cells were transfected either with GFP or TRIM25 in combination with EBOV NP and/or HA-Ub. Lysates were immunoprecipitated with anti-HA antibody and analysed by western blotting as in (D).

(G) HEK293T LacZ CRISPR control and HEK293T TRIM25 CRISPR KO cells were infected with a fixed volume of EBOV trVLPs concentrated on a 20% sucrose-cushion. Cell were lysed at the depicted time points after infection and lysates analysed by western blot for HSP90 and EBOV NP.

Supplemental Figure S4 (related to Figure 7). EBOV trVLP replication is dependent on the entry factor NPC1 and it is sensitive to transcription inhibitor T705 (Favipiravir)

(A) Cellular lysates from HEK293T LacZ CRISPR-TIM1, HEK293T NPC1 CRISPR KO-TIM1 and HEK293T NPC1 CRISPR KO-TIM1 cells with restored expression of NPC1 (+NPC1) were analysed by western blot for HSP90 and NPC1.

(B) The cells lines used in (A) were transduced either with BlaVP40-EBOV-GP or BlaVP40-VSV-G virus-like particles, and 24 hours later the percentages of cells presenting cleavage of CCF2-AM dye were determined by flow cytometry as readout for viral particle entry.

(C) EBOV trVLP normalized reporter activity on the upper mentioned cell lines (p1) transfected with EBOV RNP proteins and infected the following day with a fixed amount of EBOV trVLPs. Reporter activities were measured 24 hours later.

(D) Quantification of intracellular viral RNA levels on HEK293T-TIM1 target cells 3 and 24 hours post-infection with a fixed amount of EBOV trVLPs. Prior to infection the cells were transfected with EBOV RNP expressing plasmids together with GFP (grey), TRIM25 (blue) or ZAP-L (red). Strand-specific reverse transcription primers were used on total RNA extracted from cells to generate cDNAs for minigenomic RNA (vRNA), complementary RNA (cRNA), and mRNA, followed by RT-qPCR analysis.

(E) Relative quantification of NP-associated RNA on HEK293T LacZ CRISPR-TIM1 cells transfected with GFP (grey), TRIM25 (blue) or ZAP-L (red) prior to infection with wild-type or CpG low EBOV trVLPs. 3 hours post-infection cells were UV cross-linked, and EBOV NP from incoming virions was immunoprecipitated from lysates with an anti-NP antibody. Following proteinase K treatment, pulled-down RNAs were extracted with Qiazol / chloroform, random hexamer primers used to generate cDNAs, and RT-qPCR analysis performed using a primers/probe set targeting EBOV VP40 RNA. Values are presented as percentage of absolute RNA copy numbers on cells transfected with GFP.

(F) HEK293T LacZ CRISPR, HEK293T ZAP CRISPR KO and HEK293T TRIM25 CRISPR KO cells stably expressing TIM1 were transfected with GFP (grey), TRIM25 (blue) or ZAP-L (red) as depicted in the panels, and later infected with wild-type (solid bars) or CpG low (striped bars) EBOV trVLPs. Relative quantification of NP-associated RNA was determined as in (E).

(G) EBOV trVLP reporter activities on HEK293T-TIM1 target cells (p1), transfect with RNP proteins and pre-treated overnight with increasing amounts of T-705 (Favipiravir) prior to infection. Reporter activities measured 24 hours after infection.

(H) Relative quantification of intracellular viral RNA levels on HEK293T-TIM1 p1 target cells pre-treated with increasing amounts of T-705 compound and infected with EBOV trVLPs as in (G). Random hexamer primers were used to generate cDNAs and RT-qPCR analysis was performed using qPCR primers/probe sets targeting the VP40 mRNA or *gapdh* as endogenous control. Data presented as fold change compared to control (no T-705) based on $\Delta\Delta$Ct values.

(I) Graphical representation of CpG dinucleotides localization on a monocistronic genome containing a *Renilla* reporter gene flanked by the 5'-leader and 3'-trailer regions of EBOV genome (upper panel), and its Low-CpG variant (bottom panel) in which all CpGs in the *Renilla* ORF were silently mutated.

CpG dinucleotides present on the trailer and leader regions are represented in blue, while in yellow are represented the CpG dinucleotides present on the *Renilla* reporter gene.

(J) Normalized reporter activity of the monocistronic genomes on HEK293T-TIM1 target transfected with EBOV RNP proteins, and either GFP (grey) or ZAP-L (red) prior to infection with increasing amounts of wild-type monocistronic VLPs (WT, solid lines) or a variant with no CpG dinucleotides on the *Renilla* ORF (CpG low, striped lines).

(K) HEK293T LacZ CRISPR-TIM1 cells were transfected with GFP (grey) or ZAP-L (red) and later infected with wild-type (solid bars) or CpG low (striped bars) monocistronic VLPs. Relative quantification of ZAP-associated RNA was determined as in (E).

(**L**) HEK293T LacZ CRISPR and HEK293T NPC1 CRISPR stably expressing TIM1 were infected with either WT or ΔGP EBOV nanoluciferase trVLPs. EBOV trVLP nanoluc reporter activities were measured 48 hpi.

(**M**) HEK293T TRIM25 CRISPR KO cells were transfected with TIM1 and either a CRISPR-resistant version of TRIM25 or YFP before infection with WT or ΔGP EBOV nanoluciferase trVLPs. EBOV trVLP nanoluc reporter activities were measured 48 hpi.

Figure 1

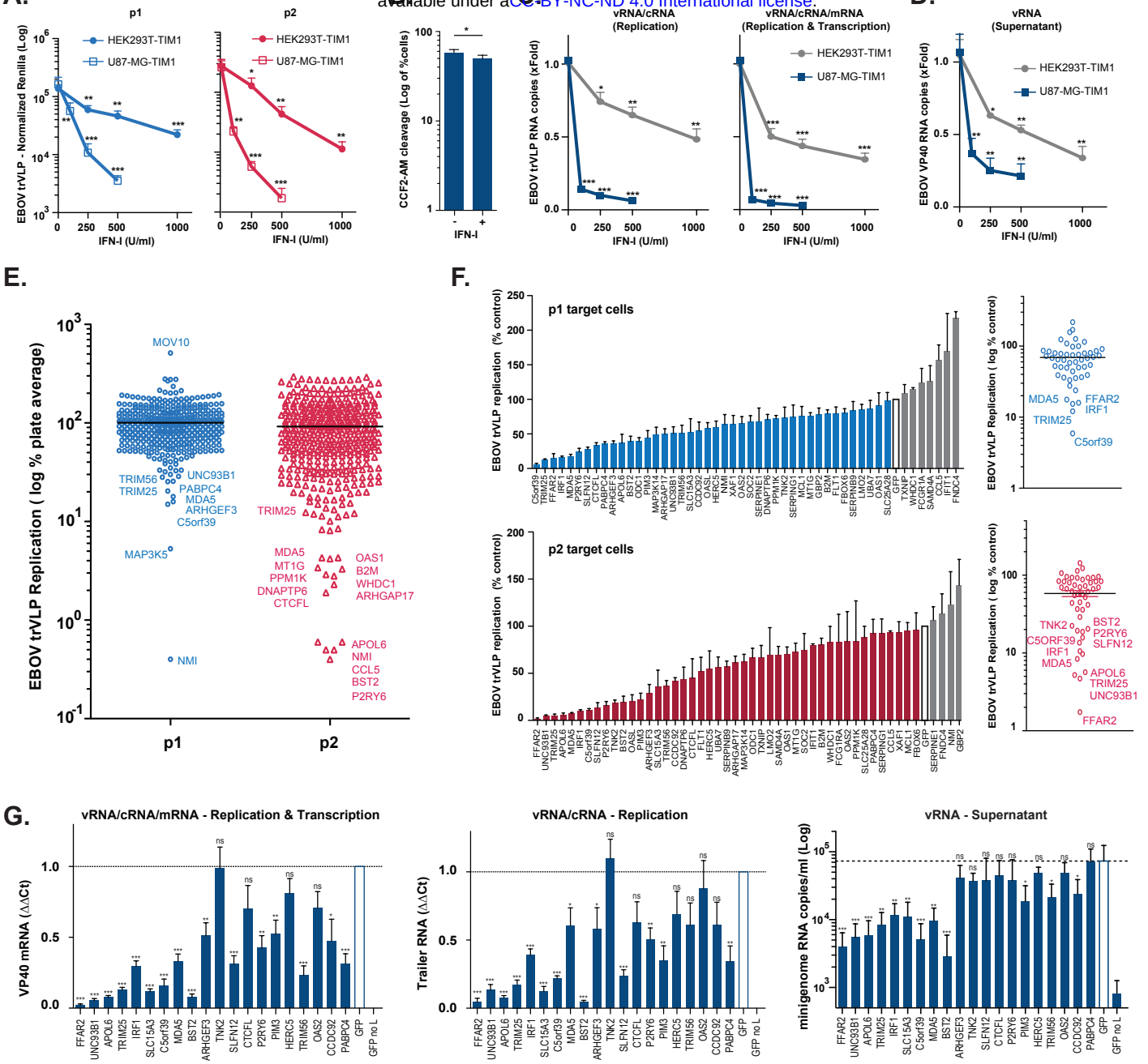

Figure 2

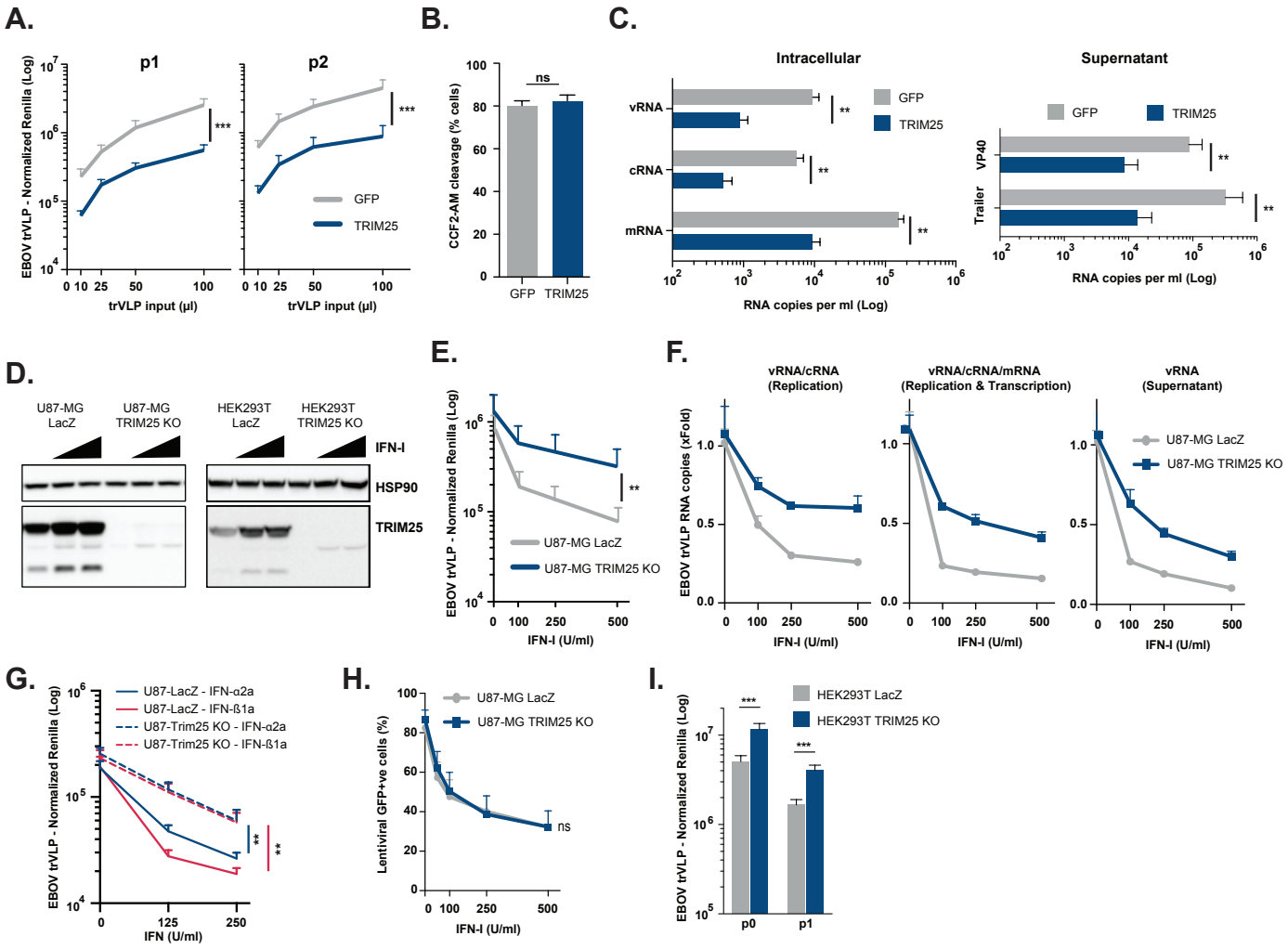

Figure 3

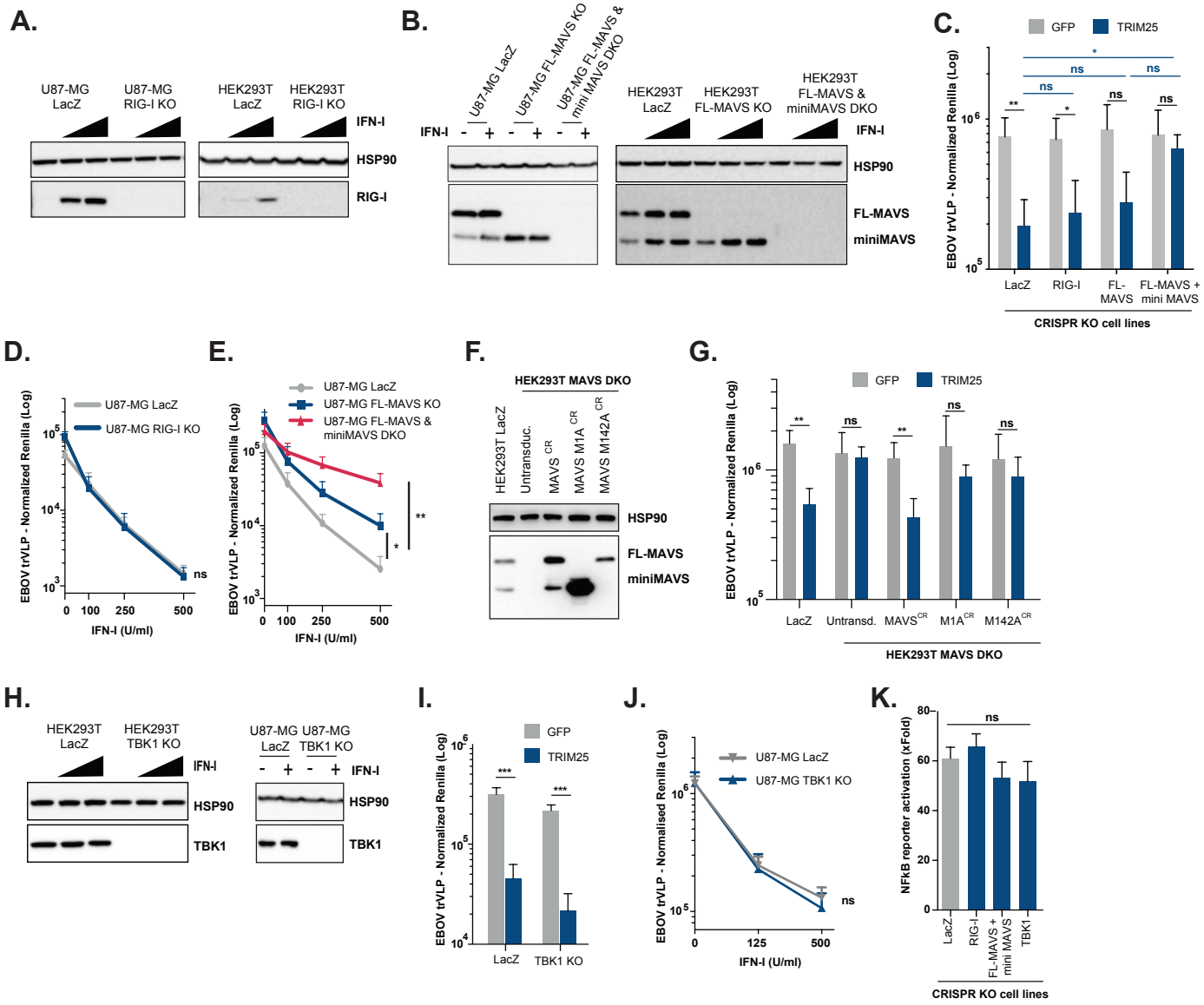

Figure 4

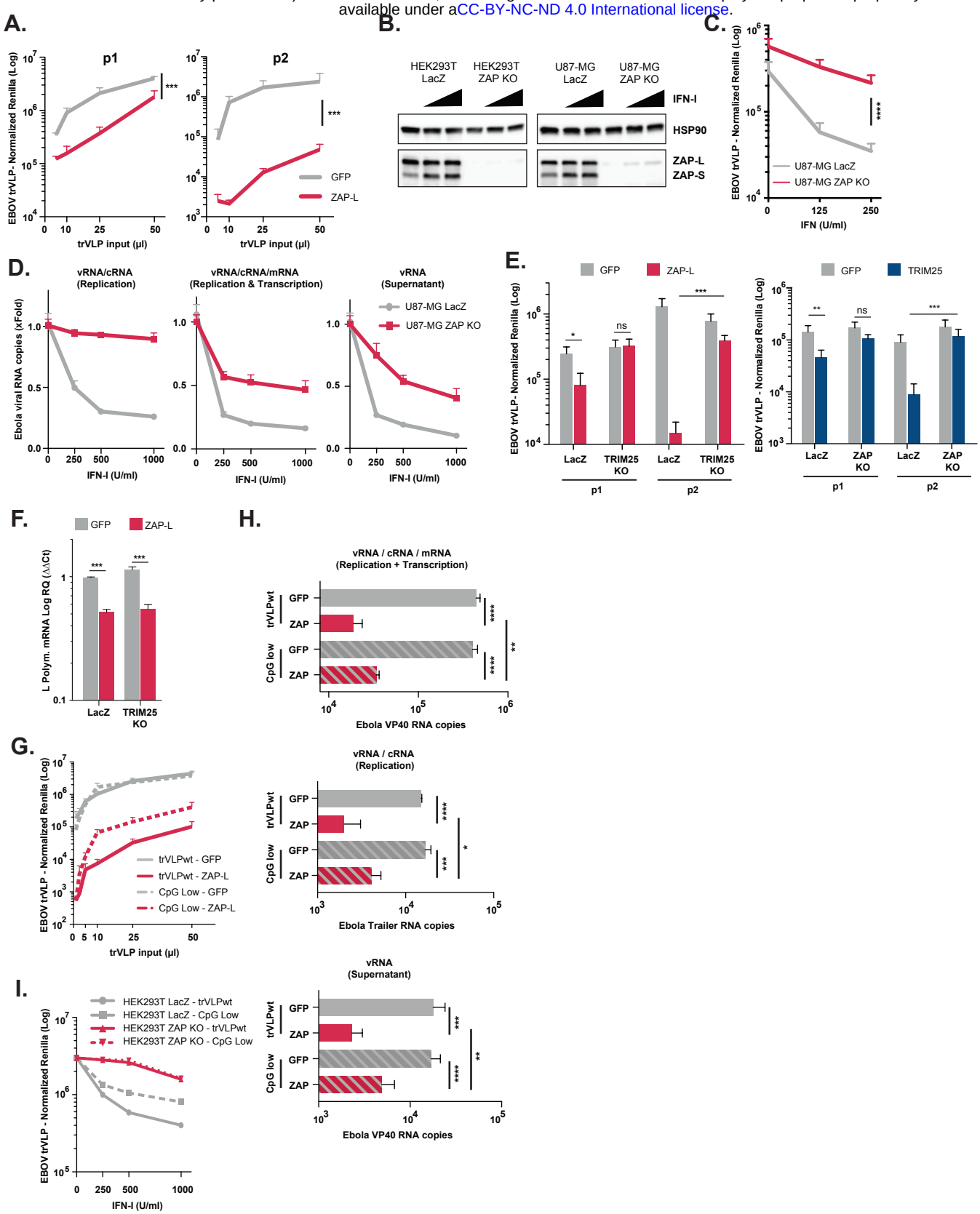

Figure 5

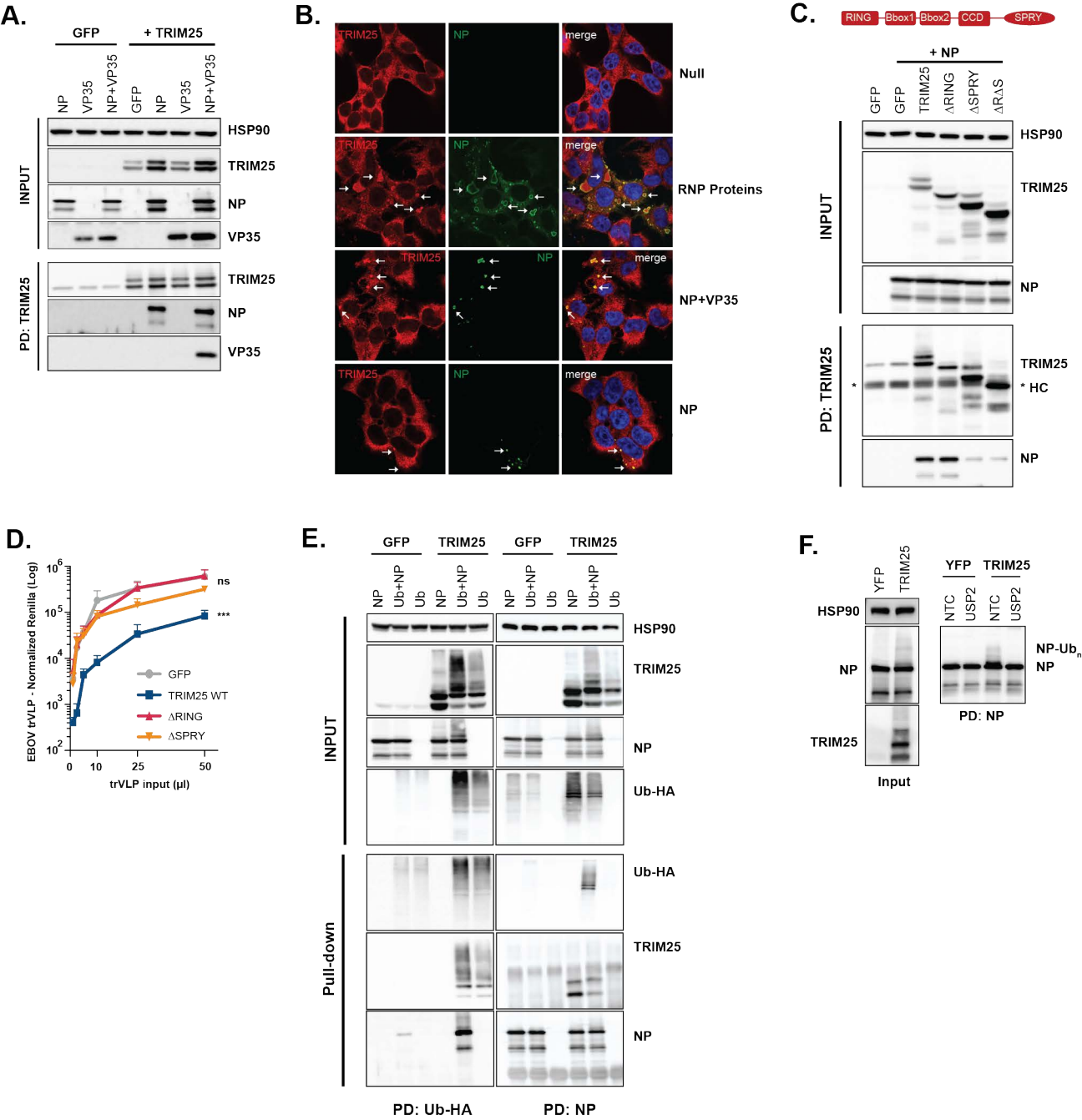
A.
GFP
+ TRIM25
NP
VP35
NP+VP35
GFP
NP
VP35
NP+VP35
INPUT
HSP90
TRIM25
NP
VP35
PD: TRIM25
TRIM25
NP
VP35
B.
TRIM25
NP
merge
Null
RNP Proteins
NP+VP35
NP
C.
RING
Bbox1
Bbox2
CCD
SPRY
+ NP
GFP
GFP
TRIM25
ΔRING
ΔSPRY
ΔRΔS
INPUT
HSP90
TRIM25
NP
PD: TRIM25
TRIM25
* HC
NP
D.
EBOV trVLP - Normalized Renilla (Log)
trVLP input (µl)
ns
***
GFP
TRIM25 WT
ΔRING
ΔSPRY
E.
GFP
TRIM25
GFP
TRIM25
NP
Ub+NP
Ub
INPUT
HSP90
TRIM25
NP
Ub-HA
Pull-down
Ub-HA
TRIM25
NP
PD: Ub-HA
PD: NP
F.
YFP
TRIM25
YFP
TRIM25
NTC
USP2
NTC
USP2
HSP90
NP
TRIM25
NP-Ub$_n$
NP
PD: NP
Input

Figure 6

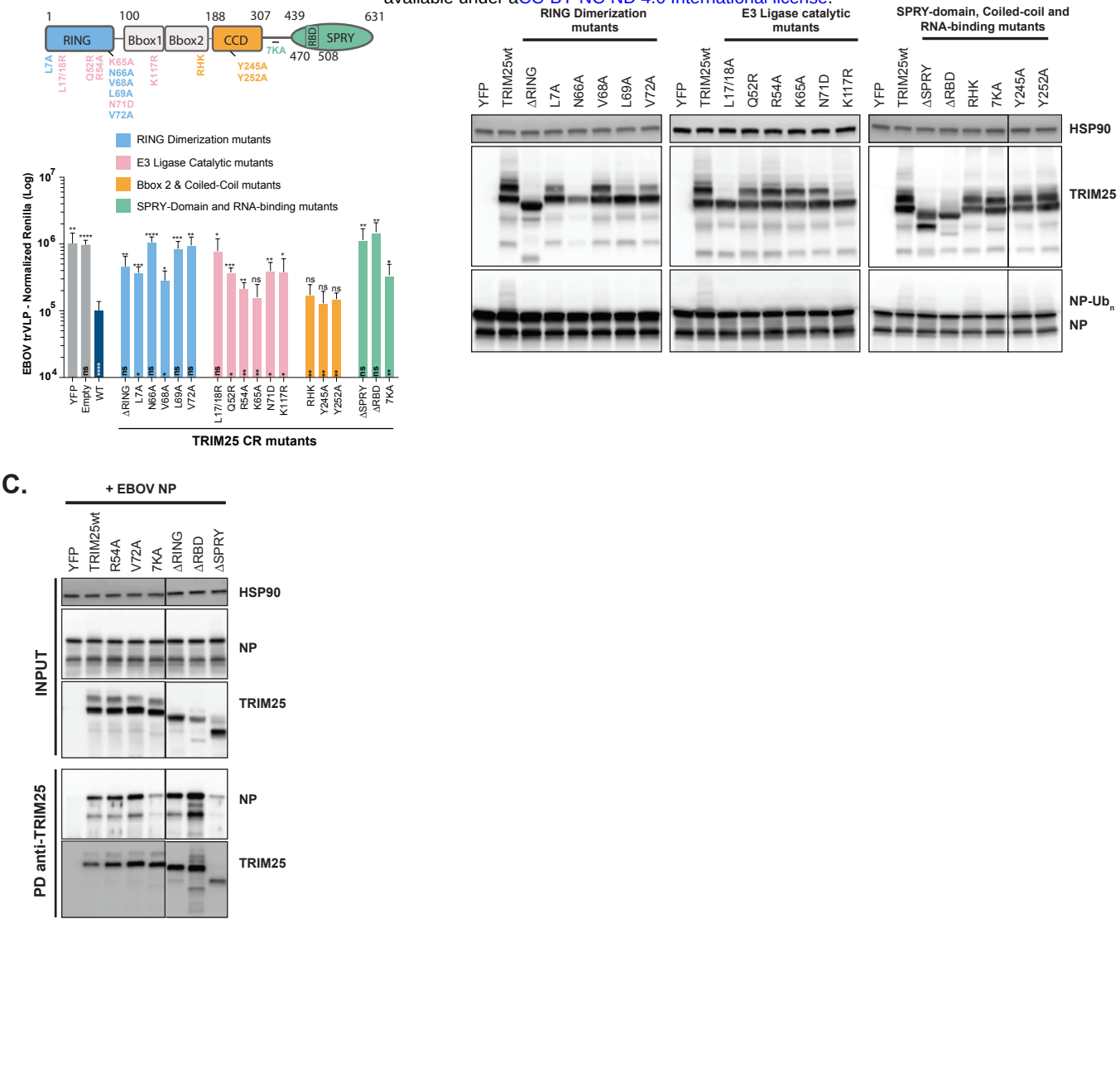

Figure 7

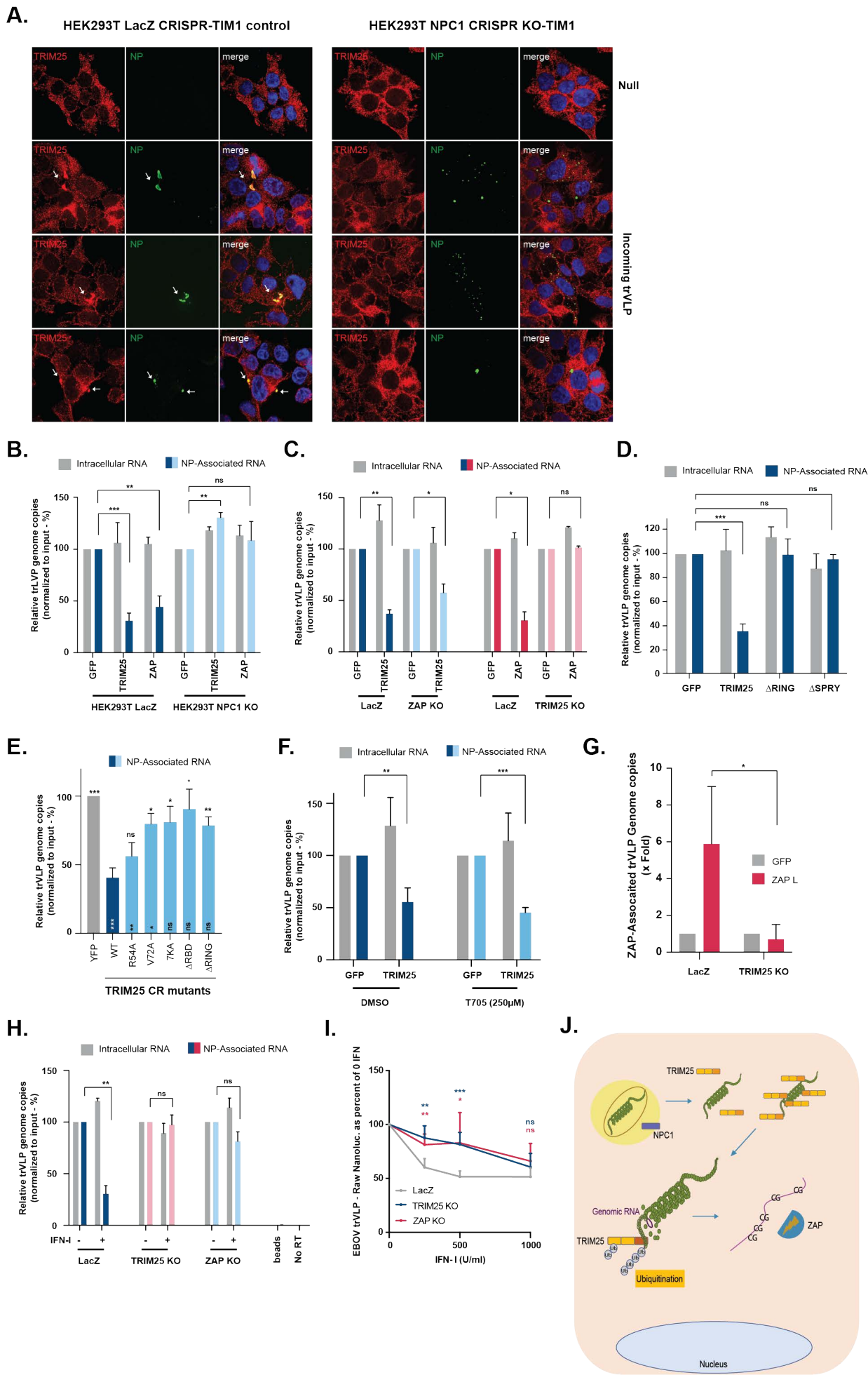
A.
HEK293T LacZ CRISPR-TIM1 control
HEK293T NPC1 CRISPR KO-TIM1
TRIM25
NP
merge
Null
Incoming trVLP
B.
Intracellular RNA
NP-Associated RNA
Relative trLVP genome copies (normalized to input - %)
GFP
TRIM25
ZAP
HEK293T LacZ
HEK293T NPC1 KO
C.
Relative trVLP genome copies (normalized to input - %)
LacZ
ZAP KO
TRIM25 KO
D.
GFP
TRIM25
ΔRING
ΔSPRY
E.
YFP
WT
R54A
V72A
7KA
ΔRBD
ΔRING
TRIM25 CR mutants
F.
DMSO
T705 (250μM)
G.
ZAP-Associated trVLP Genome copies (x Fold)
GFP
ZAP L
LacZ
TRIM25 KO
H.
IFN-I
beads
No RT
I.
EBOV trVLP - Raw Nanoluc. as percent of 0 IFN
IFN-I (U/ml)
J.
TRIM25
NPC1
Genomic RNA
ZAP
Ubiquitination
Nucleus

Figure S1 (related to Figure 1)

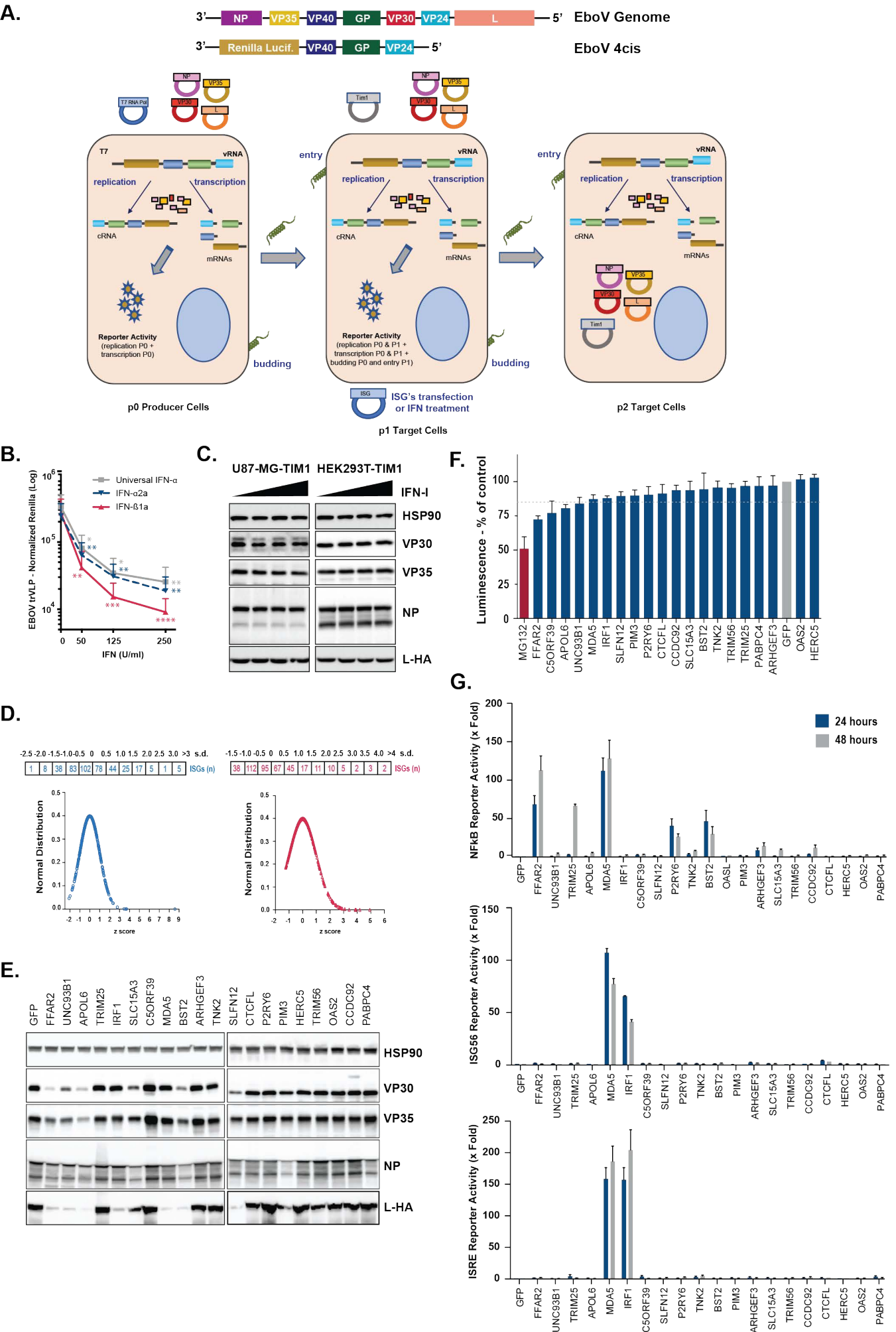

Figure S2 (related to Figure 4)

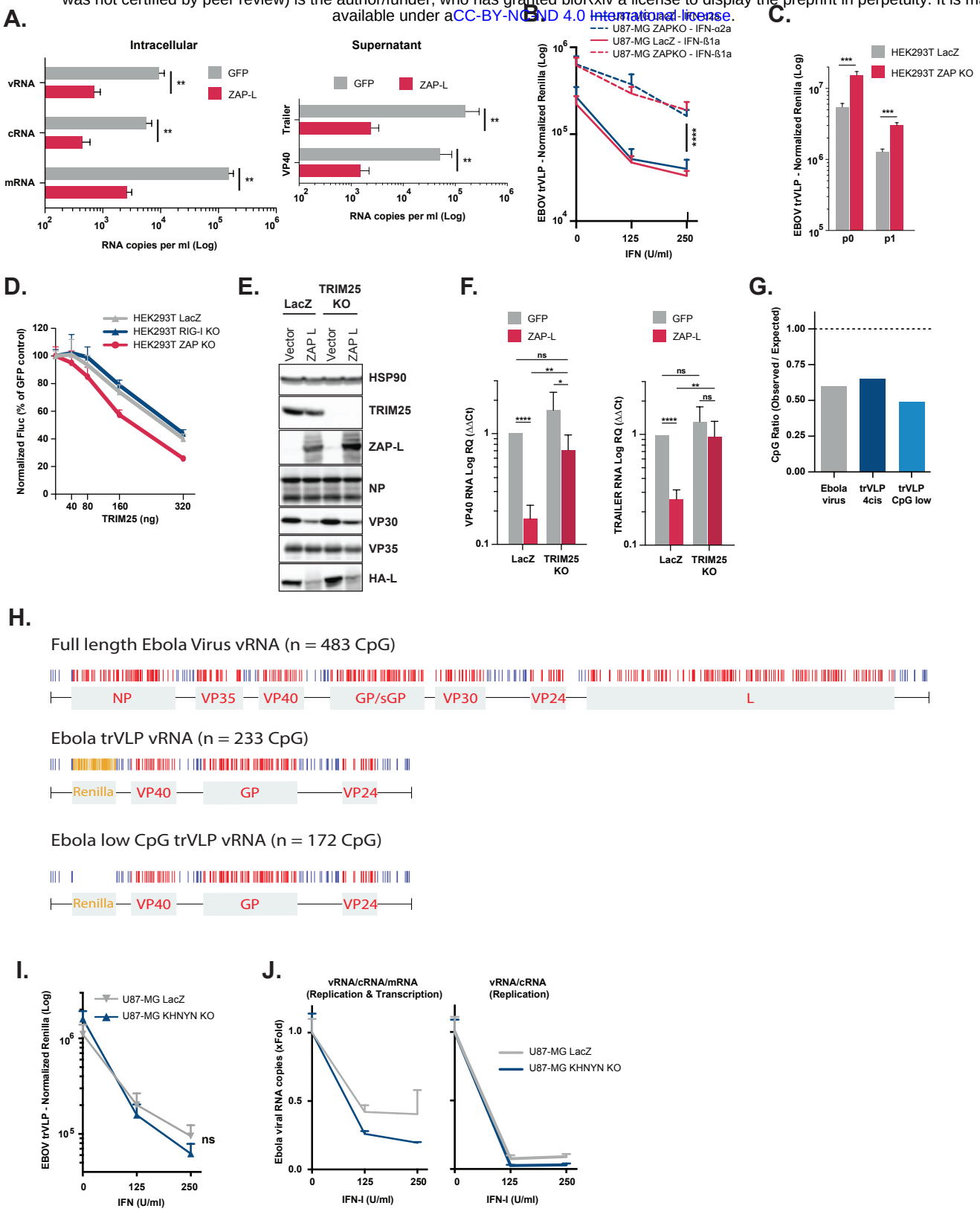

Figure S3 (related to Figure 5)

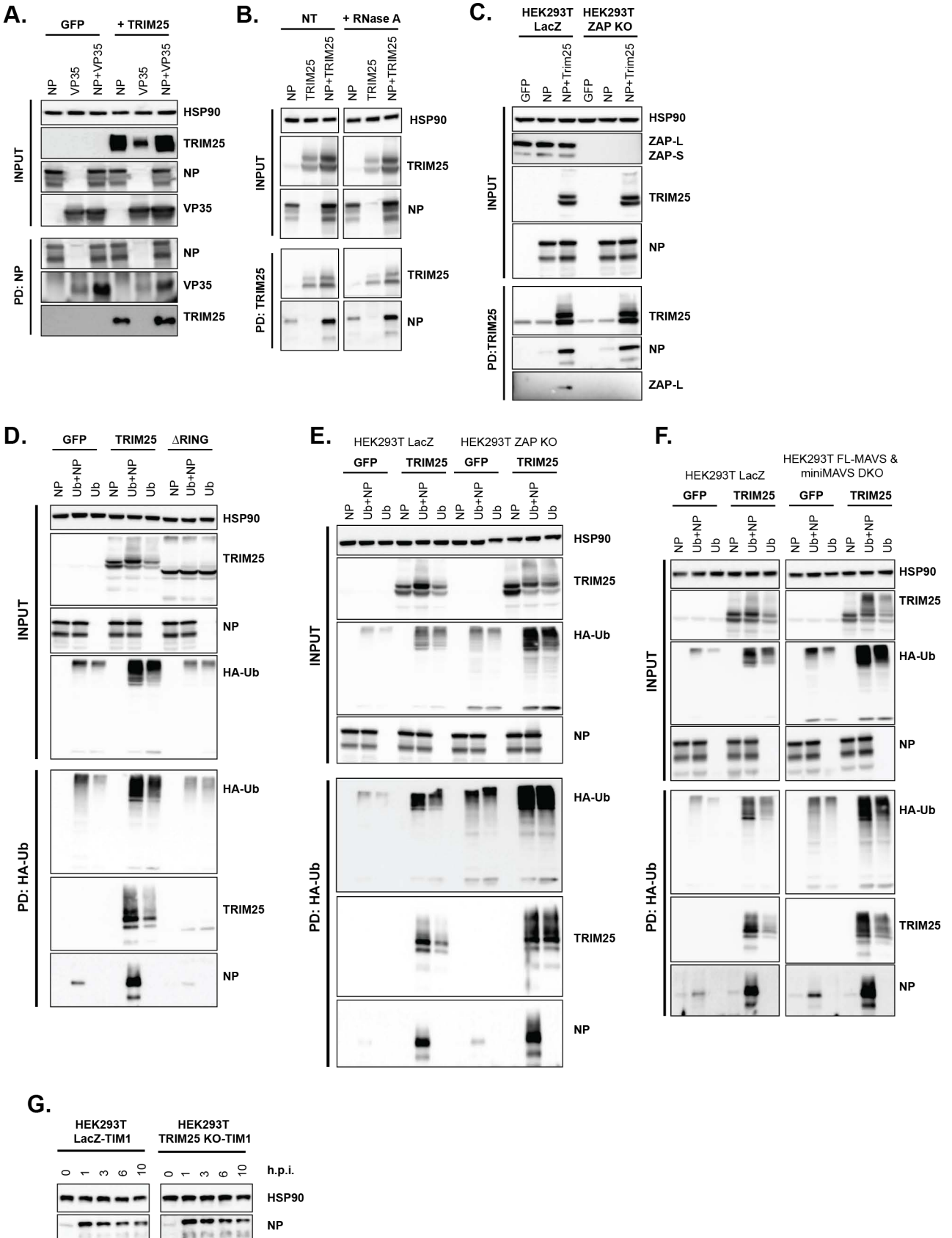

Figure S4 (related to Figure 2)

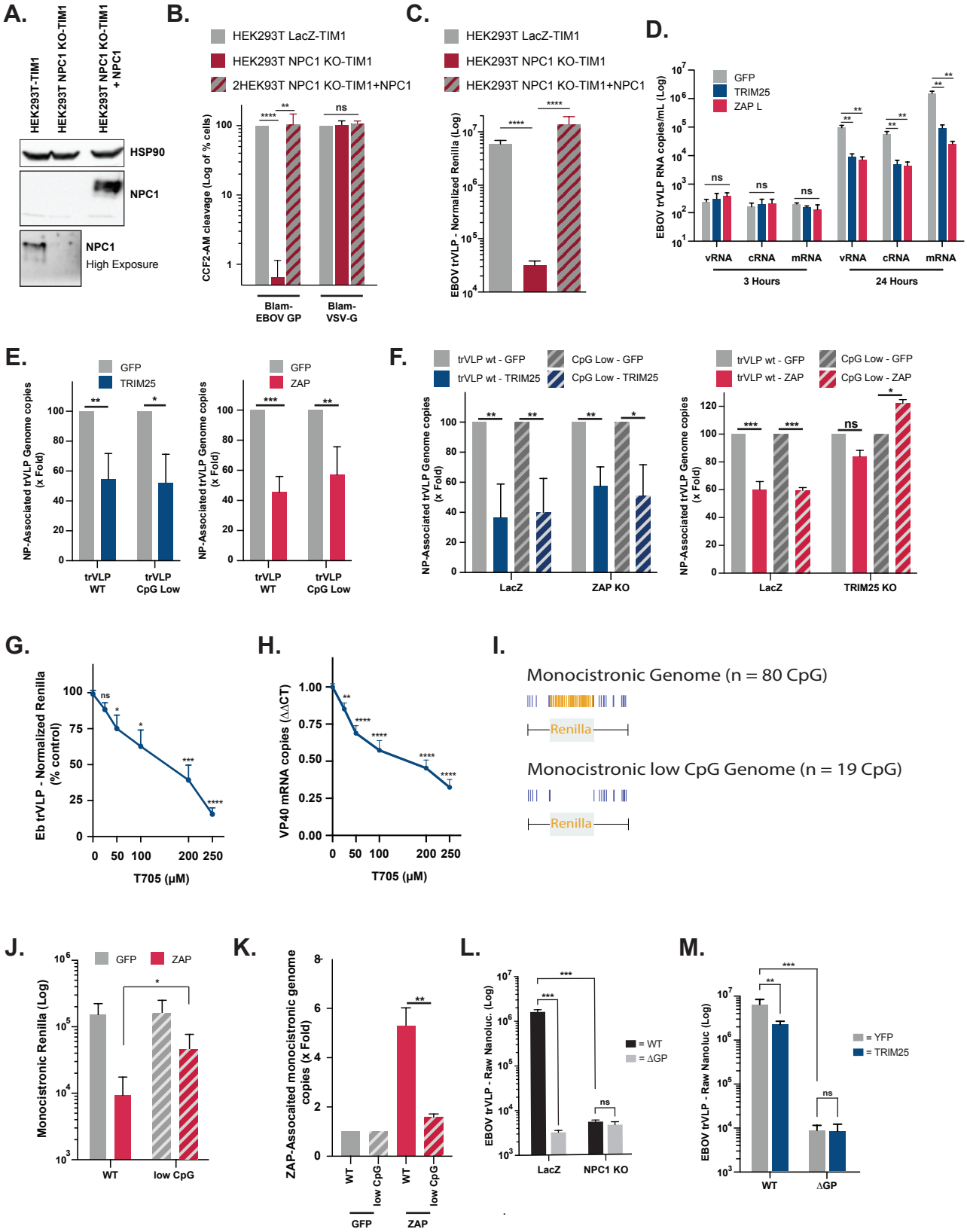

Supplemental Table 1

Large Scale ISG Screen: EboV trVLP in HEK293T cells – p1 and p2 values (Page 1 of 4)

Gene	P2 Replication (% control)	Z score	P1 Replication (% control)	Z score	Gene	P2 Replication (% control)	Z score	P1 Replication (% control)	Z score
P2RY6	0.4	-1.24	41.5	-1.23	MCOLN	28.0	-0.89	40.4	-1.25
BST2/THN	0.5	-1.24	91.8	-0.18	ZNF313	28.1	-0.89	53.5	-0.98
CCL5	0.5	-1.24	106.0	0.11	PDGFRL	28.3	-0.89	100.0	-0.01
NMI	0.6	-1.24	0.4	-2.08	PNPT1	28.7	-0.88	103.6	0.06
APOL6	0.6	-1.24	188.5	1.83	PHF15	28.7	-0.88	119.2	0.39
ARHGAP17	1.9	-1.22	57.9	-0.88	GBP5	28.9	-0.88	116.9	0.34
WHDC1	2.3	-1.21	32.0	-1.42	JAK2	29.6	-0.87	96.8	-0.08
B2M	2.8	-1.21	108.2	0.16	ATF3	30.3	-0.86	116.4	0.33
OAS1	2.9	-1.21	76.4	-0.50	C10orf10	30.5	-0.86	41.8	-1.22
CTCFL	3.3	-1.20	55.6	-0.93	AIM2	30.5	-0.86	70.3	-0.63
DNAPTP6	3.4	-1.20	58.4	-0.88	CCL19	30.6	-0.86	78.0	-0.47
PPM1K	4.2	-1.19	35.0	-1.36	RAB27A	30.9	-0.86	58.7	-0.87
MT1G	4.3	-1.19	57.1	-0.90	IFI35	31.1	-0.85	174.6	1.54
IFIH1 / MDA5	4.3	-1.19	17.9	-1.72	FBXO6	31.4	-0.85	52.3	-1.00
FNDC4	8.1	-1.14	142.9	0.88	UNC93B1	31.9	-0.84	28.2	-1.50
C5orf39	8.3	-1.14	15.0	-1.78	HLA-E	32.1	-0.84	66.7	-0.70
SOCS2	8.5	-1.14	77.3	-0.48	GTPBP2	32.5	-0.84	184.2	1.74
FCGR1A	10.1	-1.12	148.1	0.99	GLRX	32.8	-0.83	60.9	-0.82
MCL1	11.2	-1.10	124.4	0.50	CX3CL1	33.1	-0.83	212.9	2.33
ARHGEF3	11.4	-1.10	15.9	-1.76	TAP2	33.2	-0.83	145.1	0.92
FLT1	11.7	-1.10	67.9	-0.68	XAF1	33.4	-0.82	55.0	-0.95
MAP3K14	11.9	-1.09	63.6	-0.77	WARS	33.7	-0.82	112.2	0.24
OASL	12.1	-1.09	123.2	0.47	IFNGR1	34.1	-0.82	51.7	-1.01
TNK2	12.4	-1.09	165.0	1.34	SLC25A28	34.5	-0.81	105.1	0.10
GBP2	13.2	-1.08	74.2	-0.55	VIPERIN	34.7	-0.81	98.2	-0.05
GALNT2	13.7	-1.07	133.9	0.69	ZBP1	34.9	-0.81	54.1	-0.96
FFAR2	14.9	-1.06	43.0	-1.20	MYD88	35.4	-0.80	46.4	-1.12
CCDC92	15.0	-1.06	79.8	-0.43	CASP7	35.5	-0.80	71.3	-0.61
LMO2	15.4	-1.05	80.7	-0.41	NDC80	35.6	-0.80	66.9	-0.70
SLC15A3	16.0	-1.04	174.0	1.53	MAFF	36.0	-0.79	97.5	-0.06
HERC5	16.6	-1.04	77.1	-0.49	APOBEC3A	36.5	-0.79	56.2	-0.92
TXNIP	16.6	-1.03	80.5	-0.42	ZNF385B	36.6	-0.78	61.2	-0.82
UBA7	17.5	-1.02	55.8	-0.93	DEFB1	37.1	-0.78	80.9	-0.41
PIM3	17.5	-1.02	87.6	-0.27	XRN	37.1	-0.78	88.0	-0.26
TRIM25	17.7	-1.02	25.4	-1.56	SAMD4A	38.3	-0.76	62.5	-0.79
TRIM56	19.2	-1.00	25.6	-1.56	SMAD3	38.7	-0.76	80.5	-0.42
SLFN12	19.4	-1.00	56.1	-0.92	STAT2	39.9	-0.74	105.0	0.09
STEAP4	19.8	-1.00	86.3	-0.30	PUS1	39.9	-0.74	120.3	0.41
CXCL10	19.8	-0.99	90.5	-0.21	IFIT3	40.9	-0.73	92.5	-0.17
MAB21L2	19.9	-0.99	130.6	0.62	C15orf48	41.2	-0.73	63.9	-0.76
FAM46C	20.6	-0.99	38.6	-1.29	IFITM1	41.3	-0.73	109.3	0.18
MX2	21.6	-0.97	49.9	-1.05	GK	41.4	-0.72	67.8	-0.68
GBP1	21.8	-0.97	78.6	-0.46	SAT1	42.4	-0.71	93.9	-0.14
PABPC4	22.0	-0.97	20.4	-1.67	KIAA0082	42.5	-0.71	50.9	-1.03
SERPINE1	22.3	-0.96	52.2	-1.00	TNFRSF10A	43.7	-0.70	177.3	1.59
SERPING1	23.2	-0.95	68.0	-0.68	TNFAIP3	44.3	-0.69	182.0	1.69
C5orf27	23.5	-0.95	81.9	-0.39	IL28RA	44.4	-0.69	80.4	-0.42
SERPINB9	23.8	-0.94	155.3	1.14	NFIL3	45.0	-0.68	78.1	-0.47
IRF1	24.0	-0.94	33.2	-1.40	RARRES3	45.1	-0.68	97.0	-0.07
HCP5	24.5	-0.94	110.4	0.21	BIRC3	46.4	-0.66	67.0	-0.70
ODC1	24.6	-0.93	151.4	1.06	HEG1	46.5	-0.66	74.1	-0.55
TRIM14	24.7	-0.93	65.9	-0.72	C9ofr19	46.5	-0.66	85.1	-0.32
CLEC4D	25.3	-0.93	68.9	-0.66	HSPA6	46.6	-0.66	124.7	0.50
IFIT1	25.4	-0.92	96.3	-0.09	USP18	47.4	-0.65	52.6	-1.00
CNP	25.5	-0.92	156.1	1.15	DDX60	47.7	-0.65	87.9	-0.26
NCF1	26.8	-0.91	92.8	-0.16	EPAS1	48.0	-0.64	193.5	1.93
CD274	26.9	-0.91	88.2	-0.26	SAMHD1	48.2	-0.64	55.7	-0.93
IFI27	27.5	-0.90	95.5	-0.10	FAM125B	48.4	-0.64	60.8	-0.82
CEACAM1	27.6	-0.90	59.7	-0.85	STAP1	49.1	-0.63	50.5	-1.04

Large Scale ISG Screen: EboV trVLP in HEK293T cells – p1 and p2 values (Page 2 of 4)

Gene	P2 Replication (% control)	Z score	P1 Replication (% control)	Z score	Gene	P2 Replication (% control)	Z score	P1 Replication (% control)	Z score
DYNLT1	49.5	-0.62	77.0	-0.49	ISG20	68.1	-0.39	44.7	-1.16
SSBP3	49.5	-0.62	51.2	-1.03	TRAFD1	68.1	-0.39	126.7	0.54
RBM43	49.7	-0.62	75.9	-0.51	MX1	68.2	-0.39	72.0	-0.59
AKT3	49.8	-0.62	109.0	0.18	HLA-F	68.4	-0.39	125.4	0.52
ANGPTL1	50.5	-0.61	97.3	-0.07	TAP1	68.6	-0.38	98.8	-0.04
FAM70A	50.7	-0.61	75.8	-0.51	LGALS3	69.9	-0.37	85.9	-0.30
UPP2	50.7	-0.61	50.0	-1.05	HLA-C	70.2	-0.36	123.5	0.48
SIRPA	51.0	-0.60	38.2	-1.29	CASP1	70.4	-0.36	43.4	-1.19
CCND3	52.1	-0.59	163.9	1.32	RPL22	70.8	-0.35	116.2	0.33
RNF19B	52.2	-0.59	82.5	-0.37	APOL3	71.2	-0.35	75.3	-0.52
MTHFD2L	52.5	-0.59	73.4	-0.56	PSCD1	72.4	-0.34	67.5	-0.69
EIF3EIP	53.2	-0.58	147.1	0.97	SCO2	72.6	-0.33	166.5	1.37
THBD	53.3	-0.57	201.1	2.09	TRIM38	73.4	-0.32	116.5	0.33
NT5C3	53.5	-0.57	84.5	-0.33	IFI44	75.2	-0.30	79.5	-0.44
PSMB8	53.6	-0.57	80.4	-0.42	IFI44L	75.7	-0.29	30.0	-1.47
MS4A4A	54.0	-0.57	52.2	-1.00	AXUD1	75.9	-0.29	90.9	-0.20
SECTM1	54.0	-0.57	45.8	-1.14	MAFF	76.4	-0.28	102.4	0.04
ABLIM3	54.5	-0.56	53.7	-0.97	ARNTL	76.6	-0.28	154.5	1.12
FAM46A	54.9	-0.55	52.3	-1.00	TLR3	76.9	-0.28	106.4	0.12
RTP4	55.1	-0.55	87.1	-0.28	CXCL9	77.0	-0.28	85.2	-0.32
CMAH	55.2	-0.55	115.0	0.30	C9orf91	77.0	-0.28	120.6	0.42
MT1M	55.9	-0.54	148.2	0.99	IFI16	77.7	-0.27	94.9	-0.12
SOCS1	56.6	-0.53	108.5	0.17	PSMB9	77.7	-0.27	126.0	0.53
DDX58	57.1	-0.53	33.2	-1.40	IFITM3	78.3	-0.26	64.8	-0.74
BAG1	57.2	-0.53	122.4	0.45	ALDH1A1	78.9	-0.25	69.4	-0.65
UNC84B	57.3	-0.52	96.8	-0.08	ERLIN1	79.2	-0.25	72.9	-0.57
C19orf66	57.4	-0.52	96.9	-0.08	CCL8	79.3	-0.25	51.3	-1.02
B4GALT5	57.9	-0.52	104.5	0.08	INDO	79.8	-0.24	88.7	-0.25
SPTLC2	58.1	-0.51	88.3	-0.25	RNASE4	80.1	-0.24	161.0	1.26
BUB1	58.6	-0.51	74.2	-0.55	AGPAT9	80.2	-0.24	69.0	-0.66
MOV10	59.1	-0.50	513.4	8.58	DCP1A	82.3	-0.21	108.3	0.16
SAMD9L	59.4	-0.50	66.9	-0.70	HERC6	82.5	-0.21	124.0	0.49
TMEM51	60.0	-0.49	104.9	0.09	IL17RB	82.9	-0.20	152.4	1.08
VAMP5	60.2	-0.49	65.5	-0.73	JUNB	84.0	-0.19	115.9	0.32
BLZF1	60.2	-0.49	109.1	0.18	N4BP1	84.5	-0.18	59.3	-0.86
PRKD2	60.4	-0.49	150.6	1.04	EPSTI1	84.6	-0.18	90.3	-0.21
CHMP5	60.6	-0.48	126.8	0.55	TGFB1	85.1	-0.18	126.1	0.53
DDX3X	60.6	-0.48	59.7	-0.85	SAA1	85.1	-0.18	204.6	2.16
TMEM49	60.9	-0.48	118.1	0.36	PFKFB3	85.6	-0.17	137.3	0.76
SP110	61.2	-0.48	131.9	0.65	C2orf31	85.9	-0.17	125.1	0.51
CCNA1	62.6	-0.46	128.5	0.58	PCTK3	86.5	-0.16	113.5	0.27
IRF9	62.9	-0.46	90.5	-0.21	PARP12	86.7	-0.16	103.0	0.05
PARP10	63.6	-0.45	98.6	-0.04	STARD5	87.4	-0.15	115.0	0.30
SLC1A1	63.7	-0.45	51.9	-1.01	FER1L3	87.5	-0.15	69.5	-0.65
ANKRD22	64.0	-0.44	110.6	0.21	ISG15	87.6	-0.14	135.4	0.72
C4orf32	64.0	-0.44	91.9	-0.18	MT1L	87.7	-0.14	84.7	-0.33
BCL3	64.0	-0.44	128.9	0.59	IFI6	87.9	-0.14	47.4	-1.10
MAFF	64.1	-0.44	64.8	-0.74	IFITM2	88.1	-0.14	86.1	-0.30
C4orf33	64.4	-0.44	76.6	-0.50	PMAIP1	88.5	-0.13	61.8	-0.81
C1S	64.5	-0.43	50.3	-1.04	NOS2A	89.7	-0.12	76.5	-0.50
APOL2	64.6	-0.43	87.8	-0.26	PLEKHA4	90.0	-0.11	83.1	-0.36
TRIM21	65.5	-0.42	56.4	-0.92	STAT3	90.7	-0.11	61.9	-0.80
HESX1	65.9	-0.42	97.7	-0.06	EIF2AK2	91.0	-0.10	67.4	-0.69
SNN	66.7	-0.41	57.6	-0.89	ELF1	91.5	-0.10	32.8	-1.41
LIPA	66.7	-0.41	107.0	0.13	PBEF1	92.3	-0.09	127.7	0.56
LAMP3	67.1	-0.40	107.0	0.13	RIPK2	92.6	-0.08	28.7	-1.49
CCDC109B	67.2	-0.40	51.7	-1.02	DUSP5	93.1	-0.08	142.8	0.88
OPTN	67.8	-0.39	77.9	-0.47	CSDA	93.8	-0.07	164.4	1.33
DDIT4	68.0	-0.39	130.1	0.61	OGFR	94.1	-0.06	106.3	0.12

Large Scale ISG Screen: EboV trVLP in HEK293 cells – p1 and p2 values (Page 3 of 4)

Gene	P2 Replication (% control)	Z score	P1 Replication (% control)	Z score	Gene	P2 Replication (% control)	Z score	P1 Replication (% control)	Z score
EXT1	94.2	-0.06	99.2	-0.03	SLC25A30	128.3	0.37	157.1	1.18
RBM25	95.1	-0.05	77.9	-0.47	S100A8	128.4	0.37	96.7	-0.08
BCL2L14	95.1	-0.05	60.0	-0.84	SP100	129.2	0.38	82.8	-0.37
PRAME	95.9	-0.04	177.4	1.60	CRY1	130.9	0.40	115.4	0.31
GEM	95.9	-0.04	80.8	-0.41	ATP10D	131.8	0.41	102.7	0.04
BTN3A3	96.1	-0.04	106.2	0.12	IL1RN	132.0	0.41	175.7	1.56
TBX3	96.4	-0.03	168.5	1.41	IFI30	132.5	0.42	107.7	0.15
MICB	98.2	-0.01	63.5	-0.77	APOBEC3G	132.8	0.42	68.1	-0.67
GPX2	98.9	0.00	114.8	0.30	TDRD7	132.9	0.42	123.3	0.47
CD74	100.2	0.01	130.0	0.61	PTMA	133.0	0.42	99.1	-0.03
STAT1	101.6	0.03	115.6	0.31	LINCR	134.5	0.44	83.8	-0.35
RNF24	102.2	0.04	91.1	-0.20	MT1F	134.6	0.44	49.9	-1.05
GZMB	102.2	0.04	75.8	-0.51	GCA	134.7	0.45	98.5	-0.04
CYP1B1	102.4	0.04	202.7	2.12	CD163	136.0	0.46	174.2	1.53
LEPR	102.4	0.04	116.0	0.32	CPT1A	136.6	0.47	161.5	1.27
ADAMDEC1	103.3	0.05	101.6	0.02	TCF7L2	136.7	0.47	138.7	0.79
NPAS2	103.6	0.06	133.9	0.69	SLC16A1	137.5	0.48	46.8	-1.12
ADFP	104.0	0.06	103.1	0.05	PMM2	139.5	0.51	103.8	0.07
ANKFY1	104.0	0.06	92.6	-0.17	MAFB	139.6	0.51	214.0	2.36
ABTB2	104.7	0.07	144.1	0.90	THOC4	140.0	0.51	105.6	0.10
CD69	105.2	0.08	108.9	0.17	HES4	140.8	0.52	149.2	1.01
ZNF295	106.3	0.09	115.1	0.30	TIMP1	143.6	0.56	76.6	-0.50
AQP9	106.6	0.09	51.1	-1.03	IRF7	143.7	0.56	186.1	1.78
NCOA3	107.0	0.10	104.8	0.09	TAGAP	143.7	0.56	153.9	1.11
CCDC75	107.9	0.11	88.5	-0.25	LGMN	145.4	0.58	113.9	0.28
RGS1	108.4	0.12	183.2	1.72	PADI2	146.2	0.59	278.6	3.70
FKBP5	108.8	0.12	78.9	-0.45	BLVRA	146.5	0.59	86.8	-0.29
FLJ39739	108.8	0.12	104.5	0.08	SQLE	146.9	0.60	118.5	0.37
CXCL11	109.6	0.13	85.0	-0.32	NOD2	147.4	0.61	169.5	1.43
CLEC2B	109.7	0.13	142.8	0.88	GBP3	148.4	0.62	145.5	0.93
PXK	110.1	0.14	68.8	-0.66	MKX	148.7	0.62	69.7	-0.64
CCL2	111.2	0.15	43.0	-1.19	COMMD3	149.6	0.63	64.9	-0.74
IRF2	111.4	0.15	145.1	0.93	BATF2	150.7	0.65	109.8	0.19
TLK2	112.3	0.16	92.1	-0.17	DHX58	153.6	0.68	100.6	0.00
APOL1	112.5	0.17	70.4	-0.63	GCH1	154.0	0.69	57.1	-0.90
GAK	112.8	0.17	121.8	0.44	CDKN1A	154.2	0.69	153.5	1.10
PCTK2	113.3	0.18	95.6	-0.10	ENPP1	154.9	0.70	106.5	0.12
ZNF107	113.5	0.18	103.5	0.06	IL1R	155.1	0.70	46.7	-1.12
MARCK	114.2	0.19	276.4	3.65	UBE2L6	155.3	0.70	86.3	-0.29
CEBPD	115.1	0.20	116.2	0.33	PFKFB3	155.7	0.71	275.7	3.64
TYMP	115.7	0.21	96.6	-0.08	RBCK1	158.7	0.75	140.3	0.83
CES1	115.9	0.21	130.3	0.62	HSH2D	158.8	0.75	178.5	1.62
KIAA1618	116.4	0.22	134.5	0.70	RIPK2	159.8	0.76	79.2	-0.44
TREX1	116.4	0.22	99.7	-0.02	NAPA	160.1	0.76	75.3	-0.53
G6PC	116.9	0.22	133.4	0.68	CFB	161.7	0.78	107.0	0.13
IMPA2	117.4	0.23	97.7	-0.06	CLEC4A	162.0	0.79	109.9	0.19
DDX60	117.5	0.23	78.6	-0.46	IFIT5	162.7	0.80	106.0	0.11
C22orf28	119.4	0.25	98.5	-0.04	FNDC3B	163.2	0.80	103.6	0.06
ABCA9	120.2	0.26	154.0	1.11	KIAA0082	164.0	0.81	64.6	-0.75
MT1H	120.9	0.27	153.7	1.10	CD38	167.2	0.85	77.4	-0.48
SPSB1	121.0	0.27	120.4	0.41	HK2	167.7	0.86	149.8	1.02
SCARB2	121.0	0.27	57.4	-0.90	ETV6	168.2	0.87	97.4	-0.07
PPM1K	122.1	0.29	63.1	-0.78	LY6E	168.4	0.87	66.6	-0.71
MAP3K5	122.7	0.29	5.3	-1.98	TFEC	170.4	0.89	98.1	-0.05
CRP	124.0	0.31	98.4	-0.04	SLFN5	170.5	0.89	64.6	-0.75
IRF2	124.9	0.32	59.8	-0.85	LAP3	172.5	0.92	110.1	0.20
RGL-1	125.8	0.33	153.1	1.09	NRN1	172.7	0.92	91.3	-0.19
GMPR	126.4	0.34	93.6	-0.14	ZNF107	174.4	0.94	86.4	-0.29
CCL4	127.4	0.35	72.7	-0.58	PDK1	174.5	0.94	94.9	-0.12

Large Scale ISG Screen: EboV trVLP in HEK293 cells – p1 and p2 values (Page 4 of 4)

Gene	P2 Replication (% control)	Z score	P1 Replication (% control)	Z score	Gene	P2 Replication (% control)	Z score	P1 Replication (% control)	Z score
LGALS9	175.7	0.96	166.6	1.37	LRG1	246.4	1.85	132.9	0.67
IL6ST	176.3	0.97	106.9	0.13	TLR7	248.7	1.88	63.9	-0.76
RASGEF1B	179.1	1.00	72.8	-0.58	ADAR	250.4	1.90	180.5	1.66
RASSF4	183.0	1.05	118.3	0.37	TNFSF10	255.5	1.96	99.2	-0.03
DTX3L	188.2	1.12	110.6	0.21	CD80	262.4	2.05	63.1	-0.78
CCR1	189.7	1.13	70.7	-0.62	ARG2	269.5	2.14	132.9	0.67
CREB3L3	192.2	1.17	152.9	1.09	TRIM34	271.6	2.16	103.1	0.05
LOC400759	193.2	1.18	85.1	-0.32	HPSE	273.0	2.18	109.3	0.18
IL15	193.6	1.18	55.3	-0.94	ZC3HAV1	273.6	2.19	70.7	-0.62
NUP50	196.4	1.22	87.3	-0.27	PML	277.0	2.23	267.3	3.46
IGFBP2	197.3	1.23	141.9	0.86	PI4K2B	278.1	2.24	99.9	-0.01
GJA4	198.1	1.24	104.7	0.09	MASTL	280.4	2.27	161.7	1.27
HLA-G	198.5	1.25	82.1	-0.38	FLJ23556	291.6	2.41	99.0	-0.03
FUT4	199.1	1.25	234.5	2.78	PAK3	295.7	2.46	59.2	-0.86
PNRC1	200.1	1.27	80.6	-0.41	TNFSF13B	306.0	2.59	90.3	-0.21
LAMP3	206.0	1.34	143.4	0.89	ULK4	312.9	2.68	90.2	-0.21
EHD4	206.6	1.35	77.7	-0.47	MSR1	317.5	2.74	124.4	0.50
SIGLEC1	206.9	1.35	177.7	1.60	TNFAIP6	323.0	2.81	127.8	0.57
C6orf150	213.1	1.43	142.6	0.87	MAX	331.3	2.91	146.1	0.95
FAM134B	217.7	1.49	94.5	-0.12	KIAA0040	345.5	3.09	121.8	0.44
PLSCR1	221.2	1.53	63.1	-0.78	OAS3	371.0	3.41	148.0	0.99
GBP4	223.4	1.56	92.3	-0.17	IFIT2	406.4	3.85	103.0	0.05
ADM	223.6	1.56	124.9	0.51	AHNAK2	408.6	3.88	125.6	0.52
VEGFC	224.7	1.57	134.0	0.69	TRIM5	410.9	3.91	80.4	-0.42
ETV7	225.2	1.58	80.0	-0.43	OAS2	433.0	4.19	104.0	0.07
AMPH	228.5	1.62	190.9	1.88	CD9	491.6	4.92	188.2	1.82
IL15RA	229.8	1.64	135.0	0.72					

1

Table S2 – CRISPR Guides	
LacZ Guide	5'- CGA TTA AGT TGG GTA ACG CC -3'
TRIM25 CRISPR Guide	5'- GAG CCG GTC ACC ACT CCG TG -3'
ZAP CRISPR Guide	5'- ACT TCC ATC TGC CTT ACC GG -3'
RIG-I CRISPR Guide	5'- GGG TCT TCC GGA TAT AAT CC -3'
MAVS CRISPR Guide	5'- ATT GCG GCA GAT ATA CTT AT -3'
MAVS & miniMAVS CRISPR Guide 7	5'- TCT GGG GCT GAG CGT CTG CA -3'
TBK1 CRISPR Guide	5'- AGA GCA CTT CTA ATC ATC TG -3'
NPC1 CRISPR Guides	5'- GCT CAC AAA ACA GGT TCA GT -3' 5'- ACA GTC GTC TTG CTG TCG AG –3'
KHNYN CRISPR Guides	5'-GGG GGT GAG CGT CCT TCC GA-3'

2

3

Table S3 – Primers used for cloning	
EcoRI_Kz_TRIM25wt_Fwd	GCGCGAATTCGCCACCATGGCAGAGCTGTGCCCCCTGG
TRIM25 ΔRING_Fwd EcoRI	GCGCGAATTCGCCACCATGCGCGCCGTCTACCAGGCGCGACCGC
TRIM25 ΔSPRY_Rev XhoI	CGCGCGCTCGAGAATTTTAATGTAATACTCCAGGAGCTC
TRIM25wt_Rev_XhoI	CGCGCGCTCGAGCTACTTGGGGGAGCAGATGG
TRIM25wt_CR_Fwd	GAGCCGGTGACAACACCTTGCGGCCACAA
TRIM25wt_CR_Rev	TTGTGGCCGCAAGGTGTTGTCACCGGCTC
TRIM25_CR_L7A_Fwd	GCGCGAATTCGCCACCATGGCAGAGCTGTGCCCCGCGGCCGAGGAGCT
TRIM25_CR_L17/18R_Fwd	GCTGTCGTGCTCCATCTGCCGGCGACCCTTCAAGGAGCCGGTC
TRIM25_CR_L17/18R_Rev	GACCGGCTCCTTGAAGGGTCGCCGGCAGATGGAGCACGACAGC
TRIM25_CR_Q52R_Fwd	CGCCATACCTGTGCCCGCGATGCCGCGCCGTCTACCAGG
TRIM25_CR_Q52R_Rev	CCTGGTAGACGGCGCGGCATCGCGGGCACAGGTATGGCG
TRIM25_CR_R54A_Fwd	CCATACCTGTGCCCGCAGTGCGCGGCCGTCTACCAGGCGCG
TRIM25_CR_R54A_Rev	CGCGCCTGGTAGACGGCCGCGCACTGCGGGCACAGGTATGG
TRIM25_CR_K65A_Fwd	GGCGCGACCGCAGCTGCACGCGAACACGGTGCTGTGCAACG
TRIM25_CR_K65A_Rev	CGTTGCACAGCACCGTGTTCGCGTGCAGCTGCGGTCGCGCC
TRIM25_CR_N66A_Fwd	CCGCAGCTGCACAAGGCCACGGTGCTGTGCAAC
TRIM25_CR_N66A_Rev	GTTGCACAGCACCGTGGCCTTGTGCAGCTGCGG
TRIM25_CR_V68A_Fwd	AGCTGCACAAGAACACGGCGCTGTGCAACGTGGTGG
TRIM25_CR_V68A_Rev	CCACCACGTTGCACAGCGCCGTGTTCTTGTGCAGCT
TRIM25_CR_L69A_Fwd	CTGCACAAGAACACGGTGGCGTGCAACGTGGTGGAGC
TRIM25_CR_L69A_Rev	GCTCCACCACGTTGCACGCCACCGTGTTCTTGTGCAG
TRIM25_CR_N71D_Fwd	AACACGGTGCTGTGCGACGTGGTGGAGCAGTTCCTG
TRIM25_CR_N71D_Rev	CAGGAACTGCTCCACCACGTCGCACAGCACCGTGTT
TRIM25_CR_V72A_Fwd	ACGGTGCTGTGCAACGCGGTGGAGCAGTTCCTGCA
TRIM25_CR_V72A_Rev	TGCAGGAACTGCTCCACCGCGTTGCACAGCACCGT
TRIM25_CR_K117R_Fwd	GAGGCCGCCGTGAGGACGTGCTTGGTGTGC
TRIM25_CR_K117R_Rev	GCACACCAAGCACGTCCTCACGGCGGCCTC
TRIM25_CR_Y245A_Fwd	GTGGAGCAGCTACAACAAGAAGCCACGGAAATGAAGGCTCTCT
TRIM25_CR_Y245A_Rev	AGAGAGCCTTCATTTCCGTGGCTTCTTGTTGTAGCTGCTCCAC
TRIM25_CR_Y252A_Fwd	ACGGAAATGAAGGCTCTCGCGGACGCCTCAGAGACCAC
TRIM25_CR_Y252A_Rev	GTGGTCTCTGAGGCGTCCGCGAGAGCCTTCATTTCCGT
TRIM25_CR_RHK_AAA Fwd	CGACCTGGAGGCCACCCTGGCCGCAGCCCTAACTGTCATGTACAGTCAGATC
TRIM25_CR_RHK_AAA Rev	GATCTGACTGTACATGACAGTTAGGGCTGCGGCCAGGGTGGCCTCCAGGTCG

TRIM25_CR_ΔRBD_Fwd	ACCGGCCACAACAAAAAGGGGATCCACTACTGGCAGGTGGAG
TRIM25_CR_ΔRBD_Fwd	GTAGTGGATCCCCTTTTTGTTGTGGGCGGTGTTGTAGTCCAG
TRIM25_CR_7KA_Fwd 1	CGCAGAGGAAGCGGCATCCGCGGCACCTCCCCCTGTCCCTGCCTTA
TRIM25_CR_7KA_Fwd 2	ACACGCCCTGTGGCGGCGGTCTCCGCAGAGGAAGCGGCATCC
TRIM25_CR_7KA_Rev 1	TGCCGCTTCCTCTGCGGAGACCGCCGCCACAGGGCGTGTGGATTTGTG
TRIM25_CR_7KA_Rev 2	AGGGACAGGGGGAGGTGCCGCGGATGCCGCTTCCTCTGCGGAG
MAVS Not I Fwd	AAGCGCGGCCGCGCAGCAATGCCGTTTGCTGAAGACAAG
MAVS CR Fwd	ATTCAGAGCAAGCACTGCAGACGCTCAGCC
MAVS CR Rev	GGCTGAGCGTCTGCAGTGCTTGCTCTGAAT
MAVS M1A NotI Fwd	AGGCGCGGCCGCGCAGCAGCGCCGTTTGCTGAAGACAAG
MAVS M142A Fwd	AGGAGCCAAGTTACCCCGCGCCTGTCCAGGAGACCCAG
MAVS M142A Rev	CTGGGTCTCCTGGACAGGCGCGGGGTAACTTGGCTCCT
MAVS Rev XhoI	TGCTCTCGAGCTAGTGCAGACGCCGCC
XhoI_TIM1_Fwd	AGACCTCGAGATCCCATAATGCATCTTCAAGTGGTCATCTTAAGC
TIM1_Rev_NotI	ATGCGCGGCCGCTCATGGGCGTAAACTCTCAAAGAGCAC
EcoRI_NPC1_Fwd	GAATTCGCCACCATGACCGCTCGCGGCCTGGCCC
NPC1_Rev_XhoI	CGCGCTCGAGGGGGGCCTCCACATCCCGGCAGGC
P4 cis vRNA BlpI F	GACCCGTTTAGAGGCCCCAA
P4 cis low CpG TRAIL F	GGGTGCTGAAGAATGAGCAGTAAATTACCGTGCATAGTATCCTGATACTT
P4 cis low CpG TRAIL R	AAGTATCAGGATACTATGCACGGTAATTTACTGCTCATTCTTCAGCACCC
P4 cis vRNA XmaI R	TCGATCCCGGGTTAATACGACTCA

Table S4 – Primers and probes used for cDNA synthesis and RT-qPCR

Trailer qPCR_F	5'- CCA AAA CAC TAT TCC ATC TGA CAG GA -3'
Trailer qPCR_R	5'- TGC CGC AAT GAA TTT AAC GC -3'
Trailer qPCR probe	5'- ATG AGC CCA GAC CTT TCG TT -3'
VP40 qPCR_F	5'- AGT TGG ACT GGC GGA AGA AC -3'
VP40 qPCR_R	5'- CAG AGT CAA TCG GCT GGG TC -3'
VP40 qPCR probe	5'- AAG CCT GGT TTC CAA TTC GC -3'
GAPDH Taqman Assay	Applied Biosystems (Cat# Hs99999905_m1)
OligodT	5'- TTT TTT TTT TTT TTT T -3'
L-Pol RNA qPCR F	5'- CCT ACG AAC AAT GTC CGC -3'
L-Pol RNA qPCR R	5'- CTG CGG AAG GAC ATT TTG -3'
L-Pol qPCR probe	5'- TTG TTA GTG CAT GGC CGA AC -3'
EBOV -vRNA RT	5' CCT CTC TCC CTG CGT GAT AAT C -3'
EBOV +cRNA RT	5'- GCC TTC TGA TGA GCG TGG TC -3'